Experimental Investigations on Power Scaling of High-Brightness cw Ytterbium-Doped Thin-Disk Lasers

Von der Fakultät Konstruktions-, Produktions- und Fahrzeugtechnik der Universität Stuttgart zur Erlangung der Würde einer Doktor- Ingenieurin (Dr.-Ing.) genehmigte Abhandlung

Vorgelegt von

Birgit Weichelt

aus Senftenberg

Hauptberichter: Prof. Dr. rer. nat. habil. Thomas Graf
Mitberichter: Prof. Dr. rer. nat. Thomas Dekorsy

Tag der mündlichen Prüfung: 11.12.2020

Institut für Strahlwerkzeug der Universität Stuttgart

Erscheinungsjahr 2021

Experimental Investigations on Power Scaling of High-Brightness cw Ytterbium-Doped Thin-Disk Lasers

von Dr.-Ing. Birgit Weichelt
Universität Stuttgart

utzverlag München

Laser in der Materialbearbeitung
Forschungsberichte des IFSW

B. Weichelt
Experimental Investigations on Power
Scaling of High-Brightness cw
Ytterbium-Doped Thin-Disk Lasers

Laser in der Materialbearbeitung
Forschungsberichte des IFSW

Herausgegeben von
Prof. Dr. phil. nat. Thomas Graf, Universität Stuttgart
Institut für Strahlwerkzeuge (IFSW)

Das Strahlwerkzeug Laser gewinnt zunehmende Bedeutung für die industrielle Fertigung. Einhergehend mit seiner Akzeptanz und Verbreitung wachsen die Anforderungen bezüglich Effizienz und Qualität an die Geräte selbst wie auch an die Bearbeitungsprozesse. Gleichzeitig werden immer neue Anwendungsfelder erschlossen. In diesem Zusammenhang auftretende wissenschaftliche und technische Problemstellungen können nur in partnerschaftlicher Zusammenarbeit zwischen Industrie und Forschungsinstituten bewältigt werden.

Das 1986 gegründete Institut für Strahlwerkzeuge der Universität Stuttgart (IFSW) beschäftigt sich unter verschiedenen Aspekten und in vielfältiger Form mit dem Laser als einem Werkzeug. Wesentliche Schwerpunkte bilden die Weiterentwicklung von Strahlquellen, optischen Elementen zur Strahlführung und Strahlformung, Komponenten zur Prozessdurchführung und die Optimierung der Bearbeitungsverfahren. Die Arbeiten umfassen den Bereich von physikalischen Grundlagen über anwendungsorientierte Aufgabenstellungen bis hin zu praxisnaher Auftragsforschung.

Die Buchreihe „Laser in der Materialbearbeitung – Forschungsberichte des IFSW" soll einen in der Industrie wie in Forschungsinstituten tätigen Interessentenkreis über abgeschlossene Forschungsarbeiten, Themenschwerpunkte und Dissertationen informieren. Studenten soll die Möglichkeit der Wissensvertiefung gegeben werden.

Table of contents

List of symbols

Symbol	Meaning	Value	SI-Unit
Latin Letters			
B	Quality factor of the Fermi-Dirac distribution		
c	Speed of light (vacuum)	2.998×10^8	m/s
d	Thickness of the disk		
d_{opt}	Optimum disk thickness		
d_p	Diameter of the pump spot on the disk		
d_m	Diameter of the mode on the disk		
E_{min}	Threshold density		
E_p	Pump power density		
E_{sat}	Saturation density		
$E_{t,eff}$	Effective pump power density		
f	Focal length		
$f_{B,trans}$	Bleaching factor		
h	Planck constant	6.626×10^{-34}	Js
k_B	Boltzmann constant	1.38157×10^{-23}	J/K
K_{th-opt}	Thermo-optical constant		
L_{int}	Internal losses of the disk		
m	Order number of the Gaussian distribution		
M^2	Beam quality factor		
M_r	Number of laser radiation passes through the disk		
M_p	Number of pump beam passes through the disk		
n	Refractive index		
N_{dop}	Doping concentration		
P_{out}	Laser output power		
r_{pump}	Radius of the pump spot on the disk		
R_T	Thermal shock resistance		
T	Temperature		
$T_{OC,opt}$	Optimum output coupler transmission		
Z_l	Partition function of the lower laser level		

Symbol	Meaning	Value	SI-Unit
Z_u	Partition function of the upper laser level		

Greek Letters

α_{th}	Thermal expansion		
λ_p	Pump wavelength		
λ_{em}	Emission wavelength		
σ_{abs}	Effective absorption cross section		
σ_{em}	Effective emission cross section		
τ_{fl}	Fluorescence lifetime		

Abbreviations

AR	*Anti-Reflection*
CVD	*Chemical Vapor Deposition*
cw	*continuous wave*
FEM	*Finite Element Method*
FOM	*Figure Of Merit*
GWS	*Grating Waveguide Structure*
HEM	*Heat Exchange Method*
HR	*High-Reflection*
OPD	*Optical Phase Distortion*
R	*Reflectivity*
ROC	*Radius Of Curvature*
TSSG	*Top Seeded Solution Growth*
VBG	*Volume Bragg Grating*
Yb:LuAG	*Ytterbium-doped Lutetium-Aluminum-Garnet*
Yb:Lu$_2$O$_3$	*Ytterbium-doped Lutetium-Oxide*
Yb:YAB	*Ytterbium-doped Yttrium-Aluminum-Borate*
Yb:YAG	*Ytterbium-doped Yttrium-Aluminum-Garnet*
ZPL	*Zero Phonon Line*

Publications

Some parts of this thesis are published in the following journal papers and conference proceedings:

Journal Papers (peer-reviewed)

K.S. Wentsch, B. Weichelt, F. Druon, P. Georges, M. Abdou Ahmed and T. Graf, "Yb:CaF$_2$ thin-disk laser," Opt. Express(2014) no.2 p.1524.

B. Weichelt, K.S. Wentsch, A. Voss, A. Gross, V. Wesemann, D. Rytz, M. Abdou Ahmed and T. Graf, "Yb:YAl$_3$(BO$_3$)$_4$ as gain material in thin-disk oscillators: demonstration of 109 W of IR output power," Opt. Express (2013) Vol. 21, Issue 22, p. 25708-25714.

M. Vogel, M. Rumpel, B. Weichelt, A. Voss, M. Häfner, C. Pruss, W. Osten, M. Abdou Ahmed and T. Graf, "Single-layer resonant-waveguide grating for polarization and wavelength selection in Yb:YAG thin-disk lasers," Opt. Express (2012) no.4 p.4024.

B. Weichelt, A. Voss, M. Abdou Ahmed and T. Graf, "Enhanced performance of thin-disk lasers by pumping into the zero-phonon line," Opt. Letters (2012) no.15 p.3045.

S. Ricaud, A. Jaffres, K. Wentsch, A. Suganuma, B. Viana, P. Loiseau, B. Weichelt, M. Abdou Ahmed, A. Voss, Th. Graf, D. Rytz, C. Hönninger, E. Mottay, P. Georges and F. Druon, "Femtosecond Yb:CaGdAlO$_4$ Thin-Disk oscillator," Opt. Letters (2012) no.19 p.3984.

S. Piehler, B. Weichelt, A. Voss, M. Abdou Ahmed and T. Graf, "Power scaling of fundamental-mode thin-disk lasers using intra-cavity deformable mirrors," Opt. Letters (2012) no.24 p.5033-5035.

D. Blazquez-Sanchez, B. Weichelt, A. Austerschulte, A. Voss, T. Graf, A. Killi, H. Eckstein, M. Stumpf, A. L. Matthes and U. D. Zeitner, "Improving the brightness of a multi-kW single thin-disk laser by an aspherical phase-front correction," Opt. Letters (2011) no.6 p.799.

S. Ricaud, A. Jaffres, P. Loiseau, B. Viana, B. Weichelt, M. Abdou Ahmed, A. Voss, Th. Graf, D. Rytz, M. Delaigue, E. Mottay, P. Georges and F. Druon, "Yb:CaGdAlO$_4$ Thin-Disk Laser," Opt. Letters (2011) no.21 p.4134.

K.S. Wentsch, B. Weichelt, L. Zheng, J. Xu, M. Abdou Ahmed and T. Graf, "Continuous-wave Yb doped Sc_2SiO_5 thin-disk laser," Opt. Letters (2011) no.1 p.37-39.

B. Weichelt, K. Wentsch, A. Voss, M. Abdou Ahmed and T. Graf, "A 670 W $Yb:Lu_2O_3$ thin-disk laser," Laser Phys. Letters (2011).

R. Pereira, B. Weichelt, D. Liang, P. Morais, H. Gouveia, M. Abdou-Ahmed, A. Voss and T. Graf, "Efficient pump beam shaping for high-power thin-disk laser systems," Appl. Optics (2010) no.27 p.5157.

Conference Proceedings

S. Piehler, B. Weichelt, A. Voss, M. Abdou Ahmed and T. Graf, "Active mirrors for intra-cavity compensation of the aspherical thermal lens in thin-disk lasers," Proc. of SPIE (2012).

S. Ricaud, A. Jaffres, P. Loiseau, B. Viana, B. Weichelt, M. Abdou Ahmed, A. Voss, T. Graf, D. Rytz, M. Delaigue, E. Mottay, P. Georges and F. Druon, "$Yb:CaGdAlO_4$ thin disk," Proc. of SPIE (2012) p.82350Q.

S. Günster, D. Ristau, B. Weichelt and A. Voss, "Coatings for thin-disk laser systems," Proc. of SPIE (2011) p.81680J.

S. Ricaud, A. Jaffres, K. Wentsch, A. Suganuma, B. Viana, P. Loiseau, B. Weichelt, M. Abdou Ahmed, T. Graf, D. Rytz, C. Hönninger, E. Mottay, P. Georges and F. Druon, "Yb:CALGO thin-disk femtosecond oscillator," European Conference on Lasers and Electro-Optics and XIIIth International Quantum Electronics Conference (2013).

S. Ricaud, A. Jaffres, K. Wentsch, A. Suganuma, B. Viana, P. Loiseau, B. Weichelt, M. Abdou Ahmed, A. Voss, T. Graf, D. Rytz, C. Hönninger, E. Mottay, M. Hanna, P. Georges and F. Druon, "Yb:CALGO thin-disk lasers operating in femtosecond regime," Ultrafast Optics UFOIX, Davos Congress Centre, Switzerland (2013).

S. Piehler, B. Weichelt, A. Voss, M. Abdou Ahmed and T. Graf, "Active Mirrors For kW-Class Fundamental-Mode Thin-Disk Lasers," The European Conference on Lasers and Electro-Optics and the International Quantum Electronics Conference (CLEO/Europe-IQEC), München, Germany (2013).

K.S. Wentsch, B. Weichelt, F. Druon, M. Abdou Ahmed and T. Graf, "An $Yb:CaF_2$ thin-disk laser," The European Conference on Lasers and Electro-Optics and the International Quantum Electronics Conference (CLEO/Europe-IQEC), München, Germany (2013).

B. Weichelt, K.S. Wentsch, A. Voss, A. Gross, V. Wesemann, D. Rytz, M. Abdou Ahmed and T. Graf, "109 W Yb:YAl3(BO3)4 thin-disk oscillator," (CLEO/Europe-IQEC), München, Germany (2013).

S. Piehler, B. Weichelt, A. Voss, M. Abdou Ahmed and T. Graf, "Recent advances in high-power fundamental mode thin-disk lasers using intra-cavity deformable mirrors," 9th International Workshop on Adaptive Optics for Industry and Medicine (AOIM 2013), Stellenbosch, South Africa (2013).

H. Nakao, A. Shirakawa, K. Ueda, H. Yagi, T. Yanagitani, B. Weichelt, K.S. Wentsch, M. Abdou Ahmed and T. Graf, "Yb3+-Doped $Lu_3Al_5O_{12}$ Ceramic Thin-Disk Laser," OSA (Hrsg.): 10th Conference on Lasers and Electro-Optics Pacific Rim (CLEO-PR). Kyoto, Japan (2013).

F. Druon, S. Ricaud, A. Jaffres, K.S. Wentsch, A. Suganuma, B. Viana, P. Loiseau, B. Weichelt, M. Abdou Ahmed, T. Graf, D. Rytz, C. Hönninger, E. Mottay and P. Georges, "High power cw and fs Yb:CALGO thin-disk laser using diamond heat spreader," Advanced Solid-state Lasers (ASSL 2013), Paris, France (2013).

S. Piehler, B. Weichelt, A. Voss, M. Abdou Ahmed and T. Graf, "Active mirrors for intra-cavity compensation of the aspherical thermal lens in thin-disk lasers," SPIE Lase 2012, Conference 8239 : High Power Laser Materials Processing: Lasers, Beam Delivery, Diagnostics, and Applications, San Francisco, USA (2012).

K.S. Wentsch, L. Zheng, J. Xu, B. Weichelt, M. Abdou Ahmed and T. Graf, "Ytterbium doped Sc_2SiO_5 in thin-disk laser configuration," Photonics Europe, Bruxelles, Belgium (2012).

M. Abdou Ahmed, M. Rumpel, B. Weichelt, A. Voss and T. Graf, "Sub-wavelength micro-structured planar waveguides for laser beam shaping," Stuttgart Laser Technology Forum (SLT'12),Stuttgart, Germany (2012).

F. Druon, B. Viana, S. Ricaud, D. Papadopoulos, A. Jaffres, A. Suganuma, P. Loiseau, B. Weichelt, K. S. Wentsch, M. Abdou Ahmed, A. Voss, T. Graf, C. Hönninger, E. Mottay and P. Georges, "Yb:CALGO for high-power femtosecond laser applications," Stuttgart Laser Technology Forum (SLT'12),Stuttgart, Germany (2012).

B. Weichelt, A. Voss, M. Abdou Ahmed and T. Graf, "Fundamental mode thin-disk lasers," Stuttgart Laser Technology Forum (SLT'12), Stuttgart, Germany (2012).

S. Ricaud, A. Jaffres, P. Loiseau, B. Viana, B. Weichelt, M. Abdou Ahmed, A. Voss, T. Graf, D. Rytz, M. Delaigue, E. Mottay, P. Georges and F. Druon, "Yb:CaGdAlO$_4$ thin

disk laser," SPIE (Hrsg.): Photonics West, LASE (Photonics West LASE Conference on Solid State Lasers XXI: Technology and Devices), San Francisco, USA (2012).

S. Ricaud, A. Jaffres, K. Wentsch, A. Suganuma, B. Viana, P. Loiseau, B. Weichelt, M. Abdou Ahmed, A. Voss, Th. Graf, D. Rytz, C. Hönninger, E. Mottay, P. Georges and F. Druon, "CW and femtosecond Yb:CALGO thin disk oscillator," Europhoton 2012, Stockholm, Sweden (2012).

S. Ricaud, B. Weichelt, P. Goldner, B. Viana, M. Abdou-Ahmed, A. Voss, T. Graf, D. Ritz, E. Mottay, P. Georges and F. Druon, "Yb:CaGdAlO$_4$ thin disk laser in continuous-wave,"CLEO Munich 2011, München, (2011).

B. Weichelt, D. Blazquez-Sanchez, A. Voss, A. Austerschulte, T. Graf and A. Killi, "Improving the brightness of a multi-kW thin disk laser with a single disk by an aspherical phase-front correction," SPIE Europe 2010, Bruxelles, Belgium (2010).

T. Graf, A. Voss, B. Weichelt, D. Blazquez-Sanchez, M. Vogel, A. Austerschulte, M. Abdou Ahmed, A. Popp, A. Killi, S. Unger, J. Kirchof and H. Bartelt, "Micro-Optics Applications in High-Power Laser Systems," EOS Annual Meeting 2010, Paris, France (2010).

Kurzfassung

Diodengepumpte Festkörperlasersysteme haben sich im letzten Jahrzehnt in der Materialbearbeitung immer weiter durchgesetzt, da sie die Vorteile einer faserführbaren Strahlung der Wellenlänge im 1 μm Bereich sowie eine gute Fokussierbarkeit und einer hohen Ausgangsleistung bei hohem Wirkungsgrad miteinander vereinen. Inzwischen sind auch die Anforderungen an industrielle Lasersysteme wie hohe Zuverlässigkeit und eine lange Lebensdauer für diese Systeme umgesetzt worden, so dass deren Einsatz von der Industrie akzeptiert und für bestimmte Anwendungen sogar favorisiert wird. Das Festkörperlaserkonzept des Scheibenlasers hat dabei im Vergleich zu den Faserlasern seine Stärken in einer niedrigeren Sensitivität hinsichtlich Rückreflexen vom zu bearbeitenden Werkstück und einem konzeptbedingten geringeren Auftreten von nichtlinearen Effekten im Lasermedium. Ausgehend von einem am IFSW und DLR erfundenen vielversprechenden Grundkonzept wurde der Scheibenlaser durch Firmen wie z.B. Trumpf und Jenoptik industrietauglich gemacht, indem innovative Entwicklungen im Hinblick auf wichtige Parameter wie Stabilität und Kompaktheit realisiert werden konnten.

Die vorliegende Arbeit befasst sich mit dem Kernthema der Verbesserung der Strahlqualität von Scheibenlasern mit optischen Ausgangsleistungen im Kilowattbereich. Dabei wurden Beugungsmaßzahlen im Bereich von $M^2 \approx 8$ für den multi-Kilowattbereich und das Erzielen von Grundmodebetrieb bis zu einer optischen Ausgangsleistung von circa einem Kilowatt angestrebt. Die erstgenannte Strahlqualitäts-Leistungskombination ist insbesondere zum Schneiden von noch feineren Strukturen und mit höheren Distanzen von Blechen interessant, wobei die an zweiter Stelle genannte Kombination unter Anderem auf den Einsatz in Ultrakurzpulslasersystem abzielt. Um die im Scheibenlaserresonator erzeugte Strahlqualität optimieren zu können, ist es von essentieller Bedeutung, eine möglichst genaue Information über die Deformation des Scheibenlaserkristalls im Allgemeinen und die Ausprägung der asphärischen Deformation (im 50-200 Nanometerbereich) im Speziellen zu erhalten. Aus diesem Grund wurde ein Interferometeraufbau entwickelt, der auf die bestehenden Anforderungen des Betriebes von Scheibenlasern bei Ausgangsleistungen bis zu mehreren Kilowatt zugeschnitten war und eine präzise Echtzeitmessung der Deformation des Scheibenlaserkristalls ermöglichte. Die aus diesen Messungen erhaltenen Ergebnisse konnten daher direkt zur Optimierung der Strahlqualität des jeweiligen Scheibenlasersystems herangezogen werden.

Für die experimentellen Untersuchungen wurden die laseraktiven Materialien Yb:YAG, Yb:LuAG, Yb:Lu$_2$O$_3$ und Yb:YAB verwendet. Yb:YAG und Yb:LuAG sind von der Qualität der Laserscheiben her industriell einsetzbar, wohingegen sich die laseraktiven Materialien Yb:Lu$_2$O$_3$ und Yb:YAB noch im Entwicklungsstadium befinden, aber aufgrund ihrer Eigenschaften neben einem effizienten cw-Betrieb insbesondere für den Einsatz in Ultrakurzpulsscheibenlasern prädestiniert sind. Für die vier laseraktiven Materialien wurden neben den spektralen Eigenschaften insbesondere die mechanischen Eigenschaften für den Einsatz im Scheibenlaser analysiert. Als innovatives Pumpkonzept wurde das Zero-Phonon-Line Pumpen für Pumpleistungen bis in den Kilowattbereich und mit einer spektralen Breite von weniger als einem Nanometer experimentell umgesetzt. Dies ermöglichte es, bei Yb:YAG, Yb:LuAG und Yb:Lu$_2$O$_3$ die Wärmeerzeugung im Mittel um ca. 30% zu reduzieren, was durch die längeren Pumpwellenlängen von 969 nm (Yb:YAG, Yb:LuAG) und 976 nm (Yb:Lu$_2$O$_3$) im Vergleich zum konventionellen Pumpen im Wellenlängenbereich von 940-950 nm bedingt ist. Die dadurch bedeutend geringeren thermisch induzierten Verformungen, insbesondere der asphärischen Verformung, des Scheibenlaserkristalls erlaubt neben einer Steigerung der optischen Effizienz die Beugungsverluste des Scheibenlaserresonators so stark zu reduzieren, dass Grundmodebetrieb bis in den Kilowattbereich möglich ist. Unter Verwendung dieses Pumpkonzeptes wurde ein Yb:LuAG Scheibenlaser mit einer optischen Ausgangsleistung von 742 W und nahezu beugungsbegrenzter Strahlqualität (M$^2 \approx 1.5$) bei einer gleichzeitig hohen optischen Effizienz von 58.5% demonstriert. Im Multimodebetrieb (M$^2 \approx 15$) konnte unter Verwendung von Yb:YAG ein Scheibenlaser mit einer optischen Effizienz von 72% realisiert werden. Mit dem Zero-Phonon-Line Pumpen von Yb:Lu$_2$O$_3$ konnte mit einer optischen Ausgangsleistung von 670 W die bis dato höchste mit diesem laseraktiven Material realisierte Ausgangsleistung gezeigt werden. Neben dem hohen Potential von Yb:Lu$_2$O$_3$ für den Einsatz im Scheibenlaser wurden jedoch auch dessen (momentane) Limitierungen in der Kristallqualität dargestellt, was für eine Erzeugung von beugungsbegrenzter Strahlung bis in den Kilowattbereich hinderlich ist.

Da ab einem bestimmten Ausgangsleistungslevel für die Erzeugung guter Strahlqualität immer eine Kompensation der asphärischen Deformation des Scheibenlaserkristalls notwendig wird, wurden experimentelle Untersuchungen zur Verwendung statischer Asphärenspiegeln durchgeführt. Diese wurden so konzipiert, dass sie bis zu mehreren Kilowatt Ausgangsleistung des Scheibenlasers eingesetzt werden konnten. Unter Verwendung eines Asphärenspiegels im Resonator, wurde ein Yb:YAG Scheibenlaser (eine Scheibe) mit einer optischen Ausgangsleistung von 3.4 kW und einem Strahlparameterprodukt von 2.4 mm x mrad (M$^2 \approx 8$) realisiert. Auf diesen Experimenten konnte am IFSW bei der weiteren Entwicklung von aktiv regulierten, asphärischen Spiegeln für

den Einsatz im Scheibenlaser aufgebaut werden.

Die Forschung an neuartigen Lasermaterialien zur Verwendung im Scheibenlaser konzentriert sich neben den Materialien die vorteilhafte thermische Eigenschaften besitzen vor allem auf jene, die insbesondere zur Erzeugung von ultrakurzen Pulsen geeignet sind. Ein laseraktives Material, das beides bietet, ist Yb:YAl$_3$(BO$_3$)$_4$, mit welchem zum ersten Mal ein Betrieb im Scheibenlaser gezeigt werden konnte. Im cw-Multimodebetrieb wurden dabei optische Ausgangsleistungen bis zu 109 W mit einer optischen Effizienz von 50.2% realisiert. Im niedrigeren Leistungsbereich von ≈ 20 W wurde mit Yb:YAB sogar eine optische Effizienz von über 60% erzielt. Durch Verwendung eines resonanten Beugungsgitters wurde für den Yb:YAB Scheibenlaser eine spektrale Durchstimmbarkeit im Bereich von 1001 bis 1053 nm ermittelt (maximale optische Ausgangsleistung von 36 W bei 1040 nm). Aufgrund dieser großen spektrale Breite ist Yb:YAB für zukünftige Experimente in Ultrakurzpulsscheibenlasern interessant.

Extended abstract

In the last decade, diode-pumped solid-state laser systems became more and more established and are nowadays widely used for material processing in the automotive, solar and microelectronic industry. They can produce the desired combination of fiber guidability, highly focused beams, high power and a high optical efficiency. Meanwhile, also the demands of industrial laser systems like a long lifetime and a low failure rate got realized so that the use of diode-pumped solid-state lasers is widely accepted by the companies and for certain applications even favored. Comparing the two solid state laser concepts disk and fiber, the thin-disk laser has its strength in a lower sensitivity to back reflections from the work piece and in a design-based lower occurrence of nonlinear effects inside the laser-active medium which is advantageous for pulsed laser systems. Starting from the invention of a promising new laser concept at the IFSW and DLR, the thin-disk laser emerged to a robust industrial system since innovative developments with regard to important aspects like stability and compactness were realized thanks to several companies such as for example Trumpf and Jenoptik.

The core topic of the present thesis is the improvement of the brightness of thin-disk lasers at a targeted output power of one kilowatt and beyond. For an output power of several kilowatts the intention was to approach a beam quality factor of $M^2 \approx 8$, whereas for the thin-disk lasers with an optical output power up to one kilowatt a near diffraction limited beam quality was aimed. Multi-kilowatt beams with high brightness offer advantages for fast and precise material processing applications such as remote cutting, where the beam must propagate over large distances. In the second case a thin-disk laser generating ultrashort pulses can be developed in a further stage. In order to improve the beam quality of a thin-disk laser it is essential to know very precisely how the thin disk deforms in laser operation whereby special attention has to be paid on the aspherical part of this deformation which can be in the order of a few tens of Nanometers. For this reason, an interferometric setup was developed which was optimized to measure the disk deformation during laser operation with high precision. Thus, interferometric measurements in real-time could be carried out when operating the different thin-disk lasers up to an optical output power of approximately four kilowatt. The obtained results were directly used to optimize the beam quality of each thin-disk laser individually.

For the experimental investigations the laser-active materials Yb:YAG, Yb:LuAG,

Yb:Lu$_2$O$_3$ and Yb:YAB have been used. Thin-disk laser crystals out of Yb:YAG and Yb:LuAG are available in a quality which is sufficient to implement them in industrial laser systems. On the contrary, the quality of the crystals has still to be improved to achieve high quality laser disks for the laser-active materials Yb:Lu$_2$O$_3$ and Yb:YAB. However, beside a high optical efficiency, these materials provide properties which are favorable for the generation of ultrashort pulses. Beside a comprehensive analysis of the spectral properties of the four laser-active materials, close attention was paid on the mechanical ones particularly with regard to the manufacturing of laser disks.

The innovative concept of Zero-Phonon-Line (ZPL) pumping was experimentally implemented to allow for pump powers of up to ≈ 2 kW at a narrow wavelength peak with a width of less than one Nanometer. The pumping of the laser-active materials Yb:YAG, Yb:LuAG and Yb:Lu$_2$O$_3$ at the ZPL-line allows to reduce the heat generation in the disk by approximately 30% which is due to the longer pump wavelength of 969 nm (Yb:YAG, Yb:LuAG) and 976 nm (Yb:Lu$_2$O$_3$) compared to the conventional pumping in the wavelength range of 940-950 nm. For this reason, the thermally induced deformations of the thin-disk crystal are strongly reduced and the Stokes efficiency is increased. Especially the reduction of the aspherical phase distortions which result in significantly lower diffraction losses of the fundamental mode is essential for the scaling of fundamental-mode thin-disk lasers to the kilowatt output power level. Using the ZPL-pump concept, a Yb:LuAG thin-disk laser with an optical output power of 742 W and nearly diffraction limited beam quality (M$^2 \approx 1.5$) together with an unprecedented high optical efficiency of 58.5% was demonstrated. For an Yb:YAG laser in multimode operation (M$^2 \approx 15$), this pumping principle allowed to achieve a maximum optical efficiency of 72%. Kilowatt-level ZPL-pumping of an Yb:Lu$_2$O$_3$ thin-disk laser resulted in 670 W of output power which is the highest optical output power reported to date for this laser-active material. Despite the discussion of the high potential of the implementation of Yb:Lu$_2$O$_3$ for the use in thin-disk lasers, also (current) limitations especially regarding the crystal quality are adressed in this thesis. The insufficient crystal quality currently limits the generation of fundamental-mode radiation at high output powers with this laser-active material.

Despite of the advantages of ZPL-pumping, at a certain output power level a compensation of the aspherical phase front deformation induced by the thermally deformed thin-disk crystal will always be necessary. Therefore, experimental investigations with static aspherical mirrors have been carried out. These mirrors have been designed in such a way that they can be used in thin-disk lasers operating at several kilowatts of output power. Using an aspherical mirror in the resonator, an Yb:YAG thin-disk laser generating an output power of 3.4 kW and a beam parameter product of 2.4 mm x mrad (M$^2 \approx 8$) from one disk was demonstrated. Based on the gained knowledge from the in-

vestigations with the static aspherical mirrors, actively-controlled mirror concepts were developed later on at the IFSW.

Current research focuses on novel laser-active materials with beneficial properties to obtain for e.g. a lower thermal load or to generate ultrashort pulses. An interesting laser-active material which offers both is $Yb:YAl_3(BO_3)_4$. Therefore, the first demonstration of a thin-disk laser using Yb:YAB was carried out. In multimode operation cw-output powers of up to 109 W with an optical efficiency of 50.2% were achieved. At a lower power level of about 20 W this laser-active material showed an even more efficient operation with an optical efficiency of more than 60%. In fundamental-mode operation the extracted output power was 10.4 W with an optical efficiency of 44.5% and a nearly diffraction limited beam ($M^2 = 1.39$). The broad emission bandwidth of the material was confirmed by measuring a continuous wavelength tuning range from 1001 to 1053 nm by using a resonant diffraction grating in the resonator. The maximum output power of 36 W was obtained at a wavelength of 1040 nm. Due to this broad spectral width, Yb:YAB is attractive for the generation of ultrashort pulses. This will be investigated in future experiments at the IFSW.

1   Introduction

1.1   Motivation

Among all solid-state lasers, the thin-disk laser technology has experienced a very fast growth within the last decade and is today one of the most established laser technologies resulting in the utilization of thin-disk laser systems in many industrial fields such as automotive, solar and microelectronics. This was enabled by the equivalently fast (or even faster) development of laser diodes with high efficiency and high output power, emitting in the wavelength range of 9xx nm which is required for the pumping of Yb-doped laser-active materials such as Yb:YAG. Yb:YAG is the most established laser-active material for high-power thin-disk lasers emitting at a wavelength of about 1 micron which allows to guide the emitted radiation in optical fibers over very long distances (up to the order of 100 m). Furthermore, the thin-disk concept exhibits a reduced sensitivity to back reflections which may occur during material processing. In addition to these advantages, there is an easily reachable good beam quality of thin-disk lasers (typical $M^2 < 24$) even for an output power at the multi-kilowatt level. The good beam quality is possible thanks to the approximately one dimensional cooling and the high ratio of cooled surface to pumped volume of the laser disk.

Further improvement of the brightness of thin-disk lasers allows to increase the working distances during material processing, to enable welding and cutting of finer structures and to operate with higher cutting speeds. Moreover, the fundamental-mode operation is an essential prerequisite for the operation of ultrafast laser systems. The potential of these laser systems which emit radiation with pulse durations of a few hundred femtoseconds just started to be explored in various application fields. In combination with high average powers, various new applications for material processing are imaginable. The strength and unique properties of ultrafast lasers with high peak intensities is the material ablation with almost no heat exposure of the surrounding area. This allows a very precise processing of materials like e.g. metals, ceramics, carbon fiber reinforced plastics, human tissues etc. and thus opens the way to entirely new applications.

1.2   Objectives and approaches followed

In the present thesis the emphasis is on the development of thin-disk lasers with high
brightness at the kilowatt or even multi-kilowatt (4-5 kW) output power level with the
laser-active materials Yb:YAG and Yb:LuAG. To realize this, the thermal behavior espe-
cially of the thin disk and also of the complete pump and resonator cavity has been
analyzed in detail. For the highest obtainable brightness, i.e. the fundamental-mode ope-
ration of the laser, the evolution towards the one-kilowatt level (Yb:YAG and Yb:LuAG)
is shown. The future objective of the ongoing research following the experimental in-
vestigations presented in this thesis is the development of ultrafast oscillators at this
kilowatt power level. To achieve this, different Yb- doped laser-active materials have to
be evaluated regarding their thermo-optical and spectroscopic properties and also with
regard to their mechanical and chemical stability. This research plays a major role in
numerous scientific groups and companies worldwide. Our laser development group at
the IFSW focuses mainly on Yb doped laser materials to be used in disk lasers due to the
advantages of this concept mentioned previously. Important properties of the Yb-doped
laser materials which have to be analyzed are:

- the crystal structure, melting point and melting behavior
- the absorption and emission cross sections
- the spectral linewidth and shape of the absorption and emission peaks
- the thermal conductivity
- the change of the refractive index with temperature
- the heat expansion
- the thermal shock resistance
- the hardness and the tendency of fracture

This list does not claim completeness. However, it shall illustrate how comprehensive a
laser-active material has to be evaluated in order to be able to conclude on its suitability
for high-power lasers. An overview of material properties of Yb-doped laser-active ma-
terials in general and for the thin-disk laser configuration in particular can be found in
the references [1], [2], [3] and [4]. For this thesis the two potential materials Yb:YAG
and Yb:LuAG were investigated for high-power, high-brightness thin-disk lasers. In ad-
dition, Yb:Lu$_2$O$_3$ has been analyzed, which is a promising material to reach the kilowatt
output power level at shorter pulse durations compared to Yb:YAG or Yb:LuAG. Nonet-
heless, Yb:Lu$_2$O$_3$ has a very high melting temperature resulting in a complicated crystal
growth, hence close attention is paid to the quality of the supplied thin-disk crystals.
Furthermore, one interesting candidate from the novel laser materials is Yb:YAB which
will be introduced in this work using it for the first time in thin-disk configuration. The

material quality of Yb:YAB is currently a crucial issue as well and has been evaluated bearing in mind the objective of laser operation with an output power of a few kilowatts.

The present thesis is divided into nine chapters, where the 2nd chapter describes the state of the art of the main solid-state laser types and therefore sets the starting point for the research presented here.

In chapter 3, the basic principle of the thin-disk laser is briefly explained. After that, the main spectral and mechanical properties of the four laser-active materials investigated in this thesis are discussed and the important advantages and limitations of each material are pointed out. This chapter concludes with the requirements on the laser-active materials with regard to the manufacturing and use as thin-disk crystals.

Chapter 4 emphasizes on the thermal effects inside and in front of a thin-disk crystal, which currently limit the brightness of thin-disk lasers at kilowatt output powers. Simulations and experimental analysis of these effects are presented and the possible causes are discussed. The investigations undertaken show the influence of the thermal load on the properties of the laser-active material itself and also address the contributions from the contacting method, the heat sink design and the distribution of the pump power. Another important factor is the ambient atmosphere especially in the pump cavity whose influence on the achievable brightness is also described.

The 5th chapter presents an interferometric setup which allows to precisely determine the optical phase distortions caused in front of and inside thin-disk laser crystals. The setup and the measurement method is explained and completed with an evaluation of the achievable accuracy of the interferometer.

Chapter 6 discusses a key concept to minimize the thermal load in thin-disk lasers. This concept causes a general reduction of the heat generated in the thin-disk crystal itself and is called Zero-Phonon-Line (ZPL) Pumping. The experimental realization of high-power, high-brightness thin-disk lasers with the laser-active materials Yb:YAG, Yb:LuAG and $Yb:Lu_2O_3$ by using this pumping approach is presented and explained in this chapter, which is the core part of this thesis. The necessary spectral narrowing and wavelength stabilization of the radiation of the pump diode stack for ZPL-pumping is described. The experimental investigations and performances achieved by using this pump concept is shown for both, multi-mode and near diffraction-limited continuous-wave operation. An analysis of the thermal load and the resulting deformation of the thin-disk crystals are also included in this section.

Reducing the thermal load is of course beneficial for the thin-disk laser operation in general, but the maximum achievable output power and consequently the thermally in-

duced aberrations only shift the limit where unstable laser operation takes place. In time, an element which compensates for these aberrations has to be inserted in the laser cavity. One industrial approach is the compensation with a static aspherical mirror; the demonstration of this concept with multi-kilowatt output power is reported in chapter 7. The further development from a static aspherical mirror to an actively-controlled aspherical mirror was pushed forward intensively so that as final result fundamental-mode operation at an output power close to the kilowatt level with an actively-controlled aspherical mirror could be demonstrated. This result is briefly described at the end of chapter 7.

Current research focuses on different methods to carry out the compensation of thermal effects in thin-disk laser resonators and on novel laser-active materials with beneficial properties to obtain e.g. a lower thermal load. The objective of the use of novel laser-active materials in thin-disk configuration is often to generate ultrashort pulses. In chapter 8, different interesting laser-active materials used for this purpose are briefly summarized and for one interesting material; Yb:YAB, a detailed study is presented. Yb:YAB was investigated for the first time under the aspect to use it in thin-disk lasers. The experimental results in CW-operation up to an output power level of 109 W and an outlook to further power scaling using this laser-active material are also presented.

Chapter 9 contains the summary and a general outlook for the research described in this thesis. Two final questions will be addressed briefly. What are the scaling prospects of CW fundamental-mode thin-disk lasers? And is an ultrafast thin-disk oscillator at the kilowatt average power level feasible?

2 Overview of high-power solid-state laser systems

This chapter gives a short overview of the current state of the art for high-power solid-state laser systems (at the start of the research activities reported in this document) and their ability to achieve high brightness. Here, the emphasis will be on thin-disk lasers, since the enhancement of the brightness of this laser type is the topic of the research presented here.

Nowadays, high-power solid-state laser systems (excluding semiconductor lasers) exceeding one kilowatt of output power can be divided into four different geometrical concepts, whereby each laser concept exhibits advantages and disadvantages. These types of lasers are:

- rod lasers
- fiber lasers
- slab lasers
- thin-disk lasers

The different concepts are schematically illustrated in figure 2.1:
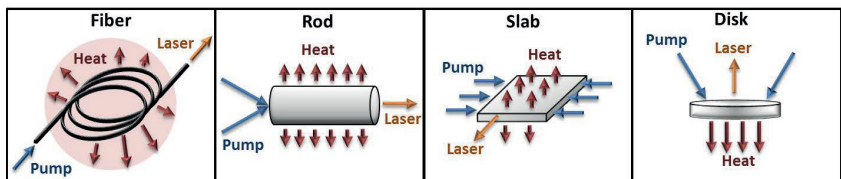
Figure 2.1: Schematic drawings of the different solid-state laser and amplifier concepts. The typical pump configurations are displayed, but also other pump and laser configurations are used in the field.

Among the solid-state lasers, the rod laser was the first laser concept which was invented and scaled to output powers of several kilowatts in a highly multimode operation. Even though rod lasers were widely used by the industry due to their simplicity and

low cost, this laser concept has one major disadvantage: a comparatively strong thermal lens which prevents fundamental-mode operation at the kilowatt output power level. In 2005, Frede et al. [5] reported the highest output power of 213 W in fundamental-mode operation (M^2= 1.15 with an optical efficiency of 23%) for this concept by using a ring oscillator which contained four longitudinally pumped Nd:YAG rods. For the other three laser concepts this power level with near diffraction-limited beam quality is already exceeded by using only one laser-active element inside the laser resonator.

In order to present the state of the art for fiber lasers in high-power cw operation, a distinction between fiber lasers in terms of oscillators and fiber amplifier systems has to be made. In fact, the availability of high gain in laser-active fibers simplifies the use in master oscillator power amplifier (MOPA) configurations. The utilization of one fiber amplifier stage makes it possible to achieve 10 kW of output power seeded by a 1 kW fiber laser oscillator. This optical scheme is e.g. used by the leading company of fiber laser systems, IPG Photonics [6]. The typical laser-active materials in fiber laser systems are Yb doped silica fibers which offer a broad gain bandwidth for wavelengths from 975 nm to 1180 nm. As a result, they can be pumped not only with high-power diode lasers at the wavelength region of 9xx nm but also in a tandem pumping configuration where one fiber laser is pumping the other at a wavelength of 1050 nm for example. The tandem-pumping method which is an in-band pumping with high brightness has also a second advantage: a very low quantum defect of less than 5% leading to high optical efficiency and very low thermal load. Together with the development of the cladding pumping, this constitutes the two important factors which resulted in an extraordinary power scaling capability of fiber laser systems with near diffraction-limited beam quality. As shown by Popp et al. [7], the high-brightness pump beam (M^2< 16) for the tandem pumping of fibers can also be provided by a thin-disk laser instead of a fiber laser. In this configuration, a very compact "brightness-conversion" fiber laser unit close to the work piece e.g. on a robot arm could be realized if a thin-disk laser was already used previously for material processing purposes. The most crucial issues of fiber lasers which are still under investigation are nonlinear effects like stimulated Raman and Brillouin scattering and the sensitivity to back reflections. An overview of the current status of fiber lasers in continuous-wave as well as in the different pulsed operation modes can be found in [8].

Slab lasers can be pumped in two configurations, either through the top and bottom of the slab or from the edges (longitudinal pumping). The edge-pumped configuration is typically applied when pumped by diode lasers. Here, the wave-guiding effect in the thin slab can be used but is not mandatory. The advantage of the slab geometry in comparison to the thin-disk is the higher gain which is achieved by the length of several tens of millimeters of the slab. The thickness of the slab is typically in the order of 1 mm,

which enables efficient heat extraction and a homogeneous cylindrical thermal lens [9]. The asymmetry of the gain medium makes it more difficult to obtain diffraction-limited beam quality in both directions. The scaling of the output power with the slab approach is performed by an increase of the length and/or width of the laser-active medium or the pump line, respectively. For the first realization of a kW-level, sub-picosecond slab laser, an Yb:KGW oscillator emitting femtosecond pulses at a repetition rate of 20 MHz in combination with two Yb:YAG slab-amplifier-stages were used [10]. The 2nd amplifier stage generated an average output power of 1.1 kW corresponding to a peak power of 80 MW. A pulse-width of 615 fs could be obtained in this laser setup. The M^2 factor was measured to be less than 3 in both directions. As can be seen from the referenced publications, the slab configuration has its strength in the area of short pulse amplification and is usually not used as a CW high-power laser source.

In the field of thin-disk laser development, the kilowatt output power level in multi-mode continuous-wave operation was already demonstrated at the IFSW in 2000 by Stewen et al [11]. The step from the laboratory setup to an industrial high-power laser system was realized soon afterwards so that thin-disk laser systems with 16 kW of output power using four disks are commercially available today. For the industrial success of the thin-disk laser the company TRUMPF Laser played a key role. So far, the highest optical output power from one thin-disk crystal which was obtained by the TRUMPF thin-disk development group in 2012 [12] is 10 kW.

In the domain of fundamental-mode thin-disk lasers, the following two publications set the benchmark at the beginning of this work. Pumping a single disk at the usual wavelength of 940 nm, Killi et al. demonstrated a fundamental-mode ($M^2 < 1.05$) output power of about 500 W from an Yb:YAG thin-disk laser with an optical efficiency of 51% [13]. However, no information about the resonator set-up and the measurement method for the beam quality factor M^2 was given. Mende et al obtained almost the same maximum output power [14] whereas in this case the fundamental-mode operation ($M^2 = 1.55$) was limited to two narrow output power ranges with a comparatively moderate optical efficiency of 36%. The further reduction of the thermal load of the thin-disk crystal is seen as a key factor for further power scaling in fundamental-mode operation and the different possibilities will be described and evaluated in this thesis.

In chapter 9 the most recent publications will be discussed to conclude and describe the further direction of this research topic and an outlook to future research will be given.

3 Basics of the thin-disk laser technology

In the previous chapter, the state of the art for high-power laser systems was illustrated to set the starting point for the present work. The current chapter provides essential information on the basic principle of thin-disk lasers and the laser-active materials which were analyzed for this thesis. The analysis was done with the objective to realize a high-power continuous-wave thin-disk laser with high brightness and as final goal even diffraction-limited beam quality in combination with kilowatt output power. This research will be continued to demonstrate a kilowatt fundamental-mode thin-disk laser capable of generating femtosecond pulses. This will require future work, however, but the goal is already considered in the investigations regarding suitable laser-active materials presented here. The sections on laser-active materials include a selection of important spectral and thermal parameters with regard to the objectives and also the evaluation of the main mechanical parameters considering the manufacturing capability of thin laser disks. So far, few researchers have addressed the problem of thin-disk manufacturing. To evaluate the suitability for the use in high-power lasers, often the theoretical crystal parameters rather than the experimentally investigated crystals were considered. For this reason, this chapter pays particular attention to the challenges which occur in the growth of large-sized crystals (section 3.3.1), the polishing of disks (section 3.3.2) at the micrometer scale and their coating requirements (section 3.3.3) to obtain the suitability for the operation at output powers at the kilowatt level. The high demands on the laser-active materials have, furthermore, to be seen in the context of the untypical high aspect ratios of thin-disk crystals.

3.1 Basic principle of the thin-disk laser

Basic idea and key point of this concept is a laser disk with a thickness in the range of 100-300 μm and a typical diameter of 10-15 mm which is directly mounted on a heat sink [15], [16]. The heat sink itself is in contact with the cooling fluid (e.g. water, liquid nitrogen etc.). The thin-disk crystal can be pumped with high intensities and still be cooled very homogeneously and efficiently due to the high ratio of cooled surface to pumped volume. The heat flow occurs almost in one dimension i.e. in the axis parallel to the laser beam. This reduces the thermally induced aberrations in the thin disk in

comparison to transversally cooled rod- and slab-type crystal geometries by orders of magnitude. Efficient heat removal at the back side of the crystal is realized by combining a heat sink material with high heat conductivity and jet impingement cooling [16], [11], [17]. To achieve an appropriate absorption length for the pump radiation in the thin crystals, different multipass pump cavity configurations can be used to realize e.g. up to 32 pump beam passes [18] or with a slightly different scheme up to 44 pump beam passes through the disk [11]. These two concepts are used industrially but they do not set the limit for the maximum realizable number of pump beam passes with regard to the optical design possibilities. An established layout for the pump cavity is the repeated imaging of pump radiation emerging from a fiber or a homogenizing rod onto the disk using a collimation lens and multiple reflections from a parabolic mirror. The pump optics unit is completed by a pair of 180 degree folding mirrors and a rear mirror for an overall double-pass [18]. A diagram showing the thin disk pump beam scheme for 24 passes and a simple I-shaped laser resonator can be seen in figure 3.1. The thin-disk crystal is passed each time in forward and backward direction due to the high-reflective coating on its backside so that 24 single passes corresponding to 12 double passes through the disk are obtained for the pump radiation.
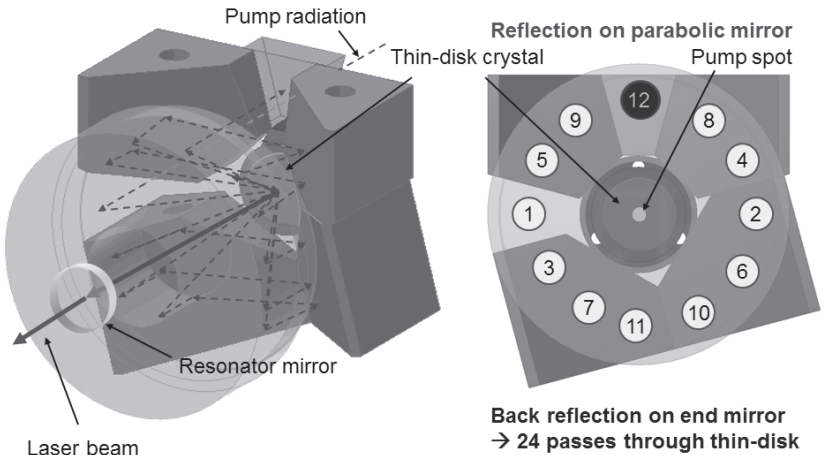

Figure 3.1: Thin-disk pump and laser principle

As mentioned above, a fiber-coupled pump diode or, at higher powers, a homogenizing rod is used for the delivery of the pump radiation. Thus, it guarantees a homogeneous pump power distribution and correspondingly a homogeneous temperature profile on

the disk. The homogeneity of the intensity distribution formed by the pump spots is additionally increased due to a rotation of the pump spot images (which depends on the angle between the two prism pairs) at each double pass. Furthermore, the overlapping multiple pump beam spots applied by the design of the pump optics allow to obtain high pump power densities on the disk. Quasi-three-level laser-active materials can therefore be used efficiently in the thin-disk concept due to a high local pump power density combined with an effective cooling. The thin-disk pumping scheme has two advantages. First, the requirements on the brightness of the pump diodes are comparatively low and second, a geometrical decoupling between pump and laser radiation is obtained. The first point allows the use of pump fibers with larger diameter (assuming a typical numerical aperture of 0.22) in comparison to what is needed for e.g. fiber lasers, which results in a cost advantage. The latter reduces the risk of damaging the pump diodes due to back reflected laser radiation.

3.2   Yb-doped laser-active materials for high-power thin-disk lasers

In thin-disk laser configuration, materials with the laser-active ion Ytterbium can exploit their full potential. The doping with Ytterbium (Yb) is favorable due to the formation of only two manifolds within the structure of most laser hosts which are separated by a large energy difference of about 10.000 cm $^{-1}$ [19]. This constellation avoids the most effective loss transitions like excited state absorption, cross relaxation and upconversion [20]. For pumping, high-power laser diodes with sufficient brightness emitting in the wavelength range between 900 and 980 nm are readily available. Furthermore, the quantum defect is very low in comparison to Neodymium (Nd) doped crystals. Nevertheless, the optimum implementation of Yb in the laser host is, like for all active ions, strongly influenced by the compound of the host material. Factors like the difference of the atomic radii of the dopant to the replaced ion or the splitting of the energy levels are correlated to the thermal conductivity, the possible doping concentration as well as the thermal population of the laser levels. As a consequence, even Yb doped laser hosts face problems due to lattice distortions caused by the implementation of the Yb-ion in the crystalline structure.

For the present work the laser-active materials Yb:YAG, Yb:LuAG, Yb:Lu$_2$O$_3$ and Yb:YAB were selected due to their specific optical and mechanical properties which are described in the following sections. The main properties of these laser-active materials are presented with regard to the use as thin-disk crystals and summarized in one

table for each material. The data available from literature were completed by calculated values for the threshold density E_{min} and the saturation density E_{sat} in laser operation as well as the thermo-optical constant K_{th-opt} and the optimum disk thickness for typical doping concentrations (N_{dop}). The parameter

$$K_{th-opt} = \frac{\partial n}{\partial T} + (n-1) \cdot \alpha_{th} \qquad [21] \qquad (3.1)$$

where n is the refractive index, T is the temperature and α_{th} the thermal expansion, determines the change of the optical path length when multiplied with the thickness of the disk and with its temperature difference between the front and backside. The thermal expansion of a laser-active material can serve as an indicator for the risk of fracture during the coating process. K_{th-opt} is used for a first estimate of the thermal behavior which can be expected in thin-disk laser operation. Together with the optimum disk thickness d_{opt} these are two key values which are typically calculated prior to the manufacturing of a laser-active material as thin-disk crystal. The parameter d_{opt} is calculated by using the following equation [22]

$$d_{opt} = \frac{1}{N_{dop}} \left[\frac{(ln\frac{M_p E_p}{E_{t,eff}})}{M_p \sigma_{abs,eff}(\lambda_p) f_{B,trans}} + \frac{L_{int} T_{OC}}{M_r(\sigma_{em,eff}(\lambda_{em}) + \sigma_{abs,eff}(\lambda_{em}))} \cdot \frac{1+f_{em,p}}{f_{B,trans}} \right],$$
$$(3.2)$$

where N_{dop} is the number density of the active ion, M_p is the number of pump-beam passes through the disk, L_{int} the resonator-internal losses and T_{OC} the output coupling of the resonator. It has to be noted that for the calculation of d_{opt} a constant temperature is assumed, which is typically not the case in real laser systems. The spectral properties of the used laser-active materials are included in the calculation by the parameters: absorption cross section at the pump wavelength $\sigma_{abs,eff}(\lambda_p)$ and the effective absorption and emission cross sections at the laser wavelength $\sigma_{em,eff}(\lambda_{em})$ and $\sigma_{abs,eff}(\lambda_{em})$, respectively. Further parameters are E_p, which is the pump power density and $E_{t,eff}$, which is the effective pump power density to obtain transparency of the laser-active medium, taking into account the superposition of the incident and multiply reflected pump beams in the disk. The parameter $E_{t,eff}$ depends on the effective emission and absorption cross sections at the pump and laser wavelength as well as the fluorescence lifetime and the pump photon energy. $f_{em,p}$ is given by dividing the effective emission cross section $\sigma_{em,eff}(\lambda_p)$ by the effective absorption cross section $\sigma_{abs,eff}(\lambda_p)$ at the pump wavelength of the laser material. To describe the depopulation of the lower laser level when

pumping the laser medium the factor $f_{B,trans}$ is used, commonly referred to as bleaching factor since it defines the threshold when transparency is reached. It is given by [22]

$$f_{B,trans} = 1 - \frac{\sigma_{abs,eff}(\lambda_p) + \sigma_{em,eff}(\lambda_p)}{\sigma_{abs,eff}(\lambda_p)} \cdot \frac{\sigma_{abs,eff}(\lambda_{em})}{\sigma_{em,eff}(\lambda_{em}) + \sigma_{abs,eff}(\lambda_{em})} \qquad (3.3)$$

For quasi-three-level Yb doped laser materials the bleaching or transparency is reached, when the minimum necessary fraction of Yb-ions is pumped to the upper laser level so that this level and the lower laser level have equal populations.

Despite the calculated values for the optimum disk thickness of the investigated laser-active materials in the different resonator configurations presented in the chapters 6,7 and 8, it can be advantageous to define a larger thickness of the disk for the polishing process. This is commonly applied e.g. to minimize the risk of fracture of the disks during polishing or to reduce the stress induced in the disks during the coating process (due to the large difference of the number of layers between an anti-reflective and a high-reflective coating). If the laser-active material has a high thermal expansion a high stress in the disk during the coating process and also during laser operation can occur. In this case, a larger disk thickness than the one theoretically determined can be beneficial as well.

In order to concentrate the determination of d_{opt} to an area of interest, mainly parameters to be used in the experimental investigations presented later on in this thesis have been used for the calculation. For this reason, a few values were considered to be fixed or to be changed solely in a defined range; for example in almost all experiments reported later the number of pump beam passes M_p through the thin disk is 24. This value was set by the available thin-disk pump module. The laser radiation passed either twice ($M_r=$ 2, I-shaped resonator) or four times ($M_r=$ 4,V-shaped resonator) through the thin-disk crystal. Furthermore, mainly doping concentrations which are likely to be grown without the formation of defects inside the crystal structure have been considered. These defects lead to additional non-radiative loss mechanisms (detailed explanations in chapter 3.3.1 and chapter 4.1.1) like e.g. the absorption of laser radiation at impurities [23] and should therefore be avoided. Additionally, the minimal possible aspect ratio with regard to the polishing and coating process was taken into account. As a result, an indicative value of an optimum thin-disk thickness of each laser-active material is given in tables 3.1, 3.2, 3.3 and 3.4 in view of the doping concentration to be used in the experiments. The value of the nominal pump power density which is necessary to calculate d_{opt} was set as well according to what was planned to be used in the experimental investigations.

As a first example, the calculated optimum disk thickness for Yb:YAG with a doping concentration of 11 at.% as a function of the number of pump beam passes is shown in Figure 3.2. The pumping wavelength is 969 nm in this case. For the calculation, a V-shaped resonator with an output coupling of $T_{OC} = 4.5\%$ and internal losses of $L_{int} = 0.15\%$ was defined. The results are plotted for pump power densities between 2.03 kW/cm^2 and 10.2 kW/cm^2. It can be seen that the dependency of the optimum thickness on the pump power density decreases strongly with increasing number of pump beam passes through the thin-disk crystal. For 24 pump beam passes, marked by the vertical line, the theoretical optimum thickness of the disk is between 144 μm (2.03 kW/cm^2) and 209 μm (10.2 kW/cm^2) in the present case. It has to be recalled that the temperature is not considered in this calculation of d_{opt}. To target a thickness of the disk in the order of 140 μm for Yb(11 at.%):YAG is apparently more benefical with regard to the power handling capability during laser operation.
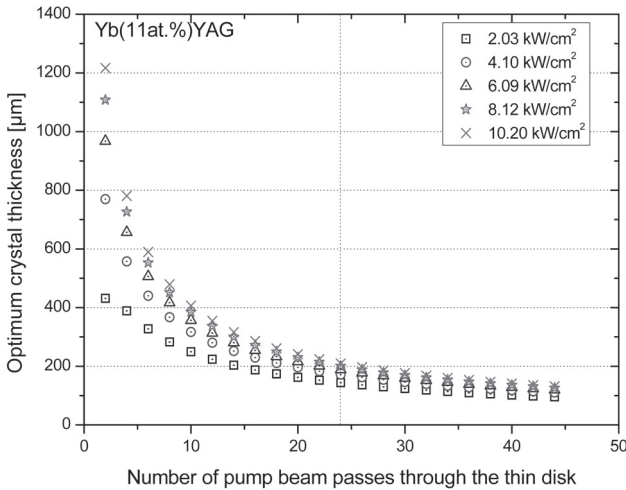
Figure 3.2: Optimum Yb:(11at.%)YAG disk thickness versus number of pump beam passes through the disk for different power densities of the incident pump radiation for a pumping wavelength of 969 nm. Considered was a V-shaped resonator configuration with an output coupling of $T_{OC} = 4.5\%$.

As a second example, the dependency of the optimum disk thickness on the number of pump beam passes for Yb:(11at.%)YAG, Yb:(11at.%)LuAG, Yb:(3at.%)Lu$_2$O$_3$ and Yb:(12at.%)YAB at a defined pump power density of 8.12 kW/cm^2 is illustrated in figure 3.3. This pump power density is chosen close to the currently feasible maximum of

approximately 9 kW/cm^2 for Yb:YAG disks and based on the consideration to generate 1 kW of output power in fundamental-mode operation with an incident pump power of 2 kW on a pump spot diameter of 5.6 mm. Again a V-shaped resonator is assumed with 4.5% of output coupling for all configurations. Even though an ouptut coupling of 4.5% is not the optimum for all four laser-active materials in this configuration, it can be seen that the variation of the optimum disk thickness for 24 pump beam passes and above is not high. At 24 passes of the pump radiation d_{opt} lies between $\approx$130 μm for Yb:(3at.%)Lu$_2$O$_3$ and $\approx$200 μm for Yb:(11at.%)YAG (λ_p = 969 nm).
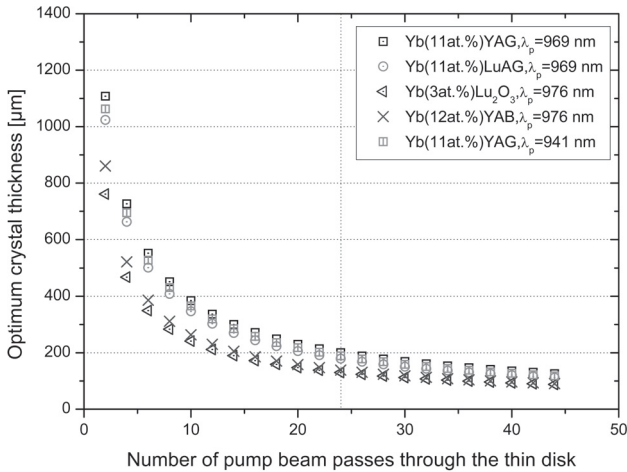

Figure 3.3: Optimum disk thickness as a function of the number of pump beam passes for Yb:(11at.%)YAG, Yb:(11at.%)LuAG, Yb:(3at.%)Lu$_2$O$_3$ and Yb:(12at.%)YAB at a power density of 8.12 kW/cm^2 of the incicent pump radiation in a V-shaped resonator. The output coupling was defined to be T_{OC} = 4.5%. The considered pumping wavelengths are listed in the legend.

In addition, the influence of the pump wavelength on the optimum disk thickness of Yb:(11at.%)YAG can be seen from the two curves with rectangular symbols. At a pump wavelength of 941 nm, the calculation resulted in lower values for the optimum disk thicknesses than for pumping at 969 nm. For 24 pump beam passes the optimum thickness of the disk would be $\approx$189 μm at the wavelength of 941 nm. This is about 11 μm thinner than for the wavelength of 969 nm where a thickness of $\approx$200 μm was determined. This suggests that for an optimum absorption of the pump radiation at 969 nm, the Yb:(11at.%)YAG thin-disks have to be manufactured either a few micrometers thicker

or the doping concentration and/or the number of pump beam passes should be increased (assuming the given conditions). The adaption via an increase of the doping concentration is in practice easier to realize for Yb:LuAG than for Yb:YAG due to defect formations in the latter laser-active material. This is due to the very similar atomic mass of Lutetium (174.97 amu) and Ytterbium (173.04 amu). On the contrary, the element Yttrium with an atomic mass of 88.91 amu has a significantly different atomic mass, which results in a higher difficulty for a "perfect" implemetation in the host lattice so that the formation of defects is more probable when doping YAG with Yb.

The aim of operating a high-power resonator in fundamental mode implies the thinnest possible disk in order to obtain low phase distortions. A doping concentration of 15% in Yb:LuAG and the use of a pump module with 44 passes through the disk would therefore be beneficial and allow a decrease of the optimum disk thickness to approximately 82 μm when pumping at a wavelength of 969 nm. Both, crystal material of Yb:(15at.%)LuAG and a pump module with 44 passes were not available during this thesis, thus it has to be a prospect for future work.

In order to evaluate the accuracy of the calculated optimum thicknesses, one should bear in mind that additionally to the neglected temperature dependence of the parameters it also depends to a large extent on the accuracy of the data available in literature. Unfortunately, the values from literature can differ quite significantly from one source to another. The values used in the calculations for each laser-active material presented here can be found together with their references in the tables of the following section (see tables 3.1, 3.2, 3.3 and 3.4).

In addition to the data accuracy, there is an obvious influence of the actual crystal quality, since parameters like the exact doping concentration N_{dop}, the fluorescence lifetime or lifetime of the upper laser level τ_{fl} and the internal losses L_{int} are defined by the growth process and the purity of the raw materials used (which are commonly supplied as powders). Furthermore, the typically manufacturing tolerance of the polishing process has to be considered which is in the order of +/- 10 μm. Altogether, the values given for d_{opt} can be used to start an investigation in thin-disk configuration of each laser-active material presented here but are not meant to replace a precise calculation by considering the points mentioned above.

Other important laser parameters for the analysis of laser-active materials are the threshold density E_{min} [24]

$$E_{min} = \frac{h \cdot c}{\lambda_p [\sigma_{abs,eff}(\lambda_p) \cdot \frac{\sigma_{em,eff}(\lambda_{em})}{\sigma_{abs,eff}(\lambda_{em})} - \sigma_{em,eff}(\lambda_p)] \cdot \tau_{fl}} \tag{3.4}$$

and the pump saturation density $E_{sat,p}$ [24]

$$E_{sat,p} = \frac{h \cdot c}{\lambda_p (\sigma_{abs,eff}(\lambda_p) + \sigma_{em,eff}(\lambda_p)) \cdot \tau_{fl}}, \tag{3.5}$$

where λ_p is the pump wavelength, h the Planck's constant and c the speed of light. The effective absorption $\sigma_{abs,eff}$ and stimulated emission $\sigma_{em,eff}$ cross sections are either defined by the pump or the emission wavelength of the laser. Both parameters were calculated for the four investigated laser-active materials according to [24].

The threshold density E_{min} defines the pump power density needed for the minimum number of excited ions in the upper laser level to obtain population inversion in the ideal case of a zero-loss laser cavity. However, with the thin-disk concept the required intensities are in general easily achieved due to the multiple passes of the pump radiation and range between 0.39 and 1.8 kW/cm^2 for the four laser-active materials presented in the following. To determine the values of $E_{sat,p}$ and E_{min}, the fluorescence lifetime τ_{fl} of the laser-active material has to be known. It is difficult to measure the fluorescence lifetime precisely because of the reabsorption effect in laser crystals and the strong dependency of this value on the purity of the raw materials used for the growth. For these reasons, quite a large variation of the values reported in literature can be found. The pump power density of > 20 kW/cm^2 where saturation takes place in Yb:YAG and Yb:LuAG is rather high. For Yb:Lu$_2$O$_3$ and Yb:YAB the pump saturation intensity is almost halved. This lower saturation intensity can become a limiting factor when the laser-active material is intended to be used in thin-disk amplifiers with high pump power densities in the tens of kilowatt per square centimeter range and has to be remembered for this case. By reaching the saturation intensity, the bleaching of the pump light absorption takes place, which results in an approximately constant output power level even at a further increase of the pump power.

Furthermore, as last important parameter, the nominal maximum doping concentration for laser operation is given in the tables (3.1, 3.2, 3.3 and 3.4) of the laser-active materials. This value can be considered as an estimation and is based on experimentally determined data reported in the literature as well as on practical knowledge gained

during the analysis of the laser-active materials. The main influencing factor on the necessary doping concentration in a laser crystal is the ion concentration. For instance, with $2.85 \cdot 10^{20}$ cm^{-3} the ion concentration in Yb:Lu$_2$O$_3$ is approximately twice as high as in Yb:LuAG with $1.42 \cdot 10^{20}$ cm^{-3}. This means that for Yb:Lu$_2$O$_3$ only half of the doping concentration is needed to obtain the same density of Yb-ions in the host when compared to Yb:LuAG. It can be assumed that a nominal lower doping concentration causes a lower distortion of the host lattice resulting in a lower probability for the formation of structural defects, but it is by far not the only influencing factor. In addition, the lattice imperfections are one major reason for the decrease of the thermal conductivity with increasing doping concentrations thus resulting in a higher temperature of the laser-active material in laser operation. To sum up, the different previously discussed parameters of each laser-active material used in this thesis together with the absorption and emission spectrum will be given and explained further in the next sections.

3.2.1   Yb:YAG

Yb:YAG is the most commonly used laser-active material in commercially available thin-disk laser systems at all power levels. This is due to the fact that Yb:YAG crystals can be grown with high quality in large sizes (diameters larger than 100 mm) and offer good laser properties up to a doping level of about 15% (see table 3.1). To evaluate the suitability of other laser-active materials, their thermal, optical, and mechanical properties are therefore systematically compared to thoses of Yb:YAG which is considered as the benchmark-material for thin-disk lasers. In this context it should be noted that a more detailed comparison of certain thermo-mechanical parameters like the heat expansion value will be given in section 3.3 and therefore doesn't appear in the following tables.

Table 3.1: Properties of Yb:YAG [22]

Properties	Yb:YAG
Pump wavelength	941/969 nm
Laser wavelength	1030 nm
Absorption bandwidth (FWHM)	12.5 at 941 nm
	2.5 at 969 nm
Emission bandwidth (FWHM)	4 nm
Quantum defect	8.6% at 941 nm
	5.9% at 969 nm
Effective absorption cross section at λ_{pump}	$0.76 \cdot 10^{-20}$ cm^2 at 941 nm
	$0.76 \cdot 10^{-20}$ cm^2 at 969 nm
Effective emission cross section at λ_{laser}	$2.1 \cdot 10^{-20}$ cm^2
Fluorescence lifetime	1040 μs
Threshold density	1.68 kW/cm^2 at 941 nm
	1.70 kW/cm^2 at 969 nm
Pump saturation density	28.7 kW/cm^2 at 941 nm
	29.2 kW/cm^2 at 969 nm
Thermal conductivity	9.8 W/(m·K) (undoped)
	6.1 W/(m·K) (10at.% Yb)
dn/dT	$7.8 \cdot 10^{-6}$ $1/K$ (undoped)
Thermo-optical constant K_{th-opt}	$13.8 \cdot 10^{-6}$ (Yb10%; 300K)
Refractive index	1.82
Ion concentration	$1.38 \cdot 10^{20}$ cm^{-3} at 1at.%
Nominal max. doping concentration for laser operation	15%
Theoretical optimum disk thickness	208 μm at 941 nm
	220 μm at 969 nm
	(Both 10% doping)

The spectra of Yb:YAG are illustrated in figure 3.4. Two main absorption peaks at the wavelengths of 941 nm and 969 nm can be observed. This results in quantum defects of 8.6 % and 5.6 %, respectively, due to the emission wavelength at 1030 nm.
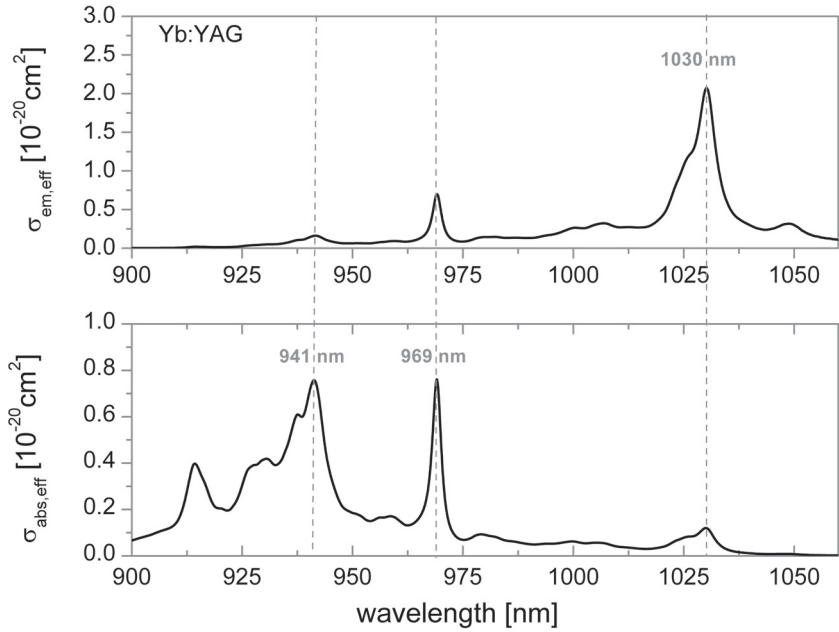
Figure 3.4: Absorption and emission spectrum of Yb:YAG [25]

3.2.2   Yb:LuAG

In the field of lithography, undoped LuAG is expected to be a good alternative high-index lens material for UV-applications. For this reason, the company Schott supported the further development of the Czochralski growth of LuAG a few years ago with the aim to obtain large-sized boule material (diameter of >80 mm, length of >300 mm). Furthermore, the cleaning and polishing process has been optimized with respect to low absorption values [26]. The production of Yb doped LuAG has also benefited from the resulting progress. As a consequence, industrial grade Yb:LuAG is now readily available as well and can be purchased e.g. from the companies FEE or Crytur. For Yb:YAG and Yb:LuAG, the optical, mechanical and thermal properties are quite similar, whereas Yb:LuAG exhibits a lower decrease of the thermal conductivity with increasing doping concentration due to the mentioned smaller difference of the atomic radius of Lu to Yb. This advantage also applies to Yb:Lu$_2$O$_3$ (see following section). Yb:LuAG possesses two main absorption peaks at the wavelengths of 938 nm and 969 nm (for material

properties see table 3.2); whereby the peak at 969 nm corresponds to the zero-phonon-line transition with an absorption cross section which is about $0.06 \cdot 10^{-20} \mathrm{cm}^2$ higher as the one of Yb:YAG. The most relevant physical properties of Yb:LuAG with regard to the use in thin-disk lasers are summarized in table 3.2. The absorption and emission spectrum is shown in figure 3.5.

Table 3.2: Properties of Yb:LuAG [25], [48], [49]

| **Properties**	**Yb:LuAG**
Pump wavelength	938/969 nm
Laser wavelength	1030 nm
Absorption bandwidth (FWHM)	18 nm at 938 nm
	2.5 nm at 969 nm
Emission bandwidth (FWHM)	5.5 nm
Quantum defect	8.9% at 938 nm
	5.9% at 969 nm
Effective absorption cross section at λ_{pump}	$0.63 \cdot 10^{-20}$ cm ^{2} at 938 nm
	$0.83 \cdot 10^{-20}$ cm ^{2} at 969 nm
Effective emission cross section at λ_{laser}	$2.55 \cdot 10^{-20}$ cm ^{2}
Fluorescence lifetime	951 μs
Threshold density	1.8 kW/cm^2 at 938 nm
	1.4 kW/cm^2 at 969 nm
Pump saturation density	35.4 kW/cm^2 at 938 nm
	26.0 kW/cm^2 at 969 nm
Thermal conductivity	8.5 W/(m·K) (undoped)
	7.6 W/(m·K) (10at.% Yb)
dn/dT	$8.3 \cdot 10^{-6} \, 1/K$
Thermo-optical constant K_{th-opt}	$13.4 \cdot 10^{-6}$ (300K)
Refractive index	1.84 (undoped)
Ion concentration	$1.42 \cdot 10^{20} \mathrm{cm}^{-3}$
Nominal max. doping concentration for laser operation	15-20 at.%
Theoretical optimum disk thickness	214 μm at 938 nm
	193 μm at 969 nm
	(Both 10% doping)
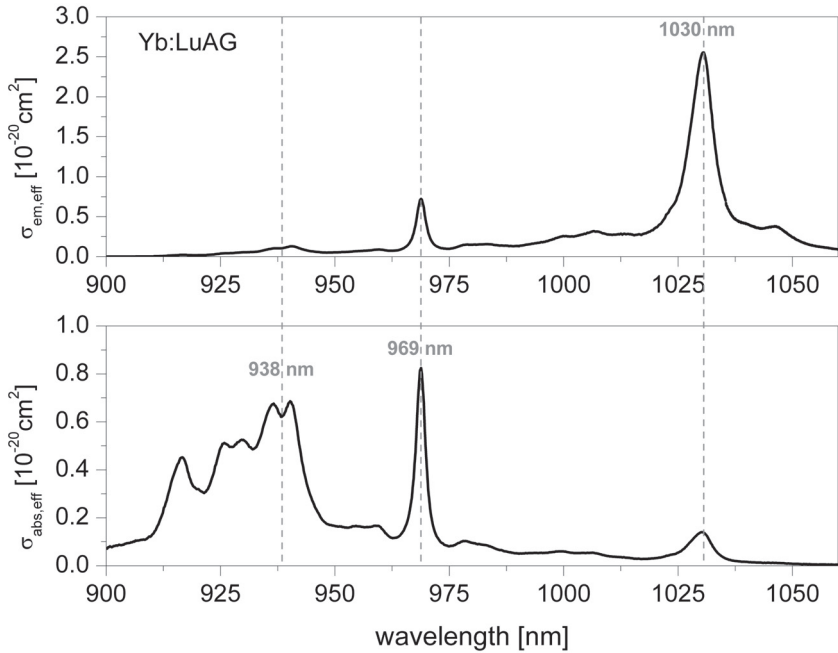
Figure 3.5: Absorption and emission spectrum of Yb:LuAG [25]

The first investigation of Yb:LuAG in comparison to Yb:YAG by using an active-mirror configuration was reported by Kasamatsu et al. in 1999 [27]. Core subject of this paper was the analysis of the thermal behavior of these two materials when pumped at a wavelength of 970 nm. More recently, the benefits from choosing Yb:LuAG with respect to Yb:YAG in thin-disk laser operation were discussed in [25]. There, a maximum output power of 5 kW could be demonstrated. In addition, the main spectral, mechanical and thermal properties of Yb:LuAG are also summarized in [25]. Noteworthy is the used Yb doping concentration of 10at.% since a larger benefit could be obtained with higher doping concentrations of 15at.% and above. At an Yb doping concentration of 10at.% the heat conductivity of Yb:YAG is approximately 19% lower than the one of Yb:LuAG. This difference increases to about 25% with a doping concentration of 15at.%. It is expected that Yb:LuAG has additionally a lower tendency to generate crystal defects and therefore non-radiative loss transitions, which is due to the nearly identical atomic mass of Lutetium and Ytterbium. However, laser operation with about 100 μm thin Yb:LuAG thin-disk crystals with 15at.% or 20at.% doping concentration has not been demons-

trated so far. In principle, Yb:LuAG with an Yb content of 15at. % is available from the company Crytur [28] but a defect-free crystal structure could not be guaranted from them. Nevertheless, this investigation has to be a prospect for future works.

3.2.3 Yb:Lu$_2$O$_3$

Yb:Lu$_2$O$_3$ belongs to the group of the sesquioxide crystals, which features good thermo-optical properties combined with a broad emission spectrum. This laser-active material allows to obtain high optical efficiencies and also shorter ultrafast pulses than Yb:YAG. Yb:Lu$_2$O$_3$ is the most promising material among the sesquioxides due to its high thermal conductivity of $\approx$ 12 W/(m·K) (Yb:YAG $\approx$ 7 W/(m·K)) for the doping concentrations typically required for efficient thin-disk laser operation. So far, one critical aspect is the limited availability of Yb:Lu$_2$O$_3$ crystals with a sufficient size and quality for high-power laser operation (kilowatt level). The reason is undoubtedly the quite demanding growth process of the single crystals from their melt due to a melting temperature of more than 2.400 °C. Currently, only the ILP Hamburg is able to grow Yb:Lu$_2$O$_3$ with good quality through the heat exchanger method [29]. This process was intensely and successfully developed over several years in order to obtain crystal qualities similar to that of Yb:YAG (T_{melt} = 1.930 °C) grown by the Czochralski method. A technology transfer of this growth process to the company FEE was initiated but appeared to be difficult so that a commercial fabrication of this material using this process lays still in the future. The material properties of Yb:Lu$_2$O$_3$ which are most relevant for thin-disk laser operation are summarized in table 3.3. To avoid the high temperatures required for drawing mono-crystalline Yb:Lu$_2$O$_3$ or other sesquioxides from their melt, rare earth-doped sesquioxide ceramics are expected to be an interesting alternative. Temperatures well below the melting point are sufficient for processes like vacuum sintering and hot pressing. Yb:Lu$_2$O$_3$ ceramic started to show its potential with the publication of the first cw-laser operation and broad spectral tunability in 2006 [30]. In the same year, Yb:Lu$_2$O$_3$ ceramic manufactured using a vacuum sintering process was tested in a mode-locked bulk laser with an output power of 532 mW and a pulse duration of 357 fs [31]. The shortest pulse duration of 65 fs using Yb:Lu$_2$O$_3$ ceramic was demonstrated by Kerr-lens mode-locking [32]. More recently, a laser based on Yb:Lu$_2$O$_3$ ceramic produced by hot pressing has been reported. The laser was operated with a maximum output power of more than 16 W and a slope efficiency of 74 % [33]. Although the powers are still lower than what was already demonstrated with crystalline material, Yb:Lu$_2$O$_3$ ceramics also have a high potential, since their production process makes it possible to obtain larger pieces of laser-active material more easily. Another novel approach to grow single crystal Yb-doped

sesquioxides is based on aqueous hydroxide solutions [34]. This hydrothermal growth takes place at temperatures in the range of 550 °C to 660 °C resulting in low thermal strain of the laser-active crystals which is advantageous for high-power laser operation. Nevertheless, the experimental verification of the suitability of hydrothermally grown Yb:Lu$_2$O$_3$ for high-power laser operation is still in progress to date.

Table 3.3: Properties of Yb:Lu$_2$O$_3$ [35], [36]

Properties	**Yb:Lu$_2$O$_3$**
Pump wavelength	949 nm/976 nm
Laser wavelength	1034 nm /1080 nm
Absorption bandwidth (FWHM)	8.6 nm at 949 nm
	2.9 nm at 976 nm
Emission bandwidth (FWHM)	13 nm
Quantum defect at λ_{laser} 1034 nm	8.2 % at 949 nm
	5.6% at 976 nm
Effective absorption cross section at λ_{pump}	0.95·10^{-20} cm^2 at 949 nm
	3.1·10^{-20} cm^2 at 976 nm
Effective emission cross section at λ_{laser}	1.26·10^{-20} cm^2 at 1034 nm
	0.44·10^{-20} cm^2 at 1080 nm
Fluorescence lifetime	820 μs
Threshold intensity 976/1034 nm	0.39 kW/cm^2
Pump saturation intensity 976/1034 nm	8.01 kW/cm^2
Thermal conductivity	12.6 W/(m·K) (undoped)
	11 W/(m·K) (3at.% Yb)
dn/dT	8.6·10^{-6} 1/K (undoped)
Thermo-optical constant K_{th-opt}	16.9·10^{-6}
Refractive index	1.91
Ion concentration	2.85·10^{20}cm^{-3} at 1at.% Yb
Nominal max. doping concentration for laser operation	>5%
Theoretical optimum disk thickness	271 μm at 949 nm
	128 μm at 976 nm
	(Both 3% doping)

Table 3.3 shows that Yb:Lu$_2$O$_3$ exhibits a significant difference between the values of the effective absorption cross section for the two main absorption pwxeaks at the wavelengths of 949 nm and 976 nm. The value of 3.1· 10^{-20} cm^2 at the wavelength of 976 nm is remarkably high. However, the general drawback of the zero-phonon absorption

line applies also for Yb:Lu$_2$O$_3$: these transitions have a comparatively narrow spectral bandwidth. The full width at half maximum (FWHM) bandwidth of the absorption peak at 976 nm in Yb:Lu$_2$O$_3$ is only 2.9 nm.
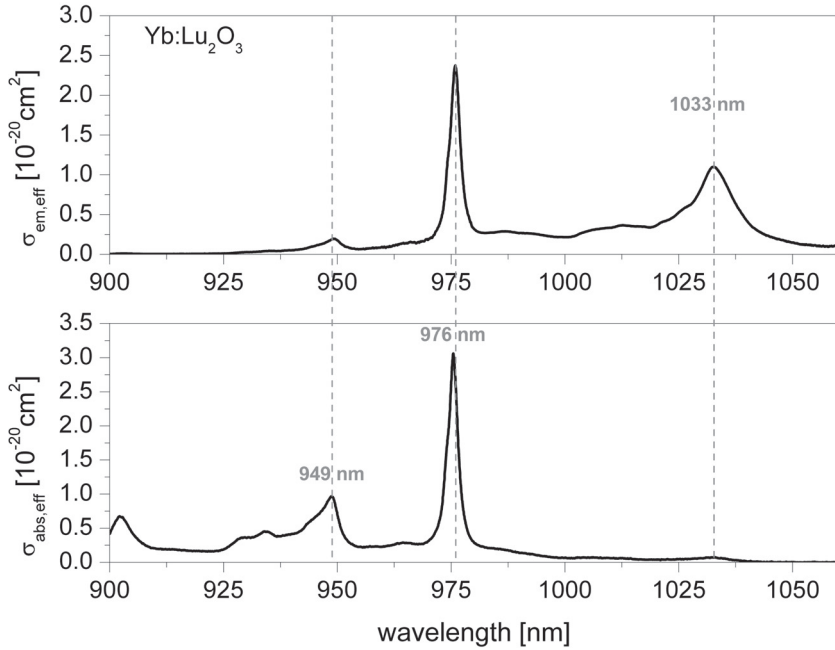

Figure 3.6: Absorption and emission spectrum of Yb:Lu$_2$O$_3$ [36]

3.2.4   Yb:YAB

The laser-active material Yb:YAl$_3$(BO$_3$)$_4$ features two interesting properties for the use in laser systems. First, the self-frequency doubling capability of the YAB host [37],[38] which generated an intense development of this material in the last decade to produce microchip lasers emitting in the green spectral region and furthermore as undoped crystal for frequency conversion by second and third harmonic generation [39]. Second, its broad gain bandwidth of >40 nm (σ-polarization) which demonstrated its potential for the use in ultrafast laser systems [40] with sub-100-fs pulse durations [41]. In addition to these properties, its good thermal conductivity of 4.7 W/(m·K) (at a doping concentration of 5.6 % [42]) indicates a sufficient ability to scale the laser output power. Yb:YAB is

a negative uniaxial crystal exhibiting a high nonlinear coefficient. Most of the research, up to now, was therefore devoted to the improvement in the use for frequency doubled operation. Some key properties of Yb:YAB are shown in table 3.4 which indicate that good laser perfomances can be expected as well when the crystal is used in the infrared spectral range.

Table 3.4: Properties of Yb:YAB [37],[43]. The values of the effective absorption and emission cross sections available from literature [37],[43] given in this table differ from the ones obtained from the measurements of the Yb12at.%:YAB samples at FEE This issue will therefore be discussed in the following section.

Properties	Yb:YAB
Pump wavelength	976 nm
Laser wavelength	1040 nm
Absorption bandwidth (FWHM)	20 nm
Emission bandwidth (FWHM)	16 nm
Quantum defect	6.2%
Effective absorption cross section at λ_{pump}	$\approx 3.4 \cdot 10^{-20}$ cm^2 [37]
Effective emission cross section at λ_{laser}	$\approx 0.8 \cdot 10^{-20}$ cm^2 [37]
Fluorescence lifetime	680 μs
Threshold intensity	0.39 kW/cm^2
Pump saturation intensity	8.8 [kW/cm^2]
Thermal conductivity	9.8 W/(m·K) (5.6at.% Yb)
dn/dT	$11 \cdot 10^{-6}$ $1/K$
Thermo-optical constant K_{th-opt}	$\sim 20 \cdot 10^{-6}$ (Nd:YAB)
Refractive index	1.76
Ion concentration	$0.57 \cdot 10^{20}$cm^{-3} at 1at.% Yb
Nominal max. doping concentration for laser operation	>12%
Theoretical optimum disk thickness	160 μm at 12at.% Yb

The company FEE performed and provided polarization-dependent transmission measurements over the wavelength range of 300 nm to 1100 nm on an 4 mm thick Yb:YAB crystal oriented along the c-axis. The values of the effective absorption and emission cross-section of Yb:YAB for p- and s-polarized radiation were derived from these measurements as explained in the following. To calculate the effective absorption cross-sections

$$\sigma_{abs,eff}(\lambda) = ln(\frac{I_{100\%}}{I_{Tmeas}(\lambda)} \cdot \frac{1}{N_{dop} \cdot l}) \tag{3.6}$$

the Lambert-Beers law was applied to the measured values, where $I_{100\%}$ is the intensity of the incident radiation and I_{Tmeas} the intensity of the radiation which is transmitted through the Yb:YAB sample with a thickness l.

From the thereby obtained effective absorption cross-sections, the effective emission cross-sections were derived by using the reciprocity relationship [44], [45]

$$\sigma_{em,eff}(\lambda) = \sigma_{abs,eff}(\lambda) \cdot \frac{Z_l}{Z_u} \cdot \exp[(E_{ZL} - h\nu)/k_B T], \tag{3.7}$$

where k_B is the Boltzmann constant and T the temperature. The Stark energy-level diagram of the $^2F_{5/2}$ and $^2F_{7/2}$ manifolds of Yb^{3+} in YAB used to calculate the partition functions Z_l and Z_u of the lower and upper laser level, respectively, and the value of the energy difference for the zero-phonon-line transition E_{ZL} have been reported in [37].
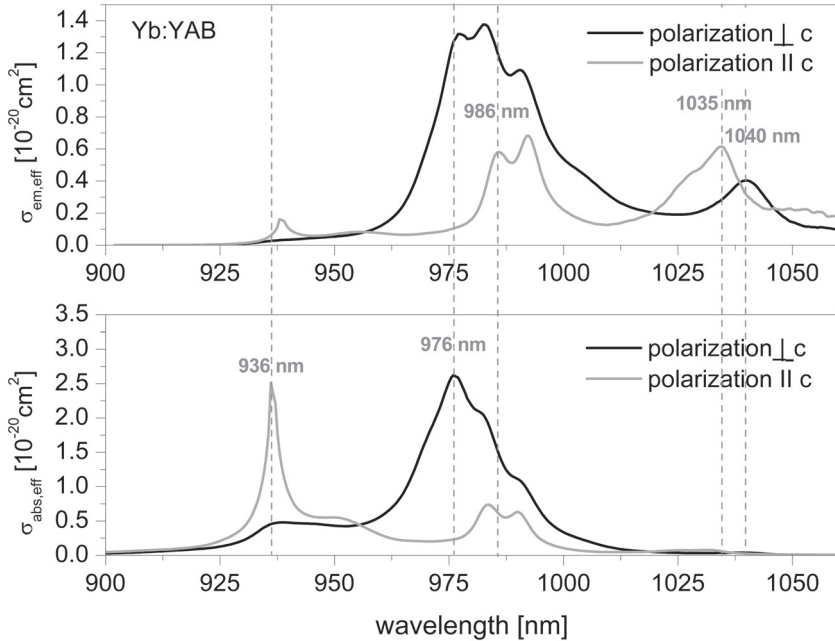

Figure 3.7: Absorption and emission spectrum of Yb:YAB at room temperature calculated from transmission measurements of a 4 mm thick sample for the wavelengths between 900 and 1060 nm.

The spectroscopic properties of Yb:YAB obtained by the calculations are shown in figure 3.7. It can be observed that for light with a polarization parallel to the c-axis an increase of noise (modulation of the line) for wavelengths above 1040 nm occurs. This can be explained by a decrease of the absorption with increasing distance from the fundamental transition as discussed in [46]. For light which is polarized perpendicular to the c-axis, the main absorption peak is at a wavelength of 976 nm. Together with the laser peak at the central wavelength of 1040 nm this results in a low quantum defect of 6.2% for Yb:YAB (see table 3.4). It should be pointed out that the FWHM bandwidth of the absorption peak at 976 nm is about 20 nm which significantly lowers the demands for the pump diodes.

However, the cross-sections reported here differ from other experimentally determined values as reported in [37] and [42]. The small difference to the values given in [37] could be explained by the use of unpolarized radiation during the measurements in [37] and furthermore by the use of a comparatively thick sample (l= 4 mm) in the transmission measurements reported here. In both cases, the Yb:YAB crystal was cut for frequency doubled operation which suggests a similar cut-angle so that this influence is considered as marginal when comparing these two results. As opposed to [37] and this work, the values of the absorption- and emission cross-sections determined by [42] differ strongly, especially the emission cross-section with a value of $\approx 4 \cdot 10^{-20}$ cm^2 for s (correspondingly σ) -polarized light is about 4 times higher (see figure 1a of the paper). The reason for this large difference seems to be a strong anisotropy of the spectroscopic properties of Yb:YAB [42] depending on the orientation of the axes of the crystal. Different measurements which have been analyzed during this thesis confirm this consideration. To conclude, there can be a benefit from applying a specific cut angle to the Yb:YAB crystal to obtain a high absorption and/or emission cross section. In view of the desired operation of the Yb:YAB laser, this possible benefit is worth to be considered for future work with this material.

3.3   Crystal properties: manufacturing requirements for high-power thin-disk laser operation

The key properties of Yb:YAG, Yb:LuAG, Yb:Lu$_2$O$_3$ and Yb:YAB have been outlined in the previous section. Beside these mainly optical properties, certain mechanical properties of the laser-active materials are of high importance for the use as thin-disk laser crystals. This section of the thesis therefore emphasizes more on essential mechanical ones, since for instance the mechanical and chemical resistance plays a decisive

role especially during the manufacturing process of the thin-disk crystals. Moreover, the manufacturing requirements regarding the surface quality and planarity of the disks are high, since all type of losses result in a decrease of the efficiency during laser operation. This is of particular importance for a low gain laser configuration like the thin-disk laser. The comparatively poor gain is obviously caused by the small thickness of the disks of a few hundred micrometers. Furthermore, laser crystals with a diameter of at least 10 mm are mandatory to realize a thin-disk laser suitable for output powers at the kilowatt level. At this high-power level, the active disk has to be as thin as possible to obtain an appropriate heat removal. This requires either a large absorption cross section, an increase of the number of pump-beam passes or an increase of the doping concentration to guarantee efficient laser operation. The limit for the minimal possible thickness of a laser disk is set by the manufacturing process (polishing and coating constraints). For instance, it is about 60-80 μm for Yb:YAG. This thickness requires an increase of the doping concentration to about 15% to guarantee efficient operation. A problem, however, is the increase of the doping concentration which leads often to the generation of additional loss transitions due to the distortion of the crystal structure when implementing the Yb^{3+} ion in the lattice. The strength of this structural distortion is more pronounced when the difference of the radius of the laser-active-ion (e.g. Yb^{3+}) to the radius of the host ion (e.g. Y^{3+}, Lu^{3+}) is high. In Yb:YAG a larger difference of the radius between Yb^{3+} to the host YAG exists than for e.g. of Yb^{3+} in LuAG, which results in a larger reduction of the length of the unit cell. It might therefore be possible that the distance between the active ions in Yb:YAG decreases more than in Yb:LuAG with increasing doping concentration [47]. In case the distance becomes very short, an interaction between the Yb^{3+} ions occurs. This mechanism and other defect formations in the crystal lattice and their influence on the laser performance are discussed in sections 3.3.1 and 4.1.1.

In general, polishing such thin disks necessitates a certain mechanical strength of the laser-active material. Thus, a high tendency of fracture (e.g. such as for Yb:KYW or Yb:CaF$_2$) makes it more difficult to handle the disk during the polishing, coating and contacting process. Moreover, the power handling capability in the thin-disk geometry is reduced. This is a drawback, especially when the aim is the usage in industrial systems. Another key parameter to keep in mind is the hardness of the material which has a similar importance during the manufacturing process as softer material is more likely to be scratched or even damaged. A summary of the most relevant properties for the manufacturing of thin-disk crystals out of Yb:YAG, Yb:LuAG, Yb:Lu$_2$O$_3$ and Yb:YAB is given in table 3.5.

Table 3.5: Relevant properties with regard to the manufacturing of thin-disk crystals out of Yb:YAG [22], Yb:LuAG [48], [49], [50],Yb:Lu$_2$O$_3$ [35] and Yb:YAB [51], [52], [53], [54]

	Yb:YAG	Yb:LuAG	Yb:Lu$_2$O$_3$	Yb:YAB
Density [g/cm^3]	4.56	6.67	9.42	3.84
Mohs hardness	8.4	8.5	6-6.5	7.5
Heat expansion coefficient [10^{-6}/K]	7.7-8.2	6.13	8.6	8.5
Thermal shock resistance [W/m]	0.76	1.24	1.47	1.15
Melting temperature [°C]	1930	2060	2450	1836

Other key factors of the materials for laser operation (especially at the high-power level) as for instance the tensile strength, the elastic modulus or the resistance against temperature changes are rarely reported in literature. The only exception is Yb:YAG. However, to be able to evaluate the mechanical stability of a laser-active material in a simple expression, Petit et al. [1] proposed to use the thermal shock resistance

$$R_T \approx \frac{\lambda_{th}}{\alpha_{th}}, \tag{3.8}$$

where λ_{th} is the thermal conductivity and α_{th} the thermal expansion coefficient. To calculate R_T, values of λ_{th} of each material were taken from the literature references given in table 3.1, 3.2, 3.3 and 3.4. The values of α_{th} and the determined values of R_T can be found in table 3.5. All four laser-active materials have a high thermal shock resistance, but the value of 0.76 of Yb:YAG is surprisingly the lowest among them. In fact, the thermal shock resistance of Yb:Lu$_2$O$_3$ is approximately twice as high as for Yb:YAG when using this calculation. This is contrary to the observations in practice reported later on. The reason is most likely the non-optimum quality of the currently available Yb:Lu$_2$O$_3$ crystals which limits the industrial break-through of this laser-active material despite his advantageous theoretical parameters. A better alternative at the moment seems to be Yb:LuAG with a still high value of 1.24 for R_T and a readily available good crystal quality which can withstand the multi-kilowatt output power level[25].

In the following sections, the production techniques of thin-disk crystals are evaluated with regard to the influence on the expected laser performance. Each manufacturing step is analyzed, and the critical factors identified. This includes a more detailed discussion of the theoretical properties of the investigated laser-active materials with respect to the actual industrial readiness level. The aim is to have a suitable crystal quality for thin-disk

lasers with an output power at the kilowatt level that additionally allows fundamental-mode operation.

3.3.1   Defects implemented by the crystal growth

The quality of a thin-disk laser crystal is to a large extent affected by the growth process. This leads us to two important parameters: melting temperature (see last row of table 3.5) and crystallographic structure. These parameters define the applicable growth methods for each laser crystal, whereas a high melting temperature increases for instance the demands for the growth apparatus. This is due to the fact that the material to be used for the crucible needs to have higher melting temperatures than the crystal to be grown (an exception is the crystal growth by the flux method). In addition, higher melting temperatures often lead to an implementation of higher stress in the crystal, because it is more difficult to maintain a homogeneous temperature distribution during the growth and cooling process. Thereby, dislocations or even cracks are formed, indicating a residual stress in the crystal material. As an example, $Yb:Lu_2O_3$ thin-disk crystals grown by the heat exchanger method (HEM) have been analyzed regarding birefringence using the conventional method of crossed polarizers. An analyzed disk with a doping concentration of 3 at.% and a diameter of 7 mm is shown in figure 3.8. It can be seen that this disk contains numerous crystallite boundaries, which indicates high internal stress. The wavefront distortions induced by this disk to the beam are likely to be higher than without these defects. They also increase the diffraction losses of the laser cavity and can even result in a general deformation of the laser mode, especially in fundamental-mode operation. Additionally, it is assumed that this $Yb:Lu_2O_3$ thin-disk crystal features a lower resistance against thermally induced stress which is for example present in axial and radial direction of the transition area between the pumped and unpumped region of the disk during laser operation (see chapter 4.1 for the explanation of thermal effects in thin-disk crystals).
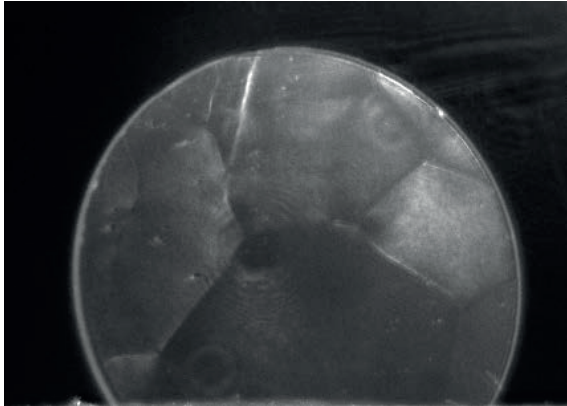
Figure 3.8: Stress in an Yb:Lu$_2$O$_3$ disk with 3 at.% doping concentration visualized by crossed
polarizers.

Another indication for high residual stress is that the Yb:Lu$_2$O$_3$ boules crack usually into
pieces when they are removed from the crucible [36] as shown in figure 3.9. From the
pieces (which are shown like delivered), the areas with low birefringence are selected to
have sufficient good material for high-power thin-disk laser operation.

$\approx$ 60 mm

Figure 3.9: Example of as grown Yb:Lu$_2$O$_3$ pieces.

In figure 3.9 another common crystal defect of laser-active materials can be seen as well: the formation of color centers due to lattice defects in the crystal structure. Color centers are well known to appear due to impurities or defaults in the crystals during the growth process and can be removed by means of annealing over several hours (typically 24-48 h) at high temperatures (typically 900-1.600 °C) [36]. After annealing the crystals are usually colorless. However, occasionally a pale yellow or brownish color of the crystals remains by which the absorption of pump and laser radiation in the disk is increased. It is furthermore problematic that a post-growth formation of color centers can occur inside the laser crystals by exposure to UV-light, since different kinds of UV-radiation can be present in several manufacturing steps for laser optics. For instance in every dielectric coating process (containing plasma) UV-radiation is generated [55] which consequently can increase the absorption of the laser material. Moreover, in case the disk gets glued onto the heat sink an UV-curable adhesive is typically used. For these reasons an analysis of the influence of UV-radiation on different samples was carried out [56]. Beforehand, it has already been communicated that the formation of color centers should be considered for thicker disks like those typically used in amplifiers and also for bonded disks with YAG as a support substrate. The question was then if it is also critical for disks where the aim is to operate at an output power at the multi-kilowatt level. Thus, an analysis of the change of the absorption due to color centers in LuAG, YAG and Yb:YAG samples has been performed. Although the detailed explanation of the optical process behind the formation of color centers in garnets by irradiation with UV-light shall not be discussed here, the interested reader may find further information in [57], where the possibility to reduce the color centers by annealing is mentioned as well and has thus been investigated for the present samples. To determine the necessary duration and temperature for the annealing process of coated thin-disk laser crystals, absorption measurements (following DIN ISO 11551 [58]) on different samples were performed at the wavelengths of 808 nm, 940 nm and 1030 nm. The absorption of the samples was first measured as delivered, then after the irradiation for different time durations with either an array of UV-LED's or a UV-oven and finally after defined annealing steps. The array of UV-LED's emitted radiation at a wavelength of 370 nm and the lamp of the UV-oven (Loctite 97035, 1 kW mercury vapor lamp) exhibited a spectrum from 220-500 nm. An increase of the absorption of the samples was observed after irradiation with both sources. However, the increase of the absorption after irradiation with the UV-LED's for a time duration of 1 minute is marginal as illustrated in figure 3.10 for the example of LuAG. It can therefore be assumed that the low increase of the absorption in the disk due to a formation of color centers during the curing of the adhesive in the gluing process by an UV-LED can be neglected. On the contrary, the irradiation for 12 minutes in an UV-oven increases the absorption significantly (approximately by 8 times). Besides the longer duration, an

influence of the higher energy of the radiation for the shorter wavelength present in the UV-oven is suspected. As a consequence the curing of adhesives with an UV-oven when gluing thin-disk crystals or the utilization of it for cleaning should be avoided in case no equipment for an annealing is available afterwards.
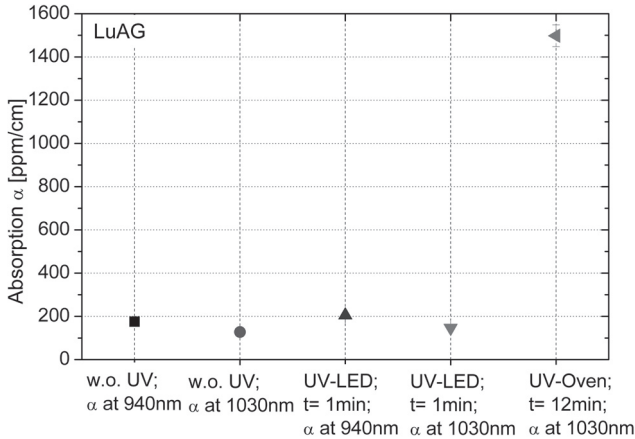

Figure 3.10: Absorption coefficient at 940 nm and 1030 nm for a 4 mm thick LuAG sample: as delivered, after 1 min irradiation with a UV-LED and after 12 min irradiation in the UV-oven.

The previously reported formation of color centers of undoped LuAG samples by irradiation of UV-light in the UV-oven was also observed for undoped YAG, Yb-doped YAG and Yb:LuAG crystals. As an example, the absorption of an 7% doped Yb:YAG disk measured at a wavelength of 808 nm after irradiation and annealing are depicted in figure 3.11. This sample was first irradiated in the UV-oven for 12 minutes and then different annealing steps were investigated. It was determined that a significant reduction of the absorption due to formation of color centers took place for temperatures exceeding 300 °C. In conclusion, an annealing of the 7% doped Yb:YAG for a duration of 24h at 450 °C resulted in an absorption that was even slightly lower than the initial one prior the performed UV-irradiation. It was also experimentally verified that this was the maximum temperature of the annealing process where no degradation of the applied coatings of the thin-disk crystals took place. A similar behaviour was observed for all analyzed samples. Thus, this annealing procedure can be recommended to be applicable for Yb:YAG and Yb:LuAG thin-disk crystals.
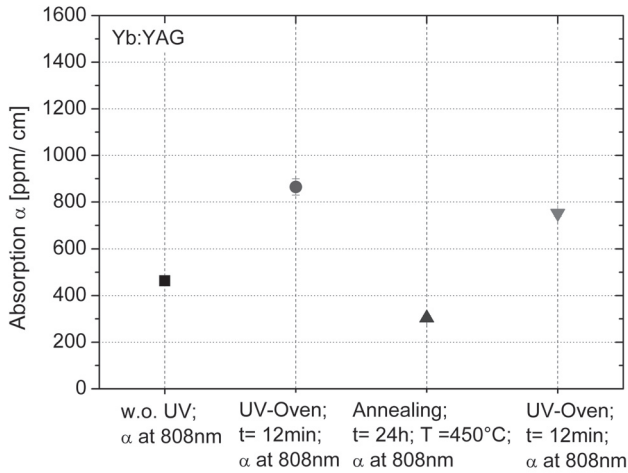
Figure 3.11: Absorption coefficient measured using a 0.9 mm thick Yb:YAG sample with 7% of doping: as delivered, after 12 min irradiation in the UV-oven, after annealing over 24 h at T= 450°C, and after a 2nd irradiation over 12 min in the UV-oven.

Finally, other intrinsic defects of laser crystals to be mentioned that severely reduce the laser performance are bubbles or striaes inside the laser-active material. These are typical scatter centers which can occur inside the complete volume of the crystal and can cause such high losses that thin-disk laser operation cannot be obtained. An example of these kind of inclusions observed inside an Yb:YAB disk are shown in figure 3.12.
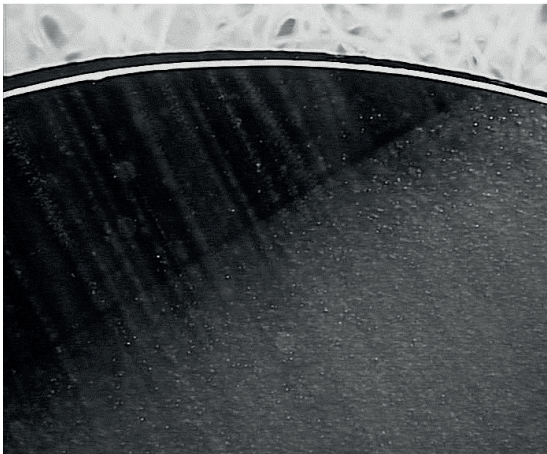
Figure 3.12: Bubbles inside an Yb:YAB thin-disk crystal.

A thin-disk crystal containing no scatter centers would appear completely transparent which would mean that the image of the used dark-field microscope would be completely dark. On the contrary, the Yb:YAB disk in figure 3.12 exhibits bubble-shaped inclusions which are spread almost over the complete bottom area of this disk section and form even striae-like structures as detectable in the upper left part of the picture.

3.3.2   Influence of the polishing on the laser performance

In order to obtain an adequately high surface quality of the thin-disk crystals, the polishing process has to be analyzed and optimized for each laser-active material individually. An important parameter thereby is e.g. the resistivity of the material against the chemical supplements of the polishing fluids. In case of Yb:Lu$_2$O$_3$, the higher sensitivity to chemicals in comparison to Yb:YAG resulted most likely in the destruction of several thin-disk crystals when using an automated polishing machine for the disk manufacturing (as communicated by the company FEE). A further point to consider is the material of the polishing cages. For laser crystals which are softer than the commonly used stainless steel cages, damage of the laser crystals at the edges takes place which reduces the disk diameter and causes scratches due to small crystal particles. Contrary to the polishing with machines, polishing by hand is more gentle so that the risk of damaging the disk is lower. The drawback of the manual polishing is the longer time needed for the process. For this reason, this method is quite costly. To analyze the surface quality and to characterize the planarity of the laser disks after polishing, microscopic (differential interference contrast microscopy and dark field microscopy) and interferometric measurement devices have been used. The microscopic methods enabled an analysis of the disks regarding surface defects and contaminations, whereby a Twymann-Green-interferometer was typically used to determine the planarity of the disks after the polishing process. The inspections showed that there are significant differences of the polishing quality of thin-disk crystals. The reason for this has been investigated further. It appeared that the quality inspection of the thin-disk crystals by the companies has often been a manual process which was done only visually by using white-light source. As a result, the inspection of the polishing quality has formerly been influenced subjectively by the examiner. To reduce the quality fluctuations of the suppliers, the DIN ISO 10110 [59] specifications were applied in order to define the requirements for the polishing of thin-disk crystals [60]. The parameters are as follows:

- Planarity: minimum λ/10
- Parallelism: 10"
- Surface defects: maximum 5/3x0.01
- Side facets: grinded

It is sufficient to specify the first three parameters for a defined free aperture of the disk, which is about 60 to 70 percent of the diameter [60]. This is appropriate due to the damages at the edges during manufacturing and the general aperture effect of each optic which is used in a resonator. A good polishing quality at the edges is not beneficial, even detrimental, as parasitic lasing due to an amplification of radiation propagating perpendicular to the optical axis can occur in certain cases [22]. Hence, the fourth specification is to grind the side facets, whereas the easiest possibility to grind is after the contacting of the disk on the heat sink. If the grinding of the side facets is performed additionally under a specific angle [17] a further reduction of the parasitic radiation is obtained. This method is especially beneficial for thin-disk amplifiers with an output energy at the multi-millijoule level, but also for oscillators operating at several kilowatt of output power.

Despite a proper specification, there are different kinds of surface defects which can appear during the polishing of the thin disks. One of these polishing defects, for example, are scratches on the front and/or backside of the thin-disk crystals (as shown in figure 3.13), another are damages on the surface due to a chemical reaction of the laser crystal with the polishing fluid (see figure 3.14).
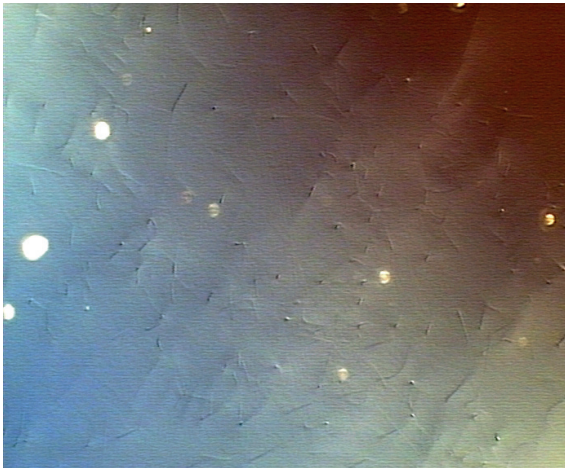

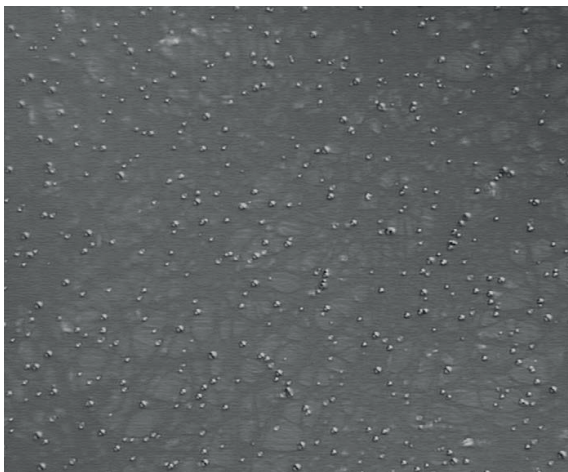**Figure 3.13:** Hole-shaped scratches on the surface of an $Yb:Lu_2O_3$ disk.

Figure 3.14: Yb:Lu$_2$O$_3$ disk with surface defects formed by a chemical reaction with the polishing fluids.

In the worst case, a complete batch of thin-disk crystals is rendered unusable during processing. However, it was determined that scratch-like defects are less critical with regard to the laser performances than other defects which are discussed in the following. For instance, absorbing defects for pump, fluorescence and laser light inside the disk, the contact layer and/or the heat sink contribute much stronger to optical damages and are assumed to cause a more significant decrease of the efficiency during laser operation.

3.3.3 Influence of the coating on the laser performance

For thin-disk crystals, the requirements of the coating especially at the high-power level are demanding. The coating techniques should provide very dense layers which result in high reflectivity values and high damage thresholds, but on the other hand exhibit low thermal resistance (HR rear side) and introduce the lowest possible stress. An important demand for the coating of thin-disk crystals, when compared to other laser designs, is the high angular acceptance for the pump radiation. The desired specifications of the coating are summarized in tables 3.6 and 3.7. The values are given for the example of Yb:YAG.

Table 3.6: Specifications AR-coating Yb:YAG

Wavelength [nm]	Angle of incidence in air [°]	Reflectivity [%]
Laser radiation (1020-1055)	0-11	<0.1
Pump radiation (938-942)	18-52	<0.3

Table 3.7: Specifications HR-coating Yb:YAG

Wavelength [nm]	Angle of incidence in Yb:YAG [°]	Reflectivity [%]
Laser radiation (1020-1055)	0-6	>99.95
Pump radiation (938-942)	12-38	>99.7

Certain differences of the demands of the coating for pump and laser radiation have to be pointed out. As mentioned above, the important aspect for the pump radiation is the large angular range, whereas a compromise is acceptable for the reflectivity with slightly lower values for the HR and marginally higher ones for the AR layer coating compared to the coatings for the laser wavelength. Contrary to this, the reflectivities for the laser radiation have a direct influence on the laser threshold and efficiency since the residual transmission acts as a loss channel for the thin-disk laser. Therefore, the goal for the HR coated rear side of the disk are values of the reflectivity exceeding 99.95%, whereas the front side should consist of a low loss (absorption, scattering) AR-coating with values below 0.1%. During the application of the coating onto the thin-disk crystal a bending of the disk occurs. This is due to the high aspect ratio between diameter and thickness in combination with the large difference of the number of layers between AR and HR-coating which create a different amount of stress on each side. Common coating materials are SiO_2 (low refractive index), Ta_2O_5 and HfO_2 (both: high refractive index) which are alternated in order to realize the desired profile of the refractive index. To achieve high reflectivities, more than 30 layers with a thickness corresponding to a quarter of the operation wavelength have to be deposited, whereas an anti-reflective behavior can already be realized with 3-5 $\lambda/4$-layers. A trade-off for the HR coating design exists between the highest possible reflectivity and the lowest possible heat resistance. Additionally, for kilowatt output power operation the damage threshold of the materials is a critical issue. For example, HfO_2 features a higher damage resistance and is therefore often used for coatings which are used in lasers emitting pulses with a pulse duration of a few picoseconds (to resist high peak powers). Its drawback is a lower refractive index than Ta_2O_5. For this reason, a higher number of coating layers is needed to obtain the same reflectivity which results in the implementation of more stress through these coa-

tings. Hence, Ta_2O_5 is often preferred as coating material for optics used in continuous wave operation. Typical coating designs and a detailed description of a novel IBS (Ion Beam Sputtering) coating system optimized for thin-disk crystals can be found in [61]. In case the contact between the thin-disk and the heat sink gets realized by soldering, a metallization [17] has to be applied on the rear side of the disk on top of the HR dielectric coating. To realize this in-situ, a separate chamber with metal-targets of Cu, Ni and Au is needed. For contamination reasons not all coating suppliers are willing to offer this option which, for a certain time, limited this type of coating design to the company Jenoptik.

Contaminations during the coating or polishing process are supposed to be the reason for the last defect mechanism to be mentioned here: the formation of particle inclusions at nanometer scale, which are possible absorption centers for both the pump and the laser radiation. Absorbing defects with even a very small size are in general much more critical than scattering defects due to the high power densities of pump and laser radiation present in a thin-disk laser. They result in localized hot spots which can deteriorate the beam quality or damage the disk. The coating damages shown in figures 3.15 and 3.16 belong to defects of this category.
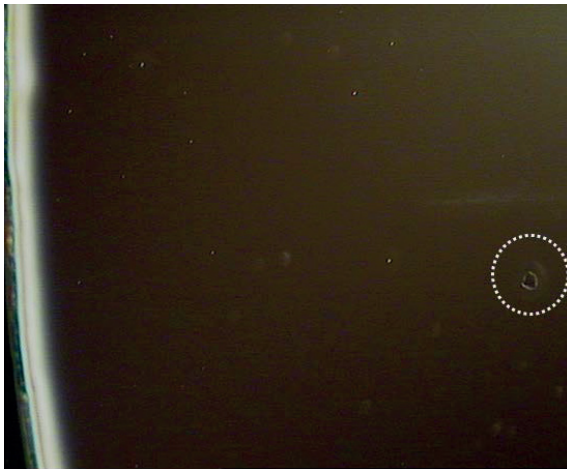

Figure 3.15: Defect in the coating: example 1, (scale of the image: 1.3 mm width x 1mm height)
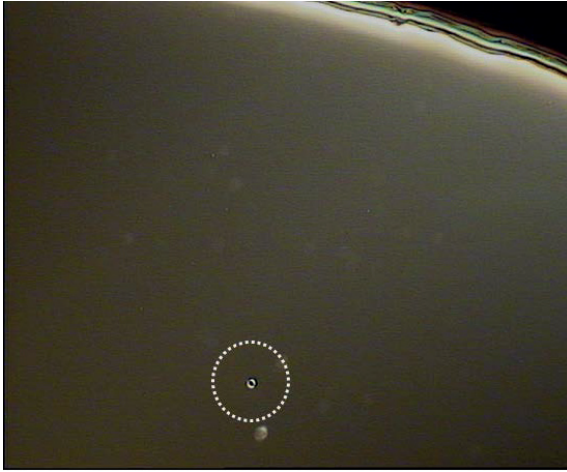
Figure 3.16: Defect in the coating: example 2, (scale of the image: 1.3 mm width x 1mm height)

Comparative studies on coatings for high-power laser optics [62] have shown that the
IBS-process has advantages regarding the quality and stability of the coating layers
when compared to IAD- (Ion Assisted Deposition) processes. This is due to the high
kinetic energy of the ions in the IBS-process in combination with low process tempera-
tures, which form a very compact, glass-like layer structure. In contrast, a more porous
micro-structure is deposited by the IAD-process. The compact layer structure of the IBS
exhibits a better thermal conductivity and less absorption and scatter centers. Critical pa-
rameters of the IBS are the adhesion of the coating and the occurrence of stresses in the
layers which were optimized for the thin-disk crystals with in-situ measurement devices
of the company sigma-physik [63]. However, other parameters like the reproducibility
of the optical constants of the material from one coating run to another and the number
and density of defects depending on the cleanliness of the coating chamber and the prior
cleaning of the samples to be coated, are also important. These parameters cannot be
influenced by the coating process alone and depend on multiple factors like for instance
human ones. Further coating techniques which have been applied for thin-disk laser cry-
stals and which show a suitability for high output powers are magnetron sputtering (MS)
and ion plating (IP). A short overview and the basics of MS and IP coating techniques
can be found in [64] and [65] respectively. These publications give an impression of the
complexity of coating depositions and the effects of different process parameters which
range from the process gas to the post-annealing.

In summary, chapter 3 outlined the criteria which were applied to select the four laser-active material investigated in this thesis and showed the challenges to manufacture thin-disk crystals out of them. The 4th chapter will address the limitations in order to scale the output power of fundamental-mode thin-disk lasers to the kilowatt level which have to be considered additionally. Nonetheless, the reported processes of manufacturing and the limitations discussed in chapter 4 represent only a snapshot of the development of thin-disk lasers since a continuous progress regarding all aspects is ongoing with the result that manufacturing capabilities are permanently improved and the mentioned limits stretched or even overcome.

4 Limitations to the power scaling of high-brightness thin-disk lasers

The advantages of laser beams featuring high power (at least kilowatt level or higher) together with high brightness have already been pointed out in chapter 1. There is no doubt that the thin-disk laser approach has the potential to reach the desired performances due to the efficient heat extraction and easy power scalability of this concept. Nevertheless, the efficient generation of several kilowatts of output power per disk at beam parameter products of less than 3 mm·mrad (corresponding to M^2 <10) is limited by a thermally induced aspherical wavefront distortion occurring inside the disk and air turbulences in front of it. Until 2009, these phase front deformations kept the fundamental-mode operation of thin-disk lasers below approximately 500 W of output power because they induce diffraction losses in the laser resonator. Thus, the topic of this chapter is the explanation of the factors influencing the brightness of thin-disk lasers and to show the limitations they impose on power scaling to output powers up to the (multi-) kilowatt level.

4.1 Thermal effects inside the thin-disk crystal

In a thin-disk laser the ratio of cooled surface to pumped volume is comparatively high and the heat flow is one dimensional, in a first approximation. The heat spreads along the axial direction of the thin-disk across the bonding layer and the heat sink to the cooling water. Assuming no defects at the edges and no aperture effect of the thin-disk, a pumping over the complete area of the thin-disk crystal would in principle be possible. In this theoretical case where the interface between pump area and un-pumped area is neglected, the thermally induced aberrations of the thin-disk would solely be defined by the homogeneity of the pump power distribution and the cooling concept. However, only pump spot diameters up to approximately two third of the disk diameter are practicable due to the aperture effect of the disk and manufacturing defects at the edges. Therefore, at the intersection between the pumped and un-pumped area in a thin-disk crystal a small radial heat flow takes place. For small diameters of the pump spot the part of the radial heat flow in relation to the overall heat dissipation is larger so that the heat is more evenly distributed between axial and radial direction. Thus, the

thermally induced variations of the refractive index of the disk in radial direction is less pronounced and can still be described as almost spherical. By increasing the diameter of the pump spot, which is certainly reasonable for power scaling, the temperature at the intersection between the pumped and un-pumped area of the disk exhibits a larger gradient since the temperature in the center of the pump spot stays almost constant in radial direction. Likewise to the refractive index, the thermal expansion of the disk is correlated to the temperature gradients. Both contributions induce a mainly aspherical phase distortion to the beam during its propagation through the thin-disk crystal. The aspherical optical phase distortion has a step-like shape. The stronger this step-like phase distortion is pronounced the higher are the diffraction losses for the fundamental-mode beam [22]. To illustrate the thermally induced optical phase distortions introduced by the thin-disk crystals during laser operation, detailed interferometric measurements and a comprehensive analysis are presented in chapter 5.

Summing up, the following thermal effects contribute to the optical phase distortion of the beam caused by a thin-disk crystal during laser operation and have to be considered in the analysis:

- Temperature dependence of the refractive index inside the laser-active material (mainly aspherical)
- Thermal expansion of the thin-disk crystal (mainly aspherical)
- Deformation of the rear side of the disk, mainly due to stress which is induced by different thermal expansions of the heat sink and the thin-disk crystal (mainly spherical)

Already at a beam parameter product of about 3 mm·mrad, the aspherical part of the phase distortion starts to cause a reduction of the efficiency and a degradation of the beam quality of the thin-disk laser. The aspherical part of the optical phase distortion should therefore be compensated with a static or adaptive mirror to guarantee a stable operation of the laser resonator as soon as the aberrations exceed a certain level. The spherical part can be taken into account to a large extent by the resonator design e.g. with the use of dynamically stable resonators [66]. A compensation with a spherically deformable adaptive mirror concept [67] is also possible but obviously more complex than the optimization of the resonator layout.

The thermally induced optical phase distortion of the beam when propagating through a thin-disk crystal during laser operation can be calculated by [22]

$$\Phi(r) = 2 \cdot \frac{2\pi}{\lambda_l} \left[\int_0^d [(n_0 + \frac{\partial n}{\partial T} \cdot (T(r,z) - T_c) + \Delta n_s(r,z) - 1] \cdot [1 + \varepsilon_z(r,z)] dz - z_0(r) \right]$$

$$(4.1)$$

where λ_l is the laser wavelength, d is the thickness of the disk, n_0 the refractive index, $\delta n/\delta T$ characterizes the change of the refractive index with temperature, T_c is the cooling temperature, Δn_s is the stress-induced change of the refractive index and ε_z the relative expansion of the length in z-direction. The point of reference is z_0 which is located at the backside of the thin-disk crystal.

Another contribution to the change of the refractive index in the laser-active material Yb:YAG has been investigated in [68] and should be discussed briefly in the present context. This contribution is the electronic lensing, which takes place due to the change of population of the excited and ground state in the Yb^{3+} active ion resulting in a different polarizability of the states. For pulsed pumping of the thin-disk crystal, a predomination of the electronic lens in comparison to the thermal lens was reported. However, the electronic lens has been evaluated [68] to approach zero for CW-pumping and is thus several orders of magnitude smaller than the thermal lens in this case. Even for the case that a measurement wavelength of 375 nm (measurement wavelength of the interferometer introduced in chapter 5) is chosen to analyze the optical phase distortions in thin-disk crystals during laser operation, the influence of the electronic lens on the measurement accuracy is still negligible. Hence, it was not taken into account in the analysis.

4.1.1   Influence of the laser-active material itself on the thermal load

The main parameters influencing the heat generation in a laser-active material and the heat extraction out of it, are the quantum defect regarding the first aspect and the heat conductivity for the latter. Heat generation and extraction are influenced by the doping concentration and the ability to implement the laser-active ion (Yb^{3+}) into the host. Here, the goal is to realize the lowest possible distortion of the structure of the host crystal. This will minimize the risk of the formation of additional non-radiative loss transitions. The heat load of each laser-active material which is caused directly by the quantum defect is pre-defined by the given pump wavelengths and cannot be influenced. The major contributing factors are therefore the non-radiative processes which can be caused by impurities, ion-ion-interaction, absorption of fluorescence radiation or spontaneous emission at impurity ions etcetera.

An evaluation of Yb-doped laser-active materials regarding their spectral and thermal properties have been reported in several publications, e.g. in [69], [16], [1]. For this purpose different figure of merits (FOM) have been introduced. In the following section the suitability of the four laser-active materials used in this thesis are analyzed with the FOMs proposed in [16]. Prior to the evaluation of the laser-active materials with FOMs,

the most relevant properties with regard to high-power cw and mode-locked thin-disk laser operation have been identified. These are the quantum defect, the emission cross section, the absorption bandwidth, the fluorescence lifetime, the gain bandwidth and the thermal conductivity. In general, the following properties are favorable:

- a large emission bandwidth is suitable to generate ultra-short pulses
- a small quantum defect to minimize the heat load
- a large emission cross section and a long fluorescence lifetime for a low laser threshold
- the availability of high-power pump diodes with reasonable brightness matching the absorption spectrum in terms of wavelength and bandwidth
- a large absorption cross section at the pump wavelength in combination with a high possible doping concentration to minimize the thickness of the disk
- a high thermal conductivity for efficient heat removal

Emission bandwidth, emission cross section and fluorescence lifetime of a laser-active ion are closely related to each other in such a way that not all the desired properties can be obtained simultaneously. For instance: for two different laser-active materials with an approximately equal fluorescence lifetime, a broad emission bandwidth typically leads to a small cross section.

The three FOMs established by Voss in [16] are explained below. They are used to quantify the favorable properties of the laser-active materials. To compare the FOMs of the considered materials, the calculated optimum disk thickness ($FOM_{opt-path}$) and the material properties listed in the tables of chapter 3 were used. The number of pump beam passes M_p is 24 for the calculations presented here. The FOM_{th-opt} describes the quality of the material with respect to the thermo-optical effects. It is defined by the ratio of the thermal conductivity λ_{th} to the thermo-optical constant K_{th-opt}

$$FOM_{th-opt} = \frac{\lambda_{th}}{K_{th-opt}} \qquad (4.2)$$

The higher the FOM_{th-opt} the better the heat extraction and/or the lower the thermal expansion of the laser-active material. A small thermal expansion is beneficial with regard to deformations and thus the thermally induced stress in the disks. Nevertheless, the high values for FOM_{th-opt} of Yb:LuAG and Yb:Lu$_2$O$_3$ (see table 4.1) can mainly be attributed to their high thermal conductivity. It should be noted that FOM_{th-opt} can have a negative value. This is the case for instance when the change of the refractive index of the laser host material with temperature is negative (like e.g. in Yb:CaF$_2$ or Yb:YLF). In

this case, the change of the refractive index with temperature acts opposed to the thermal expansion leading to a small value for K_{th-opt} and therefore a high value for FOM_{th-opt}.

To evaluate the laser-active material regarding an efficient absorption in thin-disk configuration,

$$FOM_{abs-disk} = \left| \frac{(3 \cdot M_p^2 \cdot FOM_{th-opt})}{l_{abs,eff}^2} \right| \qquad (4.3)$$

can be used, where $l_{abs,eff}$ denotes the effective absorption length of the pump radiation in the thin-disk crystal. In general, an absorption of about 90% of the pump radiation in the disk is considered as efficient [16]. The effective absorption is influenced by the doping concentration and the overlap of the pump spectrum with the absorption spectrum of the laser-active material. The $FOM_{abs-disk}$ for ZPL-pumped Yb:Lu$_2$O$_3$ amounts to $11.9 \cdot 10^{14}$ W/m^3 and is therefore about 2-10 times higher than the one of the other laser-active materials (see table 4.1). This is mainly due to the high absorption cross section of Yb:Lu$_2$O$_3$ at the ZPL pump wavelength which results in a comparatively short absorption length.

Table 4.1: Comparison of FOM_{th-opt} and $FOM_{abs-disk}$ of the laser-active materials Yb:YAG, Yb:LuAG, Yb:Lu$_2$O$_3$ and Yb:YAB.

	Yb:YAG	**Yb:LuAG**	**Yb:Lu$_2$O$_3$**	**Yb:YAB**
FOM_{th-opt} [10^6W/m]	0.44 (10at.%)	0.57 (10at.%)	0.65 (3at.%)	$\approx$0.49 (5.6at.%)
$l_{abs,eff}$ [mm]	2.36 (10at.% at 941 nm) 2.47 (10at.% at 969 nm)	2.74 (10at.% at 938 nm) 2.16 (10at.% at 969 nm)	3.05 (3at.% at 949 nm) 0.97 (3at.% at 976 nm)	1.09 (12at.% at 976 nm)
$FOM_{abs-disk}$ [10^{14} W/m^3]	1.37 (10at.% at 941 nm 1.25 (10at.% at 969 nm)	1.30 (10at.% at 938 nm) 2.09 (10at.% at 969 nm)	1.21 (3at.% at 949 nm) 11.9 (3at.% at 976 nm)	7.16 (12at.% at 976 nm)

The thermally induced optical path difference in the thin-disk crystal can be estimated with $FOM_{opt-path}$ which is given by

$$FOM_{opt-path} = \frac{1}{\Delta L_{opt}} = \frac{1}{K_{th-opt} \cdot \frac{q_{ges}}{\lambda_{th}} \cdot \frac{d^2}{3}}, \tag{4.4}$$

where ΔL_{opt} is the change of the optical path length in axial direction, q_{ges} is the heating power density in the disk and d is the thickness of the disk (here d_{opt} is used). Thus, this FOM allows an evaluation of the strength of the optical phase distortion that is expected to be present in the different thin-disk crystals during laser operation. The aim is to show the potential of the considered laser-active materials for the realization of a thin-disk laser with approximately 1 kW of output power and near diffraction-limited beam quality. For this purpose, an incident pump power of 2 kW on a pump spot diameter of 5.6 mm (E_p= 8.12 kW/cm^2) was defined for the following discussion of the four materials. To calculate the fraction of pump power which is converted into heat, the assumption of an ideal crystal quality was made so that only the quantum defect is considered. For Yb:YAB, literature data of Nd:YAB were used partly (see table 3.4) since the availability of data is limited. The calculated values of the FOMs for Yb:YAB should therefore only be considered as a rough indicator to know where to position this laser-active material with respect to the other three.

Table 4.2: Comparison of $FOM_{opt-path}$ of the laser-active materials Yb:YAG, Yb:LuAG, Yb:Lu$_2$O$_3$ and Yb:YAB.

	Yb:YAG	**Yb:LuAG**	**Yb:Lu$_2$O$_3$**	**Yb:YAB**
$FOM_{opt-path}$	44 (10at.%	51 (10at.%	40 (3at.%	115 (12at.%
	at 941 nm)	at 938 nm)	at 949 nm)	at 976 nm)
$[10^5 \text{ m}^{-1}]$	57 (10at.%	95 (10at.%	262 (3at.%	
	at 969 nm)	at 969 nm)	at 976 nm)	

These three figures of merit evaluate mainly the heat extraction capability of the laser-active materials in thin-disk configuration, under the assumption that there are no further non-radiative loss transitions or absorbing defects in the crystal structure. Therefore only the potential for high-power fundamental-mode operation at optimum crystal quality but, for instance, not the suitability to generate ultrashort pulses in particular can be analyzed with the calculated values. The comparison of the FOMs of these four laser-active materials predict the best performances for Yb:Lu$_2$O$_3$ when pumped at the ZPL-pump wavelength of 976 nm. However, also Yb:LuAG and Yb:YAB exhibit higher values for $FOM_{abs-disk}$ and $FOM_{opt-path}$ than Yb:YAG so that a high potential for good performances in thin-disk laser operation can be expected.

4.1.2   Influence of the contact layer and heat-extraction-method

After the invention of the thin-disk laser concept, three different methods have been established in order to contact the laser disk on the heat sink:

- Soldering, which requires an additional metallization on top of the HR coating on the backside of the disk
- Direct glueing of the HR coated rear side of the thin disk onto a heat sink
- Diffusion bonding of the front side of the thin disk to a support substrate which is AR coated

All three methods have different advantages and disadvantages which are discussed in the following with the aim to derive the concept which offers the best suitability for the generation of output powers at the kilowatt level with high brightness.
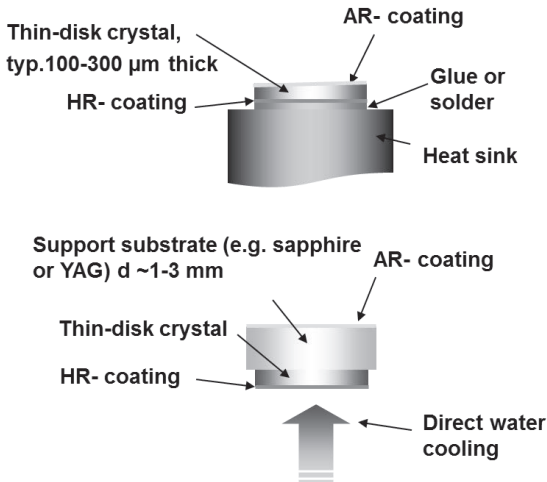
Figure 4.1: Established technical concepts of thin-disk modules. The image on top shows the concept where the water cooling is integrated in the heat sink. For the concept depicted at the bottom, the HR-coating of the thin-disk crystal is in direct contact with the cooling water.

Apart from some technical aspects, the mounting concept of the thin-disk crystal by glueing or soldering it on the heat sink is essentially the same. This is schematically shown in the top image of figure 4.1. The differences arise mainly from the contact material itself and furthermore from the necessity to apply a metallization on both adjacent

layers to be able to perform a soldering. In general, solders feature higher heat conductivities than glues so that thicker layers are permitted for comparative heat resistances. A typical thickness of a solder layer is about 50 μm, whereas for a glue the thickness should be 10 times lower or even less for efficient heat removal [17].

The advantage of the mounting concept with a support substrate on top of the thin-disk crystal (depicted at the bottom of figure 4.1) is the possibility to apply the cooling fluid directly at the backside of the disk. A disadvantage arises due to the low thickness of the thin-disk crystals of a few hundred micrometer. The support substrate therefore requires a certain thickness to mechanically stabilize the disk against the strong flow of the cooling water. The attachment of the support substrate with a typical thickness between one and three millimeter is usually realized by diffusion bonding. Materials like sapphire or YAG have been used for this purpose so far. The critical issue thereby is the non-negligible fraction of pump and laser radiation which is absorbed in the substrate. This causes strong thermally-induced aberrations inside the laser resonator. Consequently, thin-disk lasers applying this mounting method could not generate high-brightness radiation together with output powers at the kilowatt level by now. An interesting future prospect of this concept could be the use of single crystalline diamond as the substrate. It can be assumed that with the realization of diamond with low absorption, the exceptional high heat conductivity of this material will lead to a significant reduction of the thermally induced aberrations inside the substrate. However, it is still challenging to produce single crystalline diamond with a sufficient size (> 10 mm). The achievable maximum diameter is currently limited to about 9 mm [70]. Another critical issue is the further development of a bonding method which guarantees a stable contact between diamond and thin-disk crystal also for laser operation at high output powers.

Contrary to the previously discussed case, a thin-disk crystal which is mounted with the rear side on a heat sink exhibits lower thermally-induced aberrations. In this case, the only mechanism which generates heat in the disk is the laser process itself. Thus, an optimization of the heat distribution and the thermally induced aberrations is easier to obtain. For this reason, this mounting concept has been the method of choice in all experiments reported later on.

In order to develop thin-disk lasers operating at the high-power level not only the laser-active material and contact material itself have to be analyzed with regard to thermally induced-aberrations. These choices just open the discussion about parameters like hardness or stiffness and heat conductivity which has to be extended to all components present in a disk-heat-sink unit. For instance, the heat sink allows to influence the deformation and the heat extraction capability of a thin-disk crystal by a proper design. This topic shall be discussed further in the following section.

4.1.3   Influence of the heat sink on the heat extraction and deformation of thin-disk crystals

Two parameters of the heat sink directly affect the capability of heat removal and influence the deformation of the attached thin-disk crystal and thus the induced phase front deformation in the resonator. Firstly, the kind of material and secondly, the mechanical design i.e. the geometry of the heat sink. The influence of the previously discussed contact layer shall be neglected in the following considerations for the sake of simplicity.

For disks to be soldered with AuSn, the thermal expansion of the heat sink has to be adapted to the laser-active material e.g. Yb:YAG. This is due to the high melting point of AuSn of 280 °C [71]. Without adaption, the tensile strain would cause damage to the thin-disk crystal during the cooling phase of the two components after soldering. For Yb:YAG a good match of the heat expansion value is achieved when CuW containing 15 to 20 percent of copper is used for the heat sink. However, the thermal conductivity of the CuW compound is lower than for pure Cu resulting in a less efficient heat extraction. The higher stiffness of CuW is beneficial on the other hand as it reduces the overall deformation of the disk-heat-sink unit. With regard to heat conductivity and stiffness (see table 4.3) chemical vapour deposited (CVD) diamond plates are superior to all other heat sinks, but the low thermal expansion of this material makes it more difficult to solder a thin-disk crystal to it. Therefore, the mounting of thin-disk crystals on CVD-diamond heat sink plates by gluing is the method of choice for high-power thin-disk laser systems. The only drawback is the comparatively high price of CVD-diamond in comparison to other materials such as Cu, CuW, SiC etc. so that for thin-disk lasers with average output powers at the hundred watt level another choice could be more appropriate. The thermal conductivity and thermal expansion coefficient for the different heat sink materials are summarized in table 4.3.

Table 4.3: Comparison of the thermal properties of different heat sink materials investigated during this thesis.

	Thermal conductivity at 300 K	Therm. expansion coefficient at 300 K
Cu [72]	398 W/(m·K)	$17 \cdot 10^{-6}$/K
Cu20W80 [73]	235 W/(m·K)	$8.3 \cdot 10^{-6}$/K
6H-SiC (single crystal)[74]	490 W/(m·K)	$4\text{-}5 \cdot 10^{-6}$/K
CVD-diamond [75]	>1200->1800 W/(m·K)	$1 \cdot 10^{-6}$/K

One possibility to adapt the thermal expansion of the heat sink to that of the thin-disk crystal is the utilization of material compounds. Typically, metal compounds are used such as for instance the already mentioned CuW. The drawbacks of metals are a low stiffness and the abrasion by water. The latter point is a weak point especially for the industrial use of the heat sinks during long-term operation. Compounds where a ceramic is added to the copper could be an alternative. Substrates consisting of copper which is bonded to a ceramic, e.g. aluminium nitride (AlN), can be supplied from the company Curamik [76]. Different sandwich designs out of Cu and AlN slices have been investigated as a heat sink for thin-disk laser crystals [60]. For these sandwich-structures, the adaption of the thermal expansion to that of Yb:YAG has been obtained with a copper content of 50-60 %. First investigations of these sandwich-structures in the DiskModul project have been promising when using them in thin-disk lasers at moderate power levels (hundred Watt range) [60]. Nevertheless, for an utilization of AlN-Cu heat sinks at an optical output power in the kilowatt range, more comprehensive studies have to be carried out in the future.

To illustrate the influence of the heat sink material on the heat extraction out of the disk in more detail, one example is discussed in the following. The aim was to obtain a direct comparison of the heat-removal capability of copper and CVD-diamond heat sink disks for the laser-active material Yb:YAB (see material properties in chapter 3.2.4). For this purpose different FEM-simulations with COMSOL Multiphysics have been performed. It was assumed that an Yb:YAB disk (diameter= 6.3mm, thickness= 250 μm) is mounted with the same contact layer and therefore the same thermal resistance onto the heat sink. The heat sink disks had a diameter of 16 mm and a thickness of 2 mm. The optimum case for the thermal load was assumed, which is a transformation of 6.2% of the incident pump radiation into heat (that corresponds to the quantum defect of Yb:YAB). Different incident pump power levels from 100 W up to 500 W on a pump spot with a diameter of 2.6 mm were considered. The pump power densities varied from 1.9 kW cm^2 to 9.4 kW cm^2. The cooling of the heat sink was taken into account by setting the backside temperature of the heat sink to 15 °C (fixed constraint).
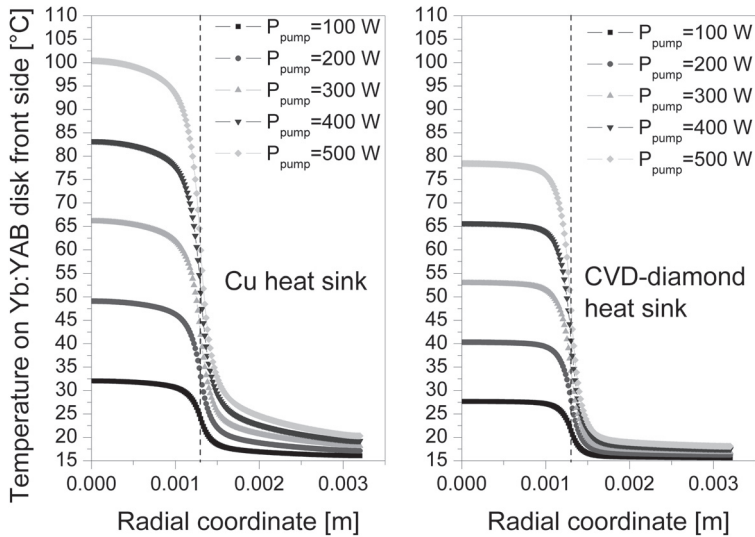
Figure 4.2: Numerically calculated temperatures on the top surfaces of the Yb:YAB thin-disk
crystals (diameter of 6.3 mm, thickness of 250 μm) for the case of a Cu (left) or
CVD-diamond (right) heat sink.

The resulting distribution of the surface temperature on the front side of the thin-disk
crystal is plotted in figure 4.2. The FEM-simulations show that the maximum tempe-
rature increase of the Yb:YAB disk can be reduced by approximately 23% when using
a heat sink consisting of CVD-diamond instead of copper. This lower temperature in-
crease, together with the higher stiffness of CVD-diamond allows to reduce the overall
deformation of the Yb:YAB disks.

The example shows that beside the already mentioned issue of higher cost, an incre-
ase of the performance of most laser-active materials in thin-disk configuration at the
high-power level can be achieved by using heat sinks made of CVD-diamond. However,
another disadvantage of CVD-diamond should be mentioned. The thermal expansion
(see table 4.3) is very low, which can result in an increase of stress in the thin-disk
crystals or even a fracture of the disk during laser operation. This is particularly criti-
cal for laser-active materials with low hardness and/or a large difference of the thermal
expansion for the different axes of the crystal.

4.1.4   Influence of the intensity distribution of the pump radiation on the brightness of the laser beam

In addition to the properties of the contact layer and the heat sink, also the intensity distribution of the pump radiation influences the achievable brightness of the oscillating laser beam. Readers for which the optical layout of a pump beam delivery of a thin-disk laser system is completely unknown (for the basic principle see chapter 3.1 and reference [18]) can find one example of a pump optics unit containing a homogenizing rod in figure 6.2. Instead of a rod, also a fiber can be used for the homogenization of the pump radiation. This is typically the case for fiber-coupled laser diodes. Both versions of homogenization use an optical collimator afterwards so that together with the parabolic mirror an image of the exit facet of either the fiber or the rod is generated on the thin-disk crystal.

It has been determined that the intensity distribution of the pump light in a thin-disk laser can introduce a radially varying gain profile due to an inhomogeneity of the pattern. This can lead to a coupling of radiation into higher-order modes and thus has to be minimized for fundamental-mode operation. A detailed theoretical analysis of the deteriorations of a laser beam induced by distortions inside the cavity such as e.g. the distribution of the pump power can be found in [77]. In practice, the mode behavior of the resonator has to be analyzed with regard to the actual condition of the pump spot on the disk at different operation points. In fact, there are different parameters which influence this intensity distribution of the pump radiation:

- Degree of homogenization of the pump radiation by the utilized rod or fiber
- Geometrical shape of the exit facet of the rod or fiber
- Number of pump beam passes (intrinsic parameter of the thin-disk pump module)
- Quality of the image obtained by the collimation optics
- Thermal deformation of the parabolic mirror at high pump power densities

By investigating these parameters one major aspect has to be adequately examined: the extraction of a Gaussian shaped fundamental mode from the laser disk with an intensity distribution of the pump radiation which has approximately a top-hat shape. This shape can be observed for a typical intensity distribution generated by imaging the end facet of a rod or fiber onto a disk (see as examples, images 4.5 and 4.6 correspondingly). The typical shape of the intensity distribution of the pump radiation for the pump sources utilized in this work is actually not a sharp top-hat but rather a Super-Gaussian profile with an exponential order varying between 8 and 12 (see calculated plots in figure 5.6). In all cases, the Gaussian fundamental laser mode does not efficiently extract the energy of the

outer gain area generated by the overlapping pump spots which leads to higher temperatures at these positions. However, the closer the intensity distribution of the image of the pump radiation gets to a Gaussian profile, the lower are these temperature differences.

Another point to consider when analyzing the intensity distribution of the pump radiation is the achievable degree of homogeneity of the optical image of the pump spot which is influenced by the guiding properties of the utilized rod or fiber. Radiation which is propagated through a fiber with a core diameter of e.g. 0.6 to 2 mm and a length of 5 m has typically a quite homogeneous intensity distribution, whereas radiation propagating through a cylindrical rod with a diameter of 5 mm and a length of 20 cm has still a rather non-uniform intensity distribution with localized intensity fluctuations after the propagation. However, a further enhancement of the degree of homogenization of the intensity distribution is obtained by the pump optics of the thin-disk pump module itself. This is due to the rotation of the image of the pump spot on the disk which is caused by the rotation (in axial direction) of one prism pair of the thin-disk pump module. For a pump module with 24 passes, the angle of rotation of the upper prism pair is 15° corresponding to a rotation of the re-imaged pump spots by 60° for each double-pass of the pump radiation through the thin-disk crystal (see details of the principle in [18]). A comprehensive insight into the topic of beam-shaping of the pump radiation for high-power thin-disk lasers can be found in [78].

Fibers or rods have typically plan-parallel end facets whereby the resulting image on the thin-disk crystal is elliptical (see figure 4.3) due to the off-axis incidence on the parabolic mirror. By using commercially available fiber-coupled laser diodes with LLK or SMA fiber connectors the end-facet is not accessible for a post-processing so that a compensation of this effect by altering the end facet is difficult to realize. Nevertheless, the rotation of the image of the pump spots by the prisms reduces this ellipticity and supports the formation of an overall circular image of the overlapping pump spots as can be seen in figure 4.4.
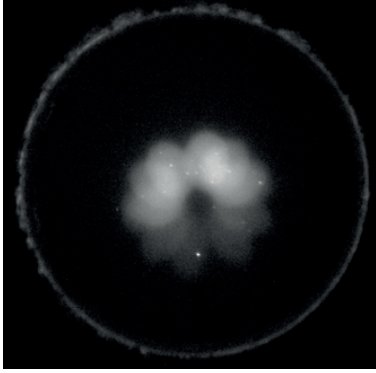
Figure 4.3: Individual, slightly elliptical images of the pump spots which occur due to a displacement of the disk in z-direction with regard to the focal plane of the parabolic mirror.
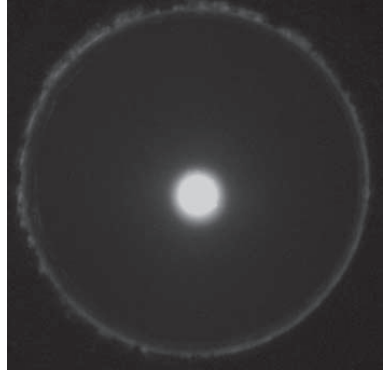
Figure 4.4: Overlapped pump spots when positioning the thin-disk crystal in the focal plane of the parabolic mirror. In both figures the images of an end facet of a fiber are shown.

Contrary to fibers, rods are often manufactured individually, which allows to polish the exit face with a defined angle in order to compensate for the slightly elliptical shape of the pump spot (an example of a homogenizing rod is displayed in figure 6.3). To illustrate the effect that an exit face with specific angle has on the intensity distribution of the pump spot image, a few examples are given in figure 4.5. The two pictures on top (4.5 a) and b)) show the images of a pump spot generated by a circular rod and the two pictures underneath (4.5 c) and d)) are the images obtained by using a rod with octahedral geometry. Both rods had an end facet which had a specific angle. In pictures 4.5 a) and b) the effect of a pump spot defocusing by the collimation lens can be seen. This is the simplest method to reduce the strong temperature gradient between pumped and unpumped area of the thin-disk crystal. A more detailed analysis of this approach to directly influence the aspherical phase front deformation was obtained with high precision interferometric measurements. The summary of the performed measurements, together with the description of the interferometric setup is given in chapter 5.
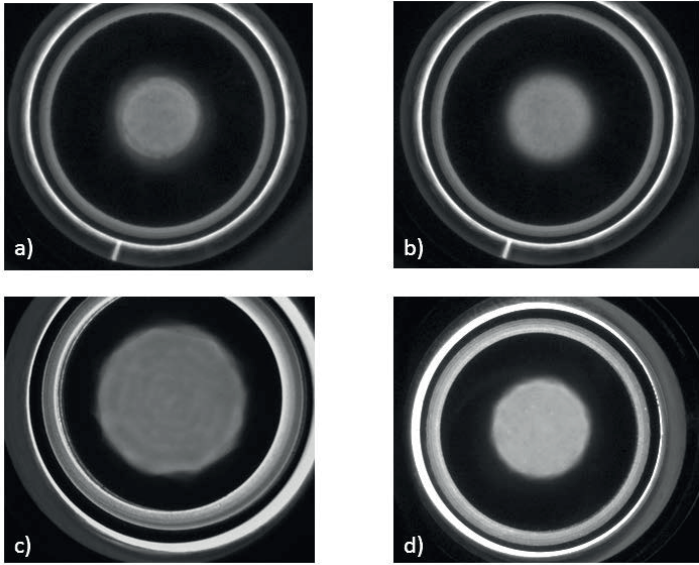
Figure 4.5: Different intensity distributions in pump spots obtained by homogenizing rods. a) sharp image of the pump spot of a circular rod with angled exit face; b) defocused image of the pump spot due to shift of a z=3 mm of the collimation optics after the circular rod; c) sharp image of the pump spot of an octahedral rod with angled exit face and 20 pump beam passes; d) sharp image of the pump spot of an octahedral rod with angled exit face and 24 pump beam passes.

In picture 4.5c) and 4.5d) images of the pump spot of a octahedral rod are shown. The difference in this case is the number of pump beam passes which is reflected by the "roundness" of the image. After 20 pump beam passes (shown in figure 4.5c)) the contour of the octahedron is still detectable, whereas by an increase of the number of pump beam passes to 24 an almost circular image shape is obtained (figure 4.5d). This "smoother" edge of the image is also beneficial with regard to a realization of a homogeneous intensity distribution of the pump radiation.
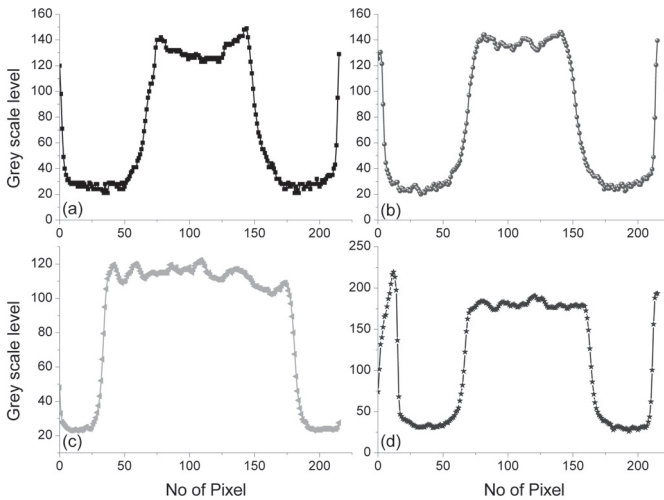
Figure 4.6: Corresponding horizontal cross-sectional profiles of the pump spot distributions shown in figure 4.5. Plots of the relative intensity (grey scale) versus the number of pixels of the CCD-camera.

The cross sections through the different intensity distributions of the pump radiation (discussed above) allow to determine more accurately the intensity variations in the central part as well as the contour of the edge of the different pump spots. A non-uniformity of the intensity distribution in a horizontal cross section of the pump spot profile indicates a potential source of optical aberrations due to a misalignment of the pump spots or a non-perfect overlap of pump spots and laser mode (can be detected with an additional IR-filter in front of the camera). Non-uniformities in the image of the pump spot should therefore be minimized. For instance, by comparing the plot in figure 4.6b to the one of figure 4.6a, lower aberrations of the fundamental mode due to a smoother profile for the case of 4.6b can be expected. The imaging of the pump spot by a CCD-camera is therefore a comparatively simple method to predict thermally induced aberrations that may be caused by an inhomogeneous intensity distribution of the pump spot.

4.2   Thermal effects in front of the thin-disk crystal

Beside the thermal effects which occur inside the thin-disk crystals, also the thermally induced optical inhomogeneity of the air in front of the disk has to be taken into account.

This is due to the high temperature of the surface of the disk of more than 100 °C at pump powers of several kilowatts. The heat transfer from the disk to the air next to the disk surface causes a temperature gradient in the ambient atmosphere, which results in a change of the density of the air. The air density decreases so that an upward laminar flow is formed (see figure 4.7) which is affected by the frictional forces. To simulate the distribution of the temperature and the velocity of the flow as depicted in figure 4.7, a simplified assembly of disk, heat sink and cooling layout was used. The additional air flows which are typically generated by the heated deflecting prisms and the parabolic mirror surfaces inside the pump cavity have been neglected. One can assume that the previously described free convection laminar flow at lower powers transforms into a more complex air flow in high-power systems exhibiting small turbulences in front of the disk.
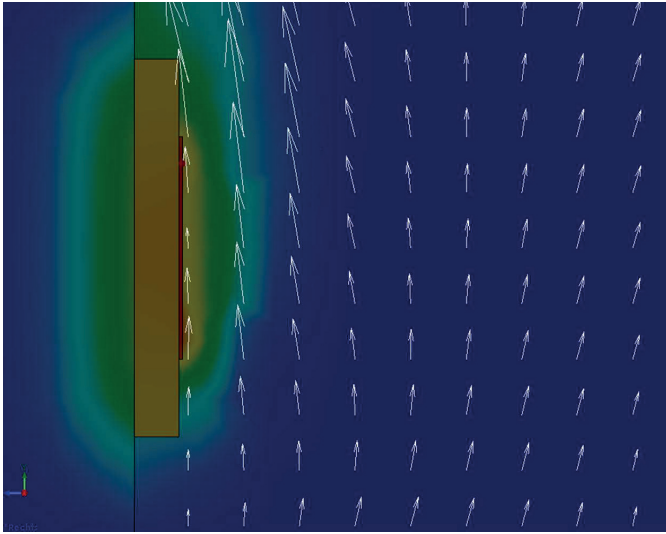
Figure 4.7: Numerical calculation of the temperature distribution and the air velocities in front of a thin-disk crystal mounted on a heat sink. False-color graphic with blue= minimum temperature (ambient air) up to red= maximum temperature (> 100°C inside the disk) and the velocity vectors.

The density- and thus the thermally induced variations of the refractive index in the air in front of the thin-disk crystal add to the phase distortions of the laser beam. These wedge-shaped wavefront distortions which occur in air under ambient atmosphere are in the order of several tens of nanometers and non-static, which makes it difficult

to compensate them. Nevertheless, these wavefront distortions are strongly reduced by operating the pump cavity in helium atmosphere. The next step in order to completely avoid them is the operation of the laser in a vacuum chamber. However, a vacuum setup is quite costly so that a thin-disk laser setup which allowed a flushing with helium was realized due to the simpler construction requirements. This setup was used for the experiments presented in the sections 5.2.1, 5.2.2 and 7.1.

Table 4.4: Comparison of thermal and optical properties of air and helium

Properties	Air	Helium
Density (25°C, 1bar)	1.22 [kg·m^{-3}]	0.44 [kg·m^{-3}]
Specific heat capacity	1007 [J/(kg·K)]	5194 [J/(kg·K)]
Heat conductivity	0.024 [W/(m·K)]	0.150 [W/(m·K)]
Refractive index (at a wavelength of 1030 nm)	$1+2.74\cdot10^{-4}$	$1+3.475\cdot10^{-5}$
Refractive index change with temperature: dn/dT (at a wavelength of 1030 nm)	$-0.88\cdot10^{-6}$ [K^{-1}]	$-0.116\cdot10^{-6}$ [K^{-1}]

The lower refractive index of helium in comparison to air results in an 8 times lower value of dn/dT. Together with a 6 times higher value for the heat conductivity (see table 4.4) this significantly reduces the phase distortions of the laser radiation passing in front of the disk. To underline the benefit of a helium atmosphere, a direct comparison of the overall phase front deviation induced in front of the disk (see figure 5.8) in air and helium is given in section 5.2.1. The measurements of the phase front deviations were performed at a pump power density of 10.7 kW/ cm^2 during laser operation. The high-precision interferometer used for this purpose is presented in the following chapter.

5 High-precision interferometer to evaluate the optical phase distortions induced by thin-disk crystals during high-power laser operation

Numerical modeling of the temperature distribution in thin-disk laser crystals [79], [80], [81] and the related thermally induced aberrations in thin-disk laser resonators was started soon after the invention of this laser concept. However, it is nowadays still difficult to obtain precise information about the optical phase distortion (OPD) solely by numerical modeling. This is due to the limited accuracy of the input data which are needed for every FEM-analysis. This applies to the material properties of the laser-active material, contact layer and the heat sink material. In addition, the heat conductivity, heat resistance, thermo-optical constants etc. have to be measured or be available in literature as well. A further difficulty arises from the large difference between the size of the thin disk, the contact layer and the heat sink, which makes it more complex to generate the correct mesh for the FEM-analysis especially at the geometrical interfaces. Instead, a calculation by defining heat resistances at the interfaces can be done, however, these values are rarely given in literature and therefore have to be determined experimentally.

A direct measurement of the distortions of the optical phase induced by the thin-disk crystal during fluorescence and laser operation is often the most accurate approach. Hence, different methods to measure the parameters such as e.g. the change of the radius of curvature of the disk or directly the OPD induced by the thin-disk crystal were investigated. From these measurement methods, the interferometric [82] and Shack-Hartmann based ones [83], [81] are most frequently used for the characterization of thermally induced aberrations. A critical point to consider for the measurement in thin-disk lasers is the permanent vibration of the thin-disk crystal which is due to the impingement cooling applied at the backside of the heat sink. Using Shack-Hartmann sensors for the analysis provides vibration insensitivity, but the resolution is lower than for interferometric setups. Therefore, only the interference stripe analysis (detection of the deformation of one interference stripe) was used as an interferometric measurement concept for this purpose up to now [82]. Another challenge regarding the measurement is the small am-

plitude of the aspherical distortion which is in the range of a few tens to hundreds of nanometer. Nevertheless, this small aspherical distortion has a strong influence on the diffraction losses of the resonator beam. A high resolution of the measurement is therefore a stringent requirement to obtain the accuracy which is needed. For this reason an interferometric measurement setup was developed which allowed the use of the phase shifting technique despite the vibration of the disk. To obtain vibration insensitivity, a simple optical method was applied which is explained in the following section. In a more recent development, the camera based shearing interferometric device of the company Phasics appeared to also be a good alternative for an accurate measurement and is therefore compared to the setup presented here at the end of this chapter.

5.1   Description of the interferometric setup

A measurement wavelength of 375 nm was chosen for the interferometer. This short wavelength permits to measure the OPD with higher sensitivity than e.g. at 1064 nm or 515 nm. Moreover the wavelength of 375 nm is close to the third harmonic of the laser wavelength at 1030 nm. This results in an anti-reflective behavior of the typical front-side coating and a high reflectivity at the backside coating of the laser disk. This also allowed an accurate measurement of the deformation of the rear side of the disk. Apart from this, the wavelength of 375 nm is spectrally well separated from the fluorescence and laser emission for all Yb doped laser-active materials ($\approx$ 900-1100 nm), which simplifies the filtering of the measurement signal.

A schematic drawing of the optical setup can be seen in figure 5.1. The basic principle of the interferometer is a common-path Mach-Zehnder configuration. The used light source was a linearly polarized (1000:1) laser diode (Oxxius S.A; OXX-375-07-CE) with a maximum output power of 15 mW. The already polarized laser beam was prepositioned regarding the forthcoming setup which means that the polarization of the laser diode was orientated at 45° to the horizontal axis. Behind the diode, a Keplerian-telescope was placed which magnified the collimated beam to a diameter of approximately 18 mm. The expanded beam then passed through a thin-film polarizer (extinction ratio >10.000:1) which was oriented parallel to the polarization state of the laser diode to further enhance the degree of polarization. After the polarizer, the beam was divided into two beams with orthogonal polarization states (horizontal- and vertical-polarization, respectively) by a polarizing beam splitter (PBS1). This polarizing beam splitter was the first element of the core part of the common-path Mach-Zehnder type interferometer which consisted in addition of a beam combiner (PBS2), two lenses (L1,L2) and two reflective mirrors

(M3, M4). One of the mirrors (M3) was mounted on a piezoelectric transducer (PZT) to perform the desired phase shifts. An important element of the interferometer was the implementation of a focusing lens (L1) in one of the interferometer arms which had its focal plane directly located on the disk. This created a reference beam which can be described as an almost ideal wave emerging from a point source. Due to its small diameter on the disk, this beam is almost insensitive to deformations and movements of the thin-disk crystal in radial direction. The second beam remained approximately collimated and served as probe beam which contains the information of the optical phase difference and therefore the path length change in the thin-disk crystal. Both beams propagate in a common path after the Mach-Zehnder part of the interferometer and are incident on the thin-disk crystal so that they experience exactly the same vibrations of the disk during a measurement. This is the key point of the interferometer to obtain the desired vibration insensitivity in order to apply the phase shifting technique.
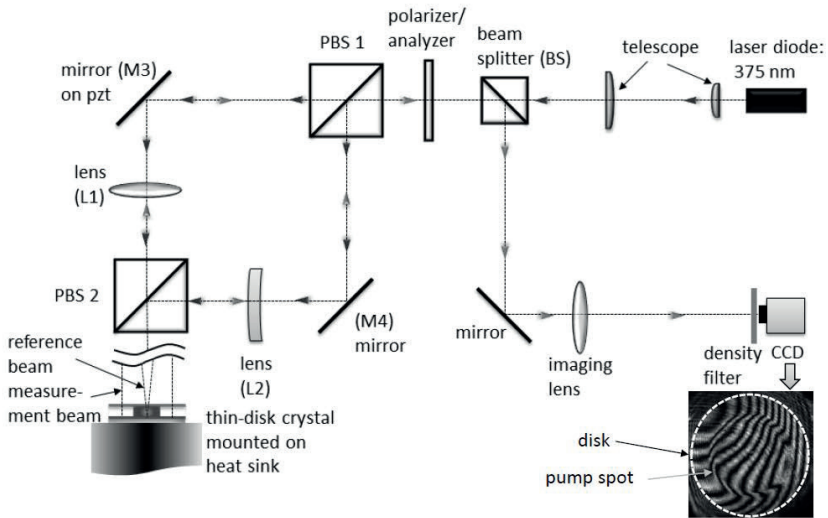
Figure 5.1: Schematic setup of the interferometer

Reference and probe beam are reflected at the HR-coated rear-side of the thin-disk crystal. The backward propagation followed approximately the same path like the incident beams. However, the propagation of the probe beam is influenced by the radius of curvature of the thin-disk laser crystal, which resulted in a focusing of this beam for the given constellation. For this reason, an additional compensating lens (L2) was implemented

in the beam path. After passing through the analyzer, the beams were redirected by a beam splitter and finally imaged on a silicon-based CCD camera. A laser-line filter at a wavelength of 375 nm in front of the camera assured a sufficient reduction of ambient radiation at other wavelengths.

The coherence length of the used laser diode is only in the order of a few 100 μm, which made it necessary to have almost equal path lengths for both arms of the interferometer. Therefore, the position accuracy of the optical elements in the Mach-Zehnder part had to be high. This was obtained by a rigid mechanical mount of the middle block (holding PBS1, PBS2, M3 and M4) manufactured within close tolerance limits, together with the usage of a 3-screw mirror mount to fine adjust the z-plane of mirror M4. The short coherence length of the laser diode on the other hand avoids spurious interferences from other optical elements in the setup.

The high resolution obtained with this interferometer can be evidenced by the image of the CCD-camera given in figure 5.1. This image was captured at a pump power density of only 0.7 kW/cm^2. In addition to the use of a comparatively short measurement wavelength of 375 nm and the application of the phase shifting technique (see section 5.1.2), the resolution of the interferometer was further enhanced by using defined polarization states, since the achievable contrast is higher compared to interferometers with non-defined ones.

To obtain not only a high relative accuracy of the interferometric measurements but also a high absolute one, specific optical properties of the LAM of the disk at the wavelength of 375 nm have to be known for an exact analysis. Therefore, the determination of the conversion factor between the laser wavelength of 1030 nm and the measurement wavelength of the interferometer of 375 nm for the laser-active material Yb:YAG was performed as described in the following section.

5.1.1 Determination of specific optical properties of Yb:YAG at the wavelength of 375 nm

In order to derive the change of the optical path length induced by an Yb:YAG disk when measuring at a wavelength of 375 nm with the previously described interferometer; the wavelength dependency of the refractive index had to be taken into account. This implied the determination of the difference between the thermo-optical constant K_{th-opt} (see chapter 3.2 for the equation) of Yb:YAG for the two wavelengths of 375 nm and 1030 nm. Beside the refractive index n, the constant K_{th-opt} furthermore depends on the

thermal expansion α_{th} and the refractive index change with temperature dn/dT. Strictly speaking, the dependence of these material parameters on the temperature and also on the Yb doping concentration should be considered. However, this was not possible in all cases due to a lack of reliable data in the literature. For instance, the refractive index at the wavelength of 375 nm was derived to be 1.872 by extrapolation of the dispersion curve of undoped YAG. It was assumed that the refractive index at a wavelength of 1030 nm is 1.818. In addition, the Yb:YAG samples used to determine the material parameters, as reported below, had not exactly the same Yb doping concentration as the thin-disk crystals used in the experiments later on. These small deviations should be mentioned and kept in mind even though it can be expected that they have only a minor influence on the overall accuracy of the determined optical phase distortions.

In reference [17] the value of dn/dT of Yb:YAG at a wavelength of 1030 nm and a temperature of 80°C was reported to be $9.84 \cdot 10^{-6}$/K. To estimate the corresponding value at a wavelength of 375 nm, the change of the optical path length $\Delta(n \cdot L)$ with temperature was determined experimentally by using the fringe counting method. For this purpose, a 10x10x10 mm large sample of Yb-doped (12%) YAG was placed in one arm of the Mach-Zehnder part of the interferometer and subjected to different temperature increases ΔT. Holder and heating device had been constructed in such a way that a very efficient heat input in the sample and a good isolation of the sample to the surrounding was guaranteed. This was necessary in order to minimize the measurement error due to the temperature difference between sample and ambient air. The value of dn/dT for temperatures between 80°C and 150°C was calculated according to [84] by:

$$\frac{dn}{dT} = n \cdot \left(\frac{1}{n \cdot L} \cdot \frac{\Delta(n \cdot L)}{\Delta T} - \frac{1}{L} \cdot \frac{\Delta L}{\Delta T} \right), \qquad (5.1)$$

where L is the geometrical length of the YAG sample, and yielded $30.0 \pm 0.9 \cdot 10^{-6}$/K. This value and the one of the heat expansion $\alpha = 6.34 \cdot 10^{-6}$/K (T= 300 K) given in [22] allowed to determine a conversion factor of 2.78 for K_{th-opt} of Yb:YAG between the two wavelengths of 375 nm and 1030 nm. The high value of dn/dT at a wavelength of 375 nm increases the sensitivity of the measurement of the path length change by approximately eight times when compared to a measurement at the wavelength of 1030 nm ($dn/dT = 7.3 \cdot 10^{-6}$, interferometric measurement in double pass).

5.1.2 Analysis method of the interferometric measurements

The μ-shape interferometry software of the company Trioptics (formerly FISBA OP-TIK) was used for the control and the calibration of the PZT of the interferometer and to record the interferometric patterns. Prior to the measurements with incident pump radiation, an interferogram of the unpumped ("cold") thin-disk crystal was taken as reference. In order to determine the optical phase difference with respect to the initial phase, the five-phase algorithm [85], [86] was automatically applied by the software. For this purpose five intensity distributions, each with a phase shift of $\pi/2$ between each image, were recorded. The first and the fifth interferometric pattern should be identical; as a consequence this method is examining itself which allows to minimize systematic measurement errors due to miscalibration of the phase steps. The distortions of the optical phase at a single reflection at normal incidence on the thin-disk laser crystal were calculated from the recorded phase maps. By this, all optical phase distortions, induced by the thin-disk crystal and also of the atmosphere in front of it, are considered. As an example, a measurement graph of a typical OPD induced by an Yb:YAG thin-disk crystal (mounted on a CVD-diamond heat sink) during laser operation is given in figure 5.2.
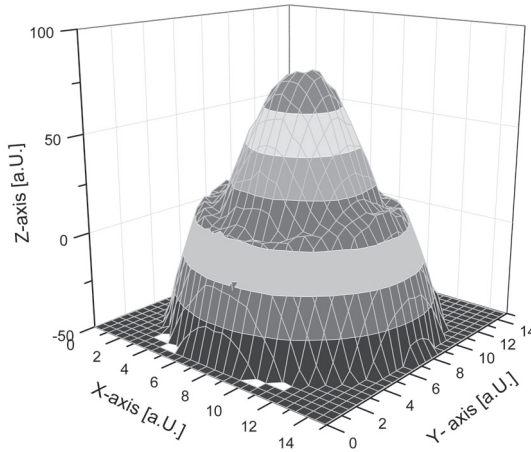
Figure 5.2: Typical OPD induced by an Yb:YAG thin-disk crystal during laser operation including the distortions in the atmosphere in front of the disk. The laser disk was mounted on a CVD-diamond heat sink. The measurement data were exported and plotted with Origin.

Two essential parameters of thin-disk lasers can be derived from the interferometric

measurements. One is the determination of the optical path difference of the wavefront
between the unpumped disk and the disk during laser operation (mainly aspherical) and
the other one is the thermally induced refractive power of the thin-disk crystal (spher-
ical). To obtain the latter one, a parabolic fit (e.g. figure 5.4) can be applied to the
measured OPD of the disk. Another possibility is the extraction of the radius of curva-
ture of the disk from the Zernike focus term provided by the software, since for every
measurement the Zernike polynomials are calculated automatically. The software provi-
des different features to export the recorded data. Either an export of a cross-section in
x- or y-direction or of a complete OPD (data matrix) can be performed (see figure 5.2).
The fit of the cross-sections allows a fast and already quite accurate analysis since the
OPD induced by the thin-disk crystal is radially symmetric in a first approximation. Ho-
wever, for a more detailed analysis, especially with regard to small, localized deviations,
the comprehensive three-dimensional (3D) fit of the phase matrix is more appropriate.
To perform the fit, conventional software like e.g. Origin or Matlab can be used.
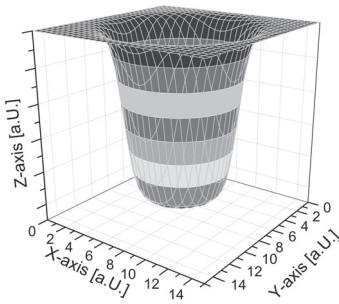
Figure 5.3: Example of a fit-function to appro-
ximate the aspherical part of the OPD induced
by the thin-disk crystal during laser operation.
To perform this fit either a higher-order Gaussi-
an distribution or a Fermi-Dirac distribution can
be used.
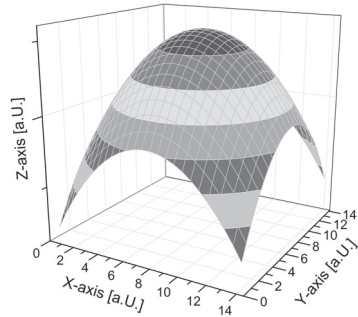
Figure 5.4: Example of a parabolic fit to ex-
tract the spherical deformation of the thin-
disk crystal during laser operation. The sphe-
rical and the aspherical distortion induced by
the laser disk possess opposite signs.

In order to obtain an accurate data analysis the choice of the fit functions is an essential
issue since the different parts (aspherical and spherical) of the thermally induced OPD
are superimposing each other. This is especially important for the exact determination
of the aspherical part of the distortions in order to be able to perform a compensation
later on. To apply a fit to the approximately step-shaped aspherical part (see figure 5.3
for an example) of the OPD, the step height and steepness of the edges has to be ap-

proached quite accurately as explained in the following. Beside the correct choice of the fit functions, the selection of suitable starting values are also important in order to allow the fit algorithm to converge towards appropriate values or even to converge at all. This is especially indispensable for a 3D-fit since the number of parameters is quite high and the spherical and aspherical contribution to the distortions induced by the laser disk additionally have opposite algebraic signs.

Taking as example the OPD of the thin-disk crystal during laser operation shown in figure 5.2, the bending of the disk which is largely spherical can also be well approximated by a 4th order polynomial function:

$$f(x,y) = (z_0 + A_2 \cdot (x - x_0)^2 + A_4 \cdot (x - x_0)^4 + B_2 \cdot (y - y_0)^2 + B_4 \cdot (y - y_0)^4), \quad (5.2)$$

whereas x_0, y_0 and z_0 define the center of the function. The approximation by a 4th order polynomial function is based on the solution for a deformation of a clamped thin plate with homogeneous rigidity and an uniformly distributed load [87]. Subtracting the fitted 4th order polynomial function from the measured OPD of the disk results in a residual distortion which is mainly ashperical. The aspherical, step-shaped distortion which is left can be well approximated by either a Fermi-Dirac or Super-Gaussian distribution.
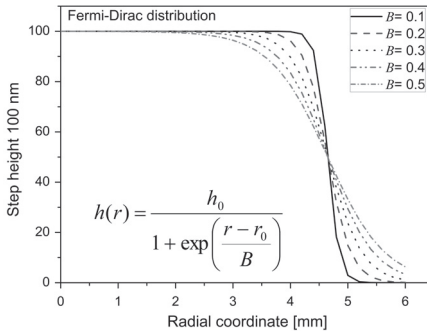
Figure 5.5: Fermi-Dirac distribution as example for a step height of 100 nm for different values of B. For a sharp image of the pump spot on the disk B is typically in the order of 0.25.
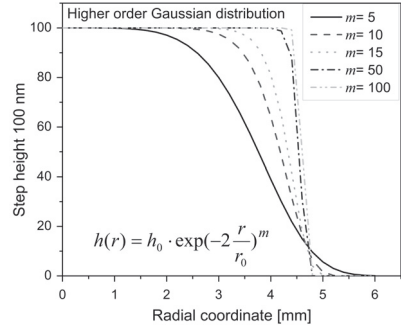
Figure 5.6: Higher order Gaussian distribution as example for a step height of 100 nm with increasing factor m. For a sharp image of the pump spot on the disk m is typically in the order of 10.

The difference between these two functions lays in the definition of the steepness of the edge, which is either defined by the order number m (Super-Gaussian distribution) or

the quality factor B (Fermi-Dirac distribution). In fact, the steepness or, in other words, roundness of the edges controls the diffraction of the circulating laser mode. Generally one can say that the higher the value of m or the lower the value of B, the sharper the edges of the aspherical part of the OPD. This results in a higher diffraction which corresponds to a larger power loss for the circulating mode inside the resonator. Depending on the distribution of the pump intensity on the laser disk either the Fermi-Dirac or the Super-Gaussian function corresponds better to the actual shape of the aspherical distortion. For this reason either the former or the latter was used to fit the aspherical part of the OPD induced by the disk during laser operation.

5.2   Results of interferometric measurements during high-power laser operation

The interferometric measurements presented in the following section have been selected to discuss two important issues of high-power thin-disk lasers:

- influence of the atmosphere in front of the disk on the OPD during laser operation
- influence of the sharpness of the pump spot image on the aspherical aberrations induced by the thin-disk crystal

In this chapter it is illustrated that measurements performed with the previously described interferometer did not only permit a detailed analysis of the thermally induced distortions of the laser disk, but also allowed to investigate the influence of the atmosphere in front of it. This topic has been already introduced briefly in chapter 4.2 and shall be discussed further with the help of the data acquired by the interferometric measurements. The measurements were conducted during laser operation whilst the laser cavity was either operated in ambient air or in helium atmosphere. A V-shaped laser resonator was used which allowed reference and probe beam of the interferometer to have their incident axis perpendicular to the laser disk. The laser disk was pumped at a wavelength of 940 nm.

5.2.1   Interferometric measurements to analyze the influence of the ambient atmosphere on thermal effects in front of the thin-disk crystal

For a given design of the disk-heat-sink-unit (here: disk glued on diamond) and diameter of the pump spot (here: 9.4 mm), the amplitude of the thermally induced OPD of the laser disk scales with the incident pump power. This correlation can be seen in figure 5.7. The measurements include the optical phase distortions in front of the

disk and were performed in helium atmosphere. The highest pump power density of 10.7 kW/cm^2 corresponds to a laser output power of $\approx$ 4 kW for the resonator configuration (multimode resonator consisting of a plane HR and a plane OC 96%) used during this experiment.
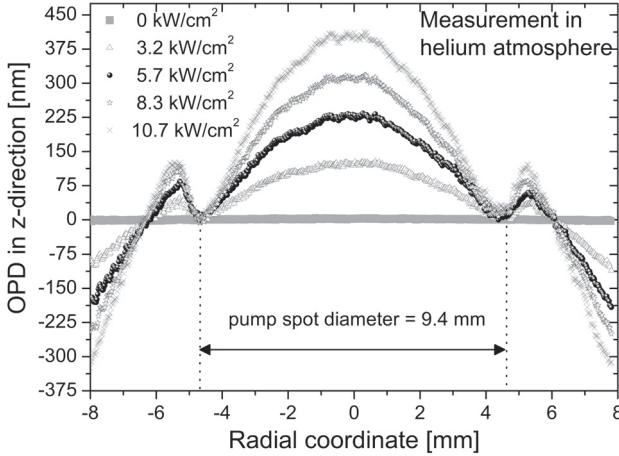

Figure 5.7: Profiles of the OPD induced by an Yb:YAG thin-disk crystal during laser operation, including the optical phase distortions in the helium atmosphere in front of the disk, for different pump power densities (pump spot diameter of 9.4 mm, pump wavelength of 940 nm). The laser disk was mounted on a CVD-diamond heat sink.

In order to analyze the effect of the atmosphere in front of the disk when operating the laser either in helium or in air, a direct comparison of the OPD of the thin-disk crystal for both cases is shown in figure 5.8 for a pump power density of 10.7 kW/ cm^2.
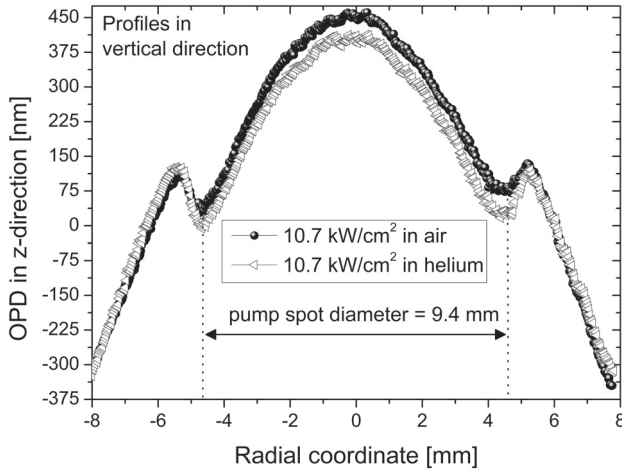
Figure 5.8: Comparison of the thermally induced OPD of the thin-disk crystal during laser operation including the distortions in front of the disk when operating the laser resonator either in air or helium atmosphere.

The difference of the two profiles arises from the fact that at several kilowatts of pump power the temperature of the disk surface is larger than 100°C and therefore a thermally induced optical inhomogeneity of the atmosphere in front of the disk takes place which is much more pronounced in air than in helium. The inhomogeneity is wedge shaped and can be identified in the graph by the tilt of the profiles of the measurement in air when compared to the one in helium. The stronger pronunciation of the wedge in air results from its higher refractive index, its larger change with temperature and its poorer heat conductivity (see table 4.4 for the properties). These parameters are significantly better in helium, which reduces the distortions in front of the disk remarkably (see section 4.2 for a more detailed discussion). In addition, distortions in an air atmosphere are more difficult to control so that a major part of the measurements were conducted with a thin-disk laser operating in a helium atmosphere. However, the difference between the two atmospheres is quite small which makes the determination so challenging. For the present case, a difference of the thermally induced OPD of the laser disk in the order of 50 nm was measured.

5.2.2 Interferometric measurements to analyze the influence of the sharpness of the pump spot image on the aspherical contribution to the OPD

The evaluation of the interferometric measurements which include the determination of the aspherical step-shaped distortions of the wavefront induced by the disk during laser operation allows to determine the influence of the distribution of the pump intensity to the oscillating mode(s) in the resonator. To emphasize this topic, a study was undertaken which analyzed the influence of the position of the pump spot image in z-direction (defocusing) on the aspherical part of the thermally induced distortions. Interferometric measurements were carried out during the operation of the previously described high-power thin-disk laser resonator in helium atmosphere. The results which are presented in the following were obtained at approximately 2 kW of laser output power (multi-mode) with a pump power density of 5.7 kW/cm^2. The defocusing of the pump-spot image was performed by moving the collimating optics in z-direction. At the position $z = 0$ of the collimating optics the pump spot image on the disk was sharp. The position of the optics was altered to the maximum defocusing position of $z = -4$ mm in defined steps. From the interferometric measurement at each position, the aspherical part of the OPD was extracted and analyzed. The Fermi-Dirac distribution was chosen as fit-function for the aspherical contribution. The results are shown in figure 5.9, together with the corresponding image of the pump spot on the disk.
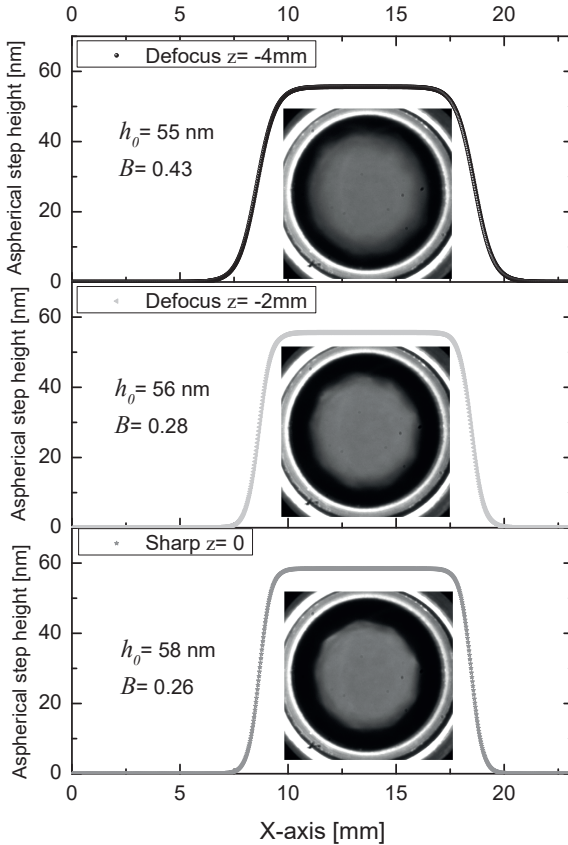
Figure 5.9: Variation of the steepness of the pump spot edge by defocusing the collimation optics. The graph shows the derived aspherical part of the OPD induced by a sharp image of the pump spot on the laser disk (bottom picture) and by two defocused images ($z=$ -2 and -4 mm) together with the corresponding pump spot images.

It can be seen that the defocusing of the pump spot mainly affects the edge steepness of the aspherical part of the OPD, whereas the amplitude h_0 remains nearly unchanged (difference $\approx$5%). This leads to the conclusion that the effect of the gain aperture of the thin-disk crystal during laser operation can be influenced with this method. A lower

steepness of the edges results in a reduction of the diffraction loss of the laser mode(s) and is thus favorable for fundamental-mode and few-mode operation. On the whole, by simple defocusing of the pump optics a better adaption of the distribution of the pump power density on the disk to the intensity distribution of the laser mode(s) can be obtained. Consequently, this method can be used to facilitate the laser operation in (transversal) fundamental-mode and few-mode lasers. This relation was experimentally verified when conducting the experiments with the goal to compensate the aspherical part of the thermally induced aberrations by suitable mirrors and which are reported in chapter 7. The method described above was also applied during the experiments to obtain fundamental-mode operation at high optical output powers (see section 6.2).

The previously described defocusing of the pump optics is only one possibility to influence the mode distribution of a thin-disk laser but apparently more effective for few-mode than fundamental-mode operation due to the following reasons. To achieve an optimum overlap for the transversal fundamental-mode, an approximately Gaussian distribution of the pump power density is required. To obtain this by applying the defocusing-method would introduce too much losses for the pump radiation, which would result in a substantial reduction of the pump power density. This method is therefore only useful to perform small adaptations. Another possibility to obtain a Gaussian distribution of the pump power density on the laser disk is to implement Gaussian refractors (for instance from the company aµs [88]) in the path of the pump beam. A proof of principle for the use of these elements in a thin-disk laser system with the goal to shape the pump spot image, was performed during this thesis. Even though the choice of the available Gaussian beam shapers was limited, a Gaussian distribution of the pump power density was obtained with one of the shapers. The Gaussian refractor which achieved this goal was 20 mm in diameter, had a divergence angle of 10 degree and was made of fused silica. For the obtained distribution of the pump power density a good overlap to the fundamental mode distribution was expected. However, the drawbacks of the Gaussian refractors available at that time (2013) was a power loss of about 6% (refraction efficiency >90%) and the increase of the divergence angle due to the structure of the elements. Unfortunately, the maximum permissible numerical aperture of the pump radiation entering in the thin-disk pump module was already reached even without the Gaussian refractor so that the increase of the divergence induced a significant loss at the entrance aperture of the module. For this reason, this investigation was restricted to a pump power of 125 W and can thus only be seen as a promising starting point for further work.

Returning to the initial topic of this chapter. By using the interferometer presented here, an exact determination of the aspherical part (amplitude as well as steepness of the edge) of the OPD thermally induced by the thin-disk crystal during laser operation can be

performed up to the multi-kilowatt output power level. It was shown that, due to the high
precision of the interferometer, even small deviations of the OPD, such as for instance
the wedge-shaped inhomogeneities of the atmosphere in front of the disk, can be detec-
ted and analyzed. However, a statement about the absolute accuracy of an interferometer
cannot be given without a precisely defined reference surface for calibration. Unfortu-
nately, a precise calibration sample was not available for this interferometric setup. To
nevertheless obtain an estimation of the accuracy of the interferometer, a comparison
with a commercially available wavefront-sensor (SID4) based on the lateral shearing
method from the company Phasics was performed. These measurements revealed that
the resolution and accuracy of the interferometer is at least as good as, if not better, than
the one of the SID4-wavefront-sensor. The specifications of a SID4-device from Phasics
can be found on the company web page and are a phase resolution of < 2 nm rms and
an accuracy of 10 nm rms.

In summary, it can be stated that by considering the points mentioned in this chapter, a
precise analysis of the OPD induced by the disk even in high-power laser operation can
be conducted with the developed interferometer. The fit-algorithm has the largest influ-
ence regarding an accurate determination of the aspherical part of the thermally induced
OPD of thin-disk crystals during laser operation. Strictly speaking, the convergence of
the algorithm was identified as the most crucial point of the analysis. This is especially
true for the 3D-evaluation of the measurement data. Thus, an appropriate starting value
is essential to facilitate the convergence of the fit-algorithm. To obtain this value, the
amplitude of the aspherical part of the OPD can be estimated by calculating the path
length change with temperature in the laser disk (see equation 7.1 in chapter 7.1).

6 Zero-Phonon-Line pumping of high-power thin-disk lasers

6.1 High-power pump source for ZPL-pumping of Yb-doped thin-disk lasers

The ZPL-pumping reduces the overall thermal load of the thin-disk laser crystal and thereby allows to enhance the laser performance of crystalline laser-active materials (LAMs). To achieve a reduction of the thermal load, the LAM is pumped directly into the lowest sublevel of the upper laser level [27]. This leads to a laser transition without any additional non-radiative process in the upper laser level which usually involves the participation of a high-energetic phonon. This excitation method is therefore commonly referred to as „zero-phonon line (ZPL) pumping" [89], though the term „direct in-band pumping" [90] is also existent in the literature. However, the drawback of the ZPL-pumping is usually the narrow spectral bandwidth of only 1-2 nm (FWHM) of the absorption peak which resulted in a rare use of this pumping concept so far. Then again, with the better availability of high-quality gratings for the spectral stabilization of laser diodes, ZPL-pumping can be realized with much lower efforts so that the implementation in practice becomes more and more beneficial. The setup for this pumping method which was realized during this thesis is described in detail in the sections 6.1.2 and 6.1.3.

6.1.1 Theoretical background of ZPL-pumping

For the research presented in this thesis, the ZPL-pumping was applied to the laser-active materials Yb:YAG, Yb:LuAG and Yb:Lu$_2$O$_3$. Their energy level schemes are shown in figure 6.1.
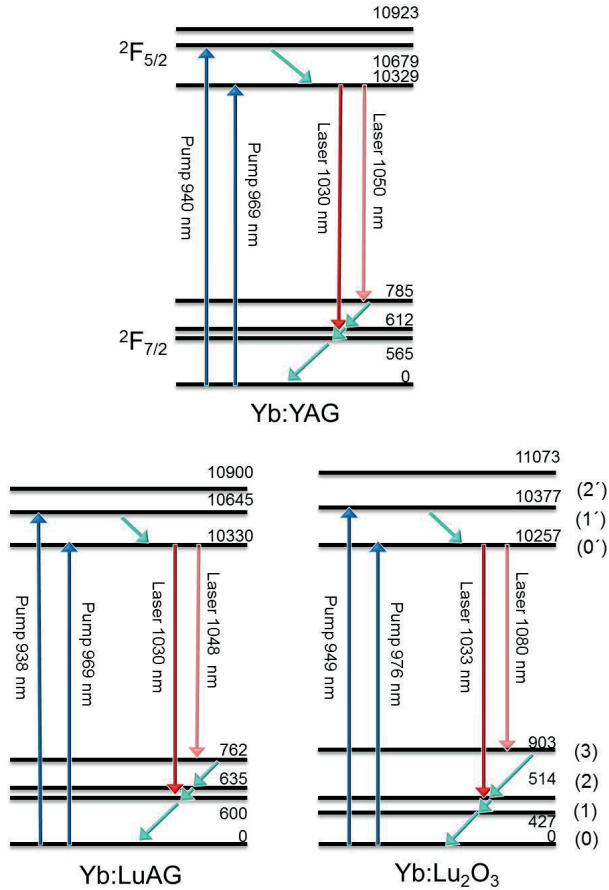
Figure 6.1: Energy levels of Yb:YAG [22], Yb:LuAG [49] and Yb:Lu$_2$O$_3$ [36], whereby $^2F_{7/2}$ corresponds to the lower and $^2F_{5/2}$ to the upper laser multiplett. The energy values are given in cm^{-1}. The arrows with an inclination of 45 degree indicate non-radiative transitions where phonons are involved.

As indicated, the ZPL-pumping takes place from the ground level (0) directly to the lowest upper laser level (0'). All three LAMs have a smaller quantum defect when ZPL-pumping is applied in comparison to the conventional pumping at the wavelengths of

938 nm, 940 nm and 949 nm, respectively. In the present case, it allows to increase the pump power by about 50% to equal the thermal load in the thin-disk crystal otherwise produced by conventionel pumping. The benefit of the ZPL-pumping in terms of quantum efficiency, heat reduction and estimated possible power increase for the three LAMs is summarized in table 6.1.

Table 6.1: Comparison between ZPL-pumping and conventional pumping

	Yb:YAG	Yb:LuAG	Yb:Lu$_2$O$_3$
Quantum efficiency [%]	8.6 at 941 nm	8.9 at 938 nm	8.2 at 949 nm
	5.9 at 969 nm	5.9 at 969 nm	5.6 at 976 nm
Heat reduction [%]	32.2	33.7	31.7
Estimated power increase [%]	47.5	50.8	46.4

In addition to the lower heat generation, the effective absorption cross section of Yb:LuAG and Yb:Lu$_2$O$_3$ is higher at the ZPL pump wavelength. This allows to reduce the thickness of the thin-disk crystals of both materials while keeping the absorption of the pump light sufficiently high. The lower thickness further improves the heat extraction capability of the disk. Another advantageous aspect of ZPL-pumping is that in case of an interruption of the laser oscillation the risk of damaging the thin-disk crystal due to overheating is substantially minimized. This is because of the strong bleaching of the absorption at the ZPL-wavelength during fluorescence operation.

Apart from the reduction of the thermally induced aspherical deformation of the wavefront in the disk by ZPL-pumping, the spherical deformation of the thin-disk crystal is lower too. This is especially beneficial for the stability of the resonator, since the spherical deformation corresponds to the thermal lens of a thin-disk laser which is in general low but not negligible when operating at high output powers. A more detailed discussion of the influence of the remaining spherical deformation on the stability of the resonator, together with the description of the used resonator layout, is therefore presented in sections 6.2.1 and 6.2.2.

6.1.2   Optical design of the pump source

Compact sized, actively cooled high-power diode laser stacks are nowadays commercially available with output powers of up to 3 kW. Their spectral bandwidth is typically 3 to 4 nm, which is appropriate for efficient pumping of Yb:YAG, Yb:LuAG and Yb:Lu$_2$O$_3$ which have broad absorption peaks at the wavelengths of 940 nm, 938 nm, and 949 nm,

respectively. The spectral width of these broad absorption bands, are in the order of 10 nm which makes the typical temperature-dependent wavelength drift of ≈ 0.3 nm/K of the diode laser stacks rather uncritical. When pumping at these absorption peaks, the control of the cooling temperature is sufficient to keep the emission wavelength of the diode stacks within the desired range. On the contrary, as already mentioned previously, the demands on the pump diodes increase when these laser-active materials shall be pumped at the ZPL-transition. In this case, the pump radiation requires a spectral bandwidth of about 2 nm (FWHM). A wavelength stabilization using an optical feedback into the diode laser stack becomes therefore necessary for efficient absorption of the pump radiation. In the present work this was realized by using Volume-Bragg-Gratings (VBG's) which were positioned directly behind the fast-axis collimation lenses of a diode laser stack. The characteristics of the diode laser stack and the optical design for the shaping of the pump beam is briefly summarized in the following.

The beam of the diode stack was already collimated in the fast-axis by means of cylindrical microlenses so that a divergence angle of less than 0.5° was obtained. In the slow-axis, the divergence was specified to be less than 9° (full angle). The radiation emitted by the diode stack (that consisted of 25 bars) had to be imaged onto the entrance facet of the available homogenizing rod as sketched in figure 6.2. This was performed by a set of crossed cylindrical lenses, which had an AR-coating for a wavelength range of 940-980 nm on both sides. Lens 1 and 3 (f_{lens1}= 233 mm, f_{lens3}= 82 mm) were used for the slow axis imaging and lens 2 (f_{lens2}= 233 mm) to image the fast-axis. The overall image at the entrance facet of the homogenizer was about 5 x 5 mm. The homogenizing rod shown in figure 6.3, had a cylindrical shape with two additional side facets (starting from the entrance facet up to a certain length) in order to break the rectangular symmetry of the diode stack. The exit facet of the rod was beveled at an angle of 30°. This was done to obtain a circular image on the thin-disk crystal which would otherwise be elliptical because of the off-axis position of the pump beams on the parabolic mirror. A bi-aspherical lens with a focal length of 80 mm was used to collimate the pump radiation after the rod.The collimation lens and the parabolic mirror (focal length of 76 mm) acted as a telescope to image the exit-facet of the homogenizer on the thin-disk crystal. All elements used for the pump beam shaping were made of fused silica.
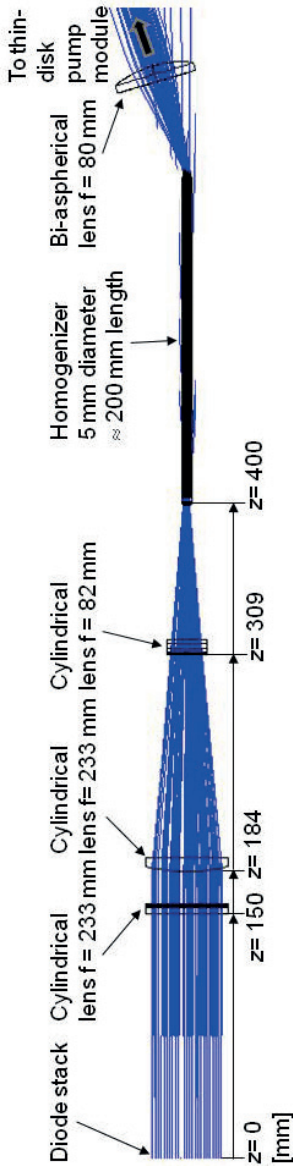
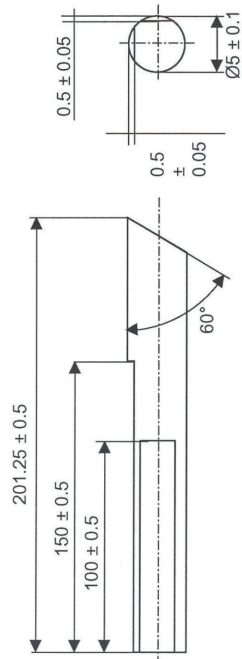**Figure 6.2:** Top view of the path of the pump beam from the diode stack to the collimation lens.

Figure 6.3: Dimensions of the homogenizing rod. Design Ch. Stolzenburg.

6.1.3   Characterization and performance of the Volume Bragg Gratings

The used VBGs were manufactured by the company Optigrate. A holographic process which generated a defined phase information inside a photo-thermo-refractive [PTR] glass was applied for the fabrication [91]. The PTR-glass consisted of Na_2O-ZnO-Al_2O_3-SiO_2-NaF-KBr doped with silver, cerium and fluorine. A modulation of the refractive index of the PTR glass was achieved [91] by coherent irradiation with a UV-laser emitting at a wavelength in the region between 280 to 350 nm together with a thermal treatment.

In order to be able to use VBG-elements in high-power laser systems, the parameters temperature and damage threshold have to be particularly considered. The used PTR-glass was specified to possess a high temperature tolerance of up to 400°C and a damage threshold of ≈ 40 J/cm^2 (for laser pulses with a duration of 8 ns). These parameters were experimentally determined and published by Glebov et al [92]. A successful implementation in a high-power pump setup was therefore considered as feasible. A thermal characterization of an uncoated PTR-glass sample inside the actual setup prior to the inscription of the Bragg grating was nevertheless carried out as briefly described in the following section.

The characterization of the PTR-glass sample by using a FTIR-spectrometer revealed an absorption inside the PTR-glass of approximately 0.70% so that a maximum temperature of 70 °C was expected for the given pump power of 2 kW. To verify this estimation experimentally, the PTR-glass sample was glued into a water cooled holder which was similar to the one planned to be used for the VBGs in the experiments afterwards. The heating of the sample was then measured for different incident output powers of the laser diode stack by using a thermal camera (InfraTec VarioCam). The recorded minimum, average, and maximum temperatures are shown in figure 6.4.

The maximum temperature at an incident optical power of 2 kW is approximately 68°C, which is in good agreement with the previously estimated temperature. Hence, a temperature of 70 °C was set as specification for the nominal operation temperature of the VBG-elements.

The free aperture of the diode stack used in this work was 43.8 mm x 10.2 mm which was larger than the producible size of the VBG´s in 2009. For this reason, the first generation of VBG's for diode stabilization (used for the research presented here) at a wavelength of 969 nm (ZPL pump wavelength of Yb:YAG and Yb:LuAG) consisted of two elements. A schematic drawing of the setup and the working principle can be seen in figure 6.5.
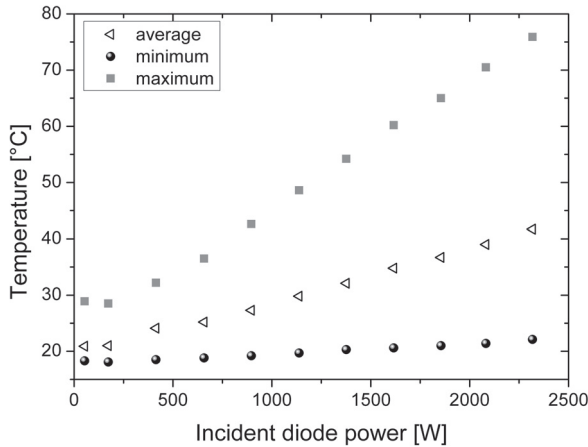
Figure 6.4: Temperature change of the PTR-glass sample with increasing incident power of the radiation from the laser diode stack.
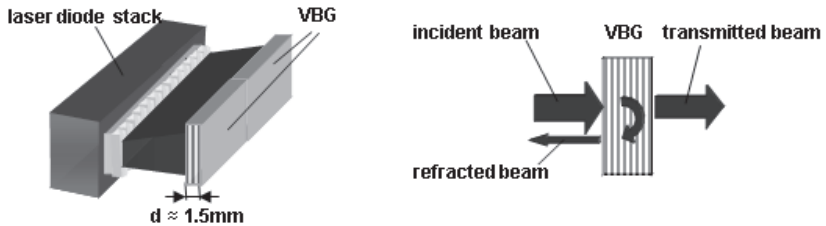

Figure 6.5: Set-up of the VBGs in combination with the diode stack. Two VBGs were used for the wavelength stabilization at a wavelength of 969 nm. Only one VBG was used for the wavelength stabilization at a wavelength of 976 nm. Tip-and tilt of the VBGs had to be aligned according to their specifications to obtain an optimal back coupling of the refracted beam into the diode stack.

The two VBGs for the wavelength of 969 nm were glued into a water cooled mount and adjusted independently from each other by taking into account the manufacturing specifications given in table 6.2. It was expected that the elements would expand with increasing temperature so that a fixation with low-strain has been chosen by using a silicon based glue. The same mounting procedure was also successfully applied later on for the VBG element with a free aperture of 46 x 12 mm (C40-01 in table 6.2) to be used for the diode stabilization at a wavelength of 976 nm to pump the ZPL-transition of Yb:Lu$_2$O$_3$.

An AR-coating with R< 0.4% (for a wavelength of 969 nm) and R< 0.15% (for a wavelength of 976 nm) was applied on both sides to avoid additional reflections and to minimize a further reduction of the amount of pump radiation by the surfaces of the VBG. The thicknesses of 1.5 mm and 1.31 mm of the VBGs was rather thin which required a careful mounting procedure. After mounting and alignment, their feedback resulted in a narrowing of the spectral bandwidth of the laser diode stack to 0.5/0.7 nm and 0.24 nm, respectively.

Table 6.2: Specifications of the used VBGs designed for a wavelength of 969 and 976 nm respectively.

Wafer ID	Diffraction efficiency (average)	Resonance wavelength (in air)	Spectral bandwidth FWHM	Grating tilt HxV	Thickness	Free aperture
	%	nm	nm	deg	mm	mm
Ce006-26	20.0	968.85	0.5	-0.5 x -0.5	1.5	22 x 11
Ce006-27	19.6	968.85	0.7	0.2 x 0.1	1.5	22 x 11
C40-01	18.7	975.7	0.24	-0.2 x -0.2	1.31	46 x 12

The setup for the VBG-locking of laser diodes that was used in the research presented here was the first experimental realization of this kind at the IFSW and publications in literature are rare. In addition, the costs of the VBGs for the desired use were high so that their specifications and their behavior at high power had to be thoroughly evaluated. The following section therefore briefly lists the points which were discussed, except the thermal issues described directly after. First of all, a trade-off between the reflectivity of the VBGs and the locking capability had to be found for the wavelength stabilization of the present laser diode stack. On the one hand the loss of the usable pump power which corresponds to the percentage of back reflected power had to be considered and on the other hand a sufficient back coupling to lock all emitters of the diode stack at the desired wavelength had to be guaranteed as well. Based on a discussion with the grating manufacturer, the reflectivity of the VBGs was specified to be approximately 20 %. The exact determination of the effectively injected part of the pump radiation into the emitters of the laser diode stack is nevertheless difficult. This is due to several reasons. Besides the requirement for accurate alignment of the VBG, the pre-adjustment of the micro-optical fast-axis-collimation lenses by the diode supplier is another important prerequisite. Any distortion of the emitted spatial pattern e.g. the appearance of the so called "smile", which is a small bend of the emitter line, results in a non-optimum locking of the diode bars. The diode stack consisted in total of 25 bars which had all to be locked by two (969 nm) or even one (976 nm) volume bragg element. Additionally, the VBG could

only be positioned with a certain distance to the diode stack. Hence, especially the higher divergence of the emitted beams in the slow axis (FWHM $\approx 7°$) can deteriorate the locking. Furthermore, the exit facets of the diode bars were not AR-coated due to cost issues.

Prior to the usage at high diode output powers, all three supplied VBG-elements were characterized regarding their thermal load and locking capability at different output power levels. The two elements designed for a wavelength of 969 nm showed higher temperatures when compared to the previously measured values for the PTR glass itself (without inscribed grating structure). Already at less than half of the total power of the diode laser stack the temperature of the VBGs exceeded 85 °C, which made it necessary to install an air cooling in order to keep the targeted temperature of about 70 °C at the maximum output power. Applying the air cooling allowed to reduce the maximum surface temperature of the VBGs to 68.8 °C when operating the diode stack close to the maximal current of 100 A which corresponds to approximately 2 kW of output power. The thermal image of the VBGs at this operating point can be seen in the bottom left picture in figure 6.6.
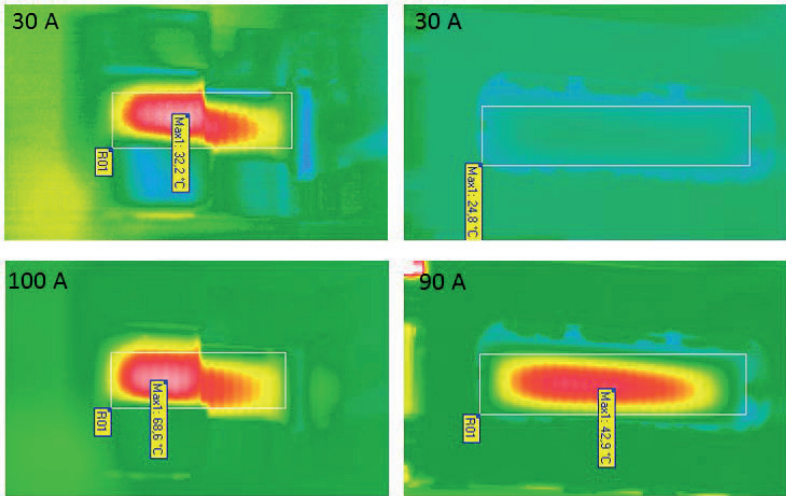
Figure 6.6: Thermal images of the VBG-elements: Left side: Two VBGs to lock at a wavelength of 969 nm. The diode laser stack operated at currents of 30A (top) and 100A (bottom). Right side: Single VBG for locking the diode laser stack at a wavelength of 976 nm. The diode current is 30 A (top) and 90 A (bottom).

However, the supplier Optigrate was able to significantly reduce the absorption of the VBG designed for a wavelength of 976 nm fabricated later. As shown in the bottom right picture of figure 6.6, even without air cooling this VBG reached a maximum surface temperature of only 42.9 °C when operating the diode laser stack at a current of 90 A. Beside the lower absorption value, Optigrate also managed to approximately double the free optical aperture of the VBG elements. This permitted the use of only one VBG-element for the wavelength stabilization at 976 nm instead of the two VBGs for the wavelength stabilization at 969 nm.

A difference in the capability to lock all emitters of the laser diode stack for the VBGs designed for the wavelength of 969 nm in comparison to the one used to lock at a wavelength of 976 nm was observed. For this reason, it was assumed that the number of emitters which where still free-running was different in both cases. The typical spectral shift of the emitters which could not be locked by the VBG(s) was ≈ 0.3 nm/K. This spectral shift was influenced by the cooling temperature and the operating current so that the contribution of the radiation emitted from the free-running emitters to the pumping process changed accordingly. On the whole, the efficiency of the locking was higher when using the VBGs designed for the wavelength of 969 nm than the one designed for the wavelength of 976 nm due to the following reasons. The desired locking wavelength of 969 nm was much closer to the central wavelength of ≈ 971 nm of the spectrum of the free-running emitters ($T_{cool,diode} = 25$°C). This appeared to be beneficial for the efficiency of the locking. Although, the efficiency of the locking with the VBGs designed for a wavelength of 969 nm was not 100%, neither, it was easier to adjust the spectrum of the free-running emitters of the diode laser stack adequately to the desired working point by adapting the cooling temperature. This for instance meant that the largest spectral overlapp between the spectrum of the free-running emitters and the absorption spectrum of Yb:YAG was obtained at a diode current of ≈ 80 A at a cooling temperature of the diode laser stack of 25°C. This optimum operation point shifted to a diode current of ≈ 95 A when the cooling temperature of the diode laser stack was set to 22°C. For this cooling tempererature, the measured spectral shift of the free-running emitters with increasing diode current is shown together with the absorption spectrum of Yb:YAG in figure 6.7. Overall, the ZPL-pumping of the Yb:YAG and Yb:LuAG at a wavelength of 969 nm was obtained with an pumping efficiency close to the theoretical maximum.
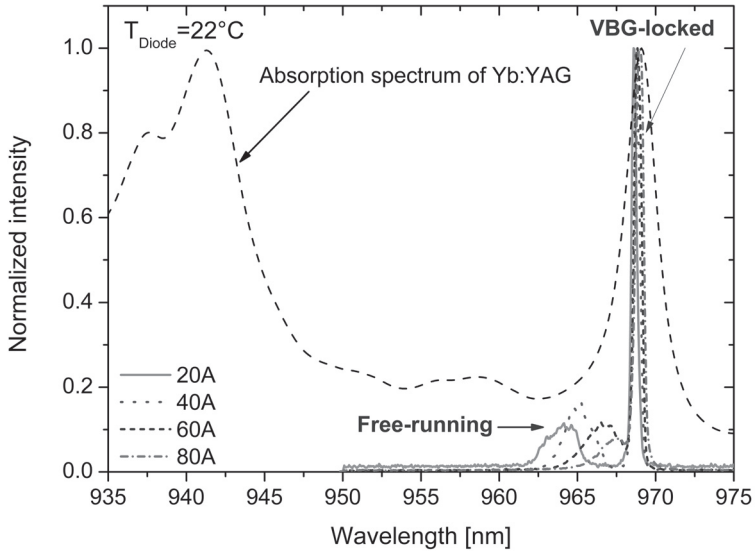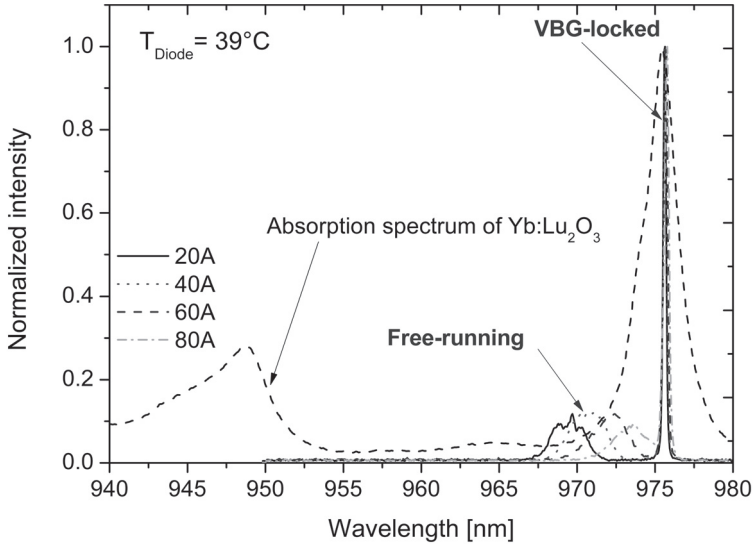
Figure 6.7: Normalized measured spectra of the pump diode for different currents (20A-80A) of the diode stack (cooling temperature = 22 °C). The locking efficiency is increasing with increasing current of the diode. The absorption spectrum of Yb:YAG is indicated by the dashed line.

Significantly lower locking- and therefore pumping-efficiencies of the diode laser stack were obtained when changing the VBGs designed for a wavelength of 969 nm to the one designed for a wavelength of 976 nm. Especially at low output power (which is equivalent to shorter wavelengths of the pump radiation), it was observed that numerous emitters of the diode laser stack could not be locked. Therefore, the cooling temperature was increased to shift the spectrum of the free-running emitters closer to the resonance wavelength of the VBG of 975.7 nm in order to facilitate the locking and to improve the overlap between the spectrum of the free-running emitters and the ZPL-absorption peak of Yb:Lu$_2$O$_3$ (see figure 6.8). However, the locking-capability was still not completely satisfactory even though the diode laser stack was finally operated at a cooling temperature of 39 °C. A reason for this insufficient locking seemed to be the remaining large difference between the center wavelength of the free-running emitters and the resonance wavelength of the VBG of about 6 nm. Besides this, it is presumed that less radiation was coupled back into the emitters of the diode laser stack by the VBG. This was most probably due to the reduced degree of freedom when only one element (976 nm) can

be adjusted instead of two (969 nm) and the lower diffraction efficiency of this VBG (976 nm) (see table 6.2). Moreover, the spectrum of the free-running emitters was still not perfectly overlapping with the ZPL-absorption peak of Yb:Lu$_2$O$_3$ as can be seen in figure 6.8.

Figure 6.8: Normalized measured spectra of the pump diode for different currents (20A- 80A) of the diode stack (cooling temperature = 39 °C). The locking efficiency is increasing with increasing current of the diode. The absorption spectrum of Yb:Lu$_2$O$_3$ is indicated by the dashed line.

6.2   Experimental results of ZPL-pumped Yb:YAG and Yb:LuAG thin-disk crystals

Thin-disk pumping optics providing 24 passes of the pump beam through the laser crystal were used for the experiments conducted with the ZPL-pump source. An efficient pump light absorption was thus guaranteed for all experiments. The maximum pump power of the diode laser stack entering the thin-disk pumping module was 1.44 kW in the present case. The pump spot was designed to have a diameter of 5.6 mm on the disk which corresponds to a pump power density of about 5.2 kW/cm^2. This pump intensity is adequately below the nominal thermally induced damage threshold for Yb:YAG

and Yb:LuAG thin-disk crystals. Typical used disk thicknesses were in the order of
100-140 μm. Both host materials feature quite similar optical, mechanical, and thermal
properties so that the only relevant difference between them was the higher thermal con-
ductivity of Yb:LuAG for the used doping concentration of about 10 at.%. A detailed
overview of the physical and spectroscopic properties of Yb:YAG and Yb:LuAG can be
found in sections 3.2.1 and 3.2.2.

6.2.1   CW-multi-mode performance of Yb:YAG and Yb:LuAG thin-disk lasers

The Yb:YAG and Yb:LuAG thin-disk crystals were glued with their HR coated backside
on CVD-diamond heat sinks in order to provide a highly efficient heat removal. All heat
sinks were water-cooled by the common impingement cooling. The temperature of the
cooling water was approximately 15 °C. The front side of the thin-disk crystals had
the typical AR-coating for pump and laser wavelengths (see section 3.3.3 for AR- and
HR-coating specifications).

The resonator consisted of a plane end mirror, the thin-disk with a radius of curvature
of about 2 m, and a plane output coupler. Its overall length was 1.3 m. This V-shaped
resonator featured a beam quality factor of $M^2 \approx 15$ and was operated with 4.5 % of out-
put coupling. Operating the thin-disk laser with ZPL-pumped Yb:YAG and Yb:LuAG
crystals allowed to obtain optical efficiencies in the order of 70 % during multimode
operation. A typical result for such a thin-disk laser using an Yb:YAG thin-disk cry-
stal is illustrated in figure 6.9. As can be seen, a maximum optical efficiency of 72 %
and a slope efficiency of 82% as indicated by the solid line was demonstrated. It can
be observed as well that the slope variates slightly. This effect was due to the influence
of the free-running emitters of the pump diode stack on the pump light absorption in
the Yb:YAG disk which varies with the operation current as explained previuously and
shown in figure 6.7. The laser performances obtained with an Yb:LuAG thin-disk cry-
stal during multimode-operation are shown in figure 6.10 for a similar resonator setup.
The maximum optical efficiency of 65 % of the Yb:LuAG laser is lower than for the
investigated Yb:YAG laser (figure 6.9). This was caused by the use of a thinner disk
in the case of Yb:LuAG due to the following reason. By choosing a disk with lower
thickness, a trade-off between an optimum absorption of the pump power and minimum
distortions of the laser beam was made. As a result, a reduction of the optical efficien-
cy of this laser during multi-mode operation was observed, but a benefit was obtained
for fundamental-mode operation as presented in the following section. Nonetheless, the

exceptionally high efficiencies realized by ZPL-pumping with the thicker Yb:YAG disk clearly point out the significant potential of this pumping method for thin-disk lasers.
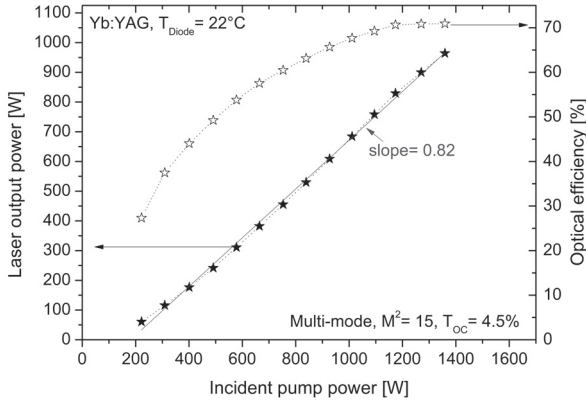

Figure 6.9: Output power and optical efficiency of an ZPL-pumped Yb:YAG thin-disk laser during multi-mode operation for a M^2 value of 15. The VBG-locked pump diode stack was operated at a cooling temperature of 22 °C.
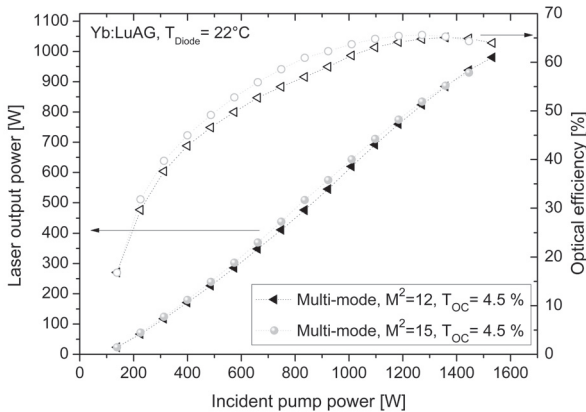

Figure 6.10: Output power and optical efficiency of an ZPL-pumped Yb:LuAG thin-disk laser during multi-mode operation for M^2 values of 12 and 15. The overall length of the resonator was 1.27 m ($M^2 \approx 12$) and 1.23 m (($M^2 \approx 15$). The VBG-locked pump diode stack was operated at a cooling temperature of 22 °C.

To determine the thermal load of the ZPL-pumped Yb:LuAG disk, the maximum temperature on the surface of the thin-disk crystal was measured as a function of the incident pump intensity. The temperature values which were determined during fluorescence and laser operation are shown in figure 6.11. During laser operation the maximum temperature reaches 72 °C at a pump power density of 5.8 kW/cm^2. The temperature during fluorescence operation (laser resonator interrupted) was always higher than in the lasing case. It was about 7 K higher at the maximum investigated pump power density of 2.8 kW/cm^2 for the fluorescence operation. The temperature behavior shown here was typical for all thin-disk crystals analyzed in ZPL-pumped configuration during this research.
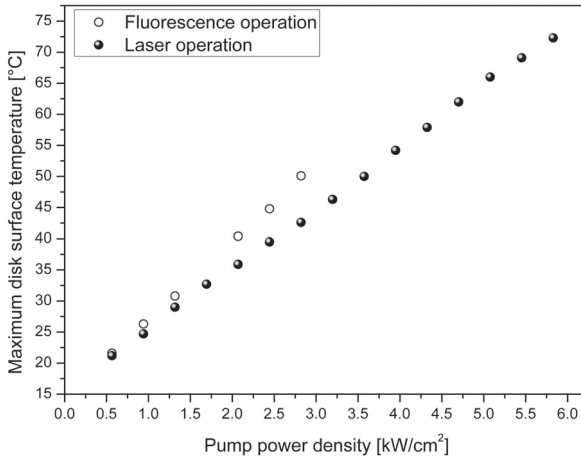
Figure 6.11: Maximum surface temperature of a ZPL-pumped Yb:LuAG disk during fluorescence and laser operation.

In order to characterize the thermal behavior of the ZPL-pumped disks further and to evaluate the induced spherical and aspherical aberrations, interferometric measurements during laser operation have been carried out. The thin-disk crystal without incident pump power was used as reference for these measurements. The deformation of the investigated thin-disk crystals remained mainly spherical up to a pump power density of 5.2 kW/cm^2 (corresponds to a pump diode current of 90 A). To exemplify this, the profiles of the OPD induced by an Yb:YAG disk are shown in figure 6.12.
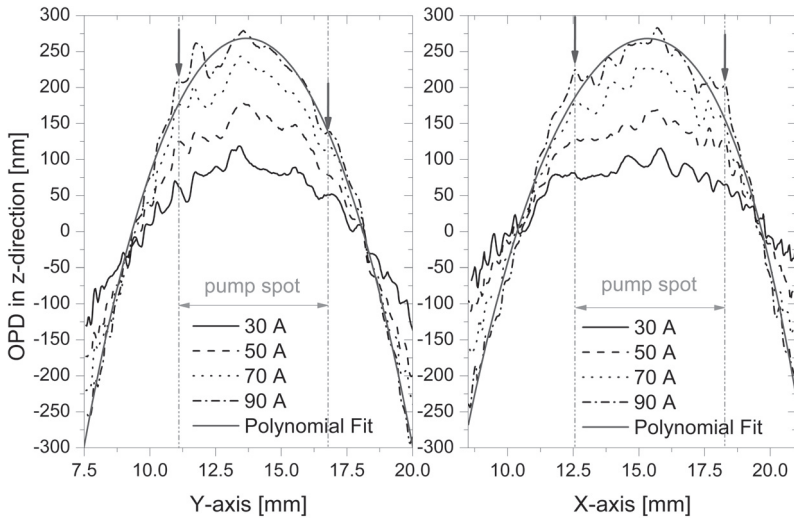
Figure 6.12: X- and Y- profiles of the OPD induced by the Yb:YAG thin-disk crystal during laser operation with increasing incident radiation of the pump diode. The VBG-locked laser diode stack was operated up to a maximum diode current of 90 A (corresponds to a pump power density of 5.2 kW/cm^2 on the disk for the present case). The temperature of the cooling water of the pump diode during these measurements was 22 °C.

At the maximum pump power density of 5.2 kW/cm^2 the profiles are approximated by a 4th order polynomial fit (thin-solid line). Solely a minor distortion at the pump spot edges as indicated by the arrows could be identified. By comparing the profiles of the OPD induced by the Yb:YAG disk during laser operation in x- and y-direction, it appears that particularly in y-direction which corresponds to the vertical direction (shown on the left side in figure 6.12) the aspherical contribution to the distortions is marginal. Nevertheless, especially in x-direction the onset of the aspherical distortions can clearly be seen, so that a reduction of the thickness of the disk was chosen as easiest solution to guarantee negligible aspherical deformations up to the maximum available pump power of the laser diode stack.

6.2.2 CW near diffraction-limited performance of Yb:YAG and Yb:LuAG thin-disk lasers

At present, only Yb:YAG and Yb:LuAG fulfill the high demands to realize thin-disk lasers at the kilowatt or even multi-kilowatt output power level in all required aspects. They are therefore currently the sole candidates to reach the 1 kW of output power during fundamental-mode operation. To extend the current state of the art (when starting this research) of a laser output power of 500 W achieved with a single thin-disk crystal, the application of ZPL-pumping for both laser-active materials was considered as the most promising approach as presented in the previous sections.

In order to obtain fundamental-mode operation, a V-shaped resonator with an overall length of 2.4 m was designed using the ABCD matrix formalism. It consisted of a convex spherical end mirror (ROC = 0.6 m), the already mentioned concave Yb:LuAG disk with a radius of curvature of about 3.6 m, and a plane output coupler (T= 4.5 %). The diameter of the fundamental mode on the disk was chosen to be 75% of the size of the pump spot ($\approx$4.2 mm) in order to suppress the oscillation of higher transverse modes. Figure 6.13 shows the measured laser output power and the calculated optical efficiency as a function of the incident pump power for cooling temperatures of the pump diode stack of 22 °C and 25 °C respectively. A reduction of the cooling temperature to 22°C allowed to shift the maximum of the optical efficiency of the thin-disk laser to the desired operating point. Running the cooling of the diode stack at this three dregree lower temperature allowed to achieve a maximum near diffraction-limited output power of 742 W with an unprecedented high optical efficiency of 58.5%.
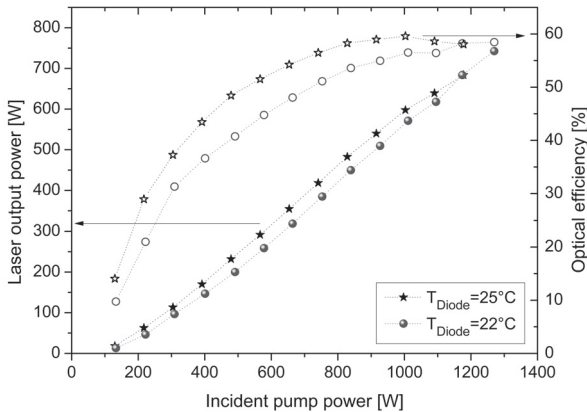
Figure 6.13: Performance of an Yb:LuAG thin-disk laser with near diffraction-limited beam quality for diode cooling temperatures of 22 °C and 25 °C.
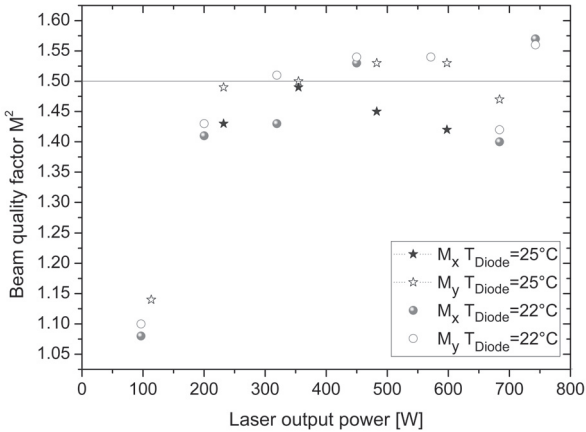
Figure 6.14: Measured beam quality factor M^2 of the laser beam in horizontal (x)- and vertical (y)-direction versus laser output power.

The beam quality factor M^2 was determined at different operating points for both cooling temperatures of the pump diode stack. For this purpose, a camera-based system using the second moment method (Spiricon M^2-200) as specified by the ISO standards was used. The measured M^2-factors are plotted versus the output power of the Yb:LuAG disk laser in figure 6.14. It can be observed that the laser operates with a beam quality factor centered around a value of 1.5, regardless of the diode cooling temperature. This is especially the case well above laser threshold, where no significant change of the M^2 value took place.

6.3   Experimental investigation on ZPL-pumped Yb:Lu$_2$O$_3$

The benefit of ZPL-pumping is high, especially for Yb:Lu$_2$O$_3$ (for material properties see chapter 3.2.3). This is due to the quite large difference between the absorption cross section of the two absorption peaks (σ_{abs}= 0.95·10^{-20} cm^2 at a wavelength of 949 nm and 3.1·10^{-20} cm^2 at 976 nm (ZPL-transition)) used for high-power diode-laser pumping. Nevertheless, the investigation on the high-power suitability of this material in general and for the use in thin-disk lasers in particular is currently only at its beginning. The interest was growing after the realization of a few rods with diameters larger than 9 mm, but diminished a bit when discovering that the quality of the material still differs significantly from boule to boule. A comprehensive characterization of the Yb:Lu$_2$O$_3$

thin-disk crystals available for this thesis was therefore performed as presented in the following. The analysis of the thermal behavior of the Yb:Lu$_2$O$_3$ thin-disk crystals during fluorescence and laser operation is described in section 6.3.1. The results obtained from the experiments with high-power multi-mode and fundamental-mode resonators are reported afterwards in sections 6.3.2 and 6.3.3.

6.3.1 Analysis of the thermal behavior of ZPL-pumped Yb:Lu$_2$O$_3$ disks during fluorescence and laser operation

The same pump configuration allowing 24 passes of the pump radiation through the disk was used as presented in section 3.1. The description of the pump setup, including the performance and the spectral characteristics of the VBG-stabilized pump diode stack at a wavelength of 976 nm can be found in chapter 6.1. To perform the analysis of the thermal load of the Yb:Lu$_2$O$_3$ disks during laser operation, a V-shaped (folded) cavity was set up providing two passes of the laser beam through the crystal. It was comprised of a plane HR-mirror, the backside HR coated concave disk, and a plane output coupling mirror (T$_{out}$ =3 %). The pump spot diameter was set to 5.6 mm. By using total resonator lengths of 950 to 1000 mm, the laser oscillated in multi-mode with M^2 values around 20. A more detailed description of the setup can be found in [93]. The laser experiments were performed with 200 and 250 μm thick Yb:Lu$_2$O$_3$ disks with an Yb-doping concentration of 3at.%. The thin-disk crystals had a diameter of 11.3 mm and radii of curvature of about 1.8 m in vertical- and horizontal direction.

In order to evaluate the thermal load of different Yb (3at.%):Lu$_2$O$_3$ thin-disk crystals during fluorescence (resonator interrupted) and laser operation, a thermal image of the surface of the disk was recorded using a thermographic camera (InfraTec VarioCam). The maximum temperature and the radial temperature distribution for different pump powers was measured. The recorded data are summarized in figure 6.15. For the sake of clarity, only values of two Yb:Lu$_2$O$_3$ thin-disk crystals are shown and discussed.

For a 200 μm thin crystal, the surface temperature increased strongly during fluorescence and also during laser operation when pumped at the ZPL-wavelength of 976 nm. This is a contradiction to the theoretically expected temperatures of this disk. The temperature curves of this 200 μm thin disk (as can be seen in figure 6.15) are additionally strongly bent, reaching a maximum of 113 °C at an incident pump power of 367 W (pump power density of 1.5 kW/cm^2) during laser operation. Contrary to this, a maximum temperature of only 52.3°C at a pump power density of 1.2 kW/cm^2 was measured for a 250 μm thin crystal during fluorescence operation. The same disk had a

maximum surface temperature of 42.3 °C at a pump power density of about 1.5 kW/cm^2 during laser operation. A linear extrapolation of the temperature curve leads to an estimated maximum surface temperature of 80 °C for a pump power density of 4.2 kW/cm^2 which corresponds to a pump power of 1 kW.
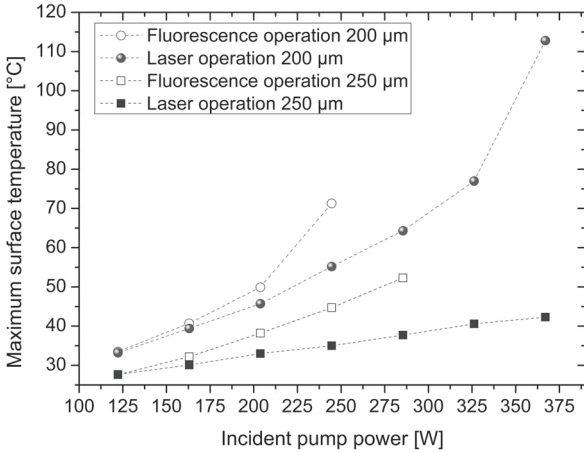

Figure 6.15: Comparison of the maximum surface temperatures of two 200 and 250 μm thick ZPL-pumped Yb:Lu$_2$O$_3$ thin-disk crystals during fluorescence and laser operation. An incident pump power of 367 W corresponds to a pump power density on the disk of 1.5 kW/cm^2.

The temperature behavior of the two Yb:Lu$_2$O$_3$ thin-disk crystals was confirmed by the obtained laser performance. For the thin-disk laser with the 250 μm thick disk, an output power exceeding 500 W was achieved. Even at the maximum output power, the laser mode was stable and the optical efficiency of the thin-disk laser still increasing. By extrapolation of the measured temperatures, a maximum surface temperature of 140°C at a pump power of 2 kW can be expected. Consequently, it should in principle be possible to reach laser output powers in the order of 1kW. Although it would have been interesting to push this laser to its power limit, the power was not further increased to avoid any damage of the disk since the availability of additional Yb:Lu$_2$O$_3$-disks was restricted. Contrary to the 250 μm thick disk, the 200 μm thin crystal from the same Yb:Lu$_2$O$_3$ boule with 3 at.% doping concentration showed significantly lower output powers and no stable laser operation at higher pump powers. Exceeding a pump power density of about 1.2 kW/cm^2 caused a lateral contraction of the laser mode resulting in unstable laser operation. The recorded temperature distributions indicated that the strong increase of

the surface temperature of the disk was limited to a small hot spot. This absorbing spot might result from localized color centers, impurities or a clustering of Yb^{3+} ions [35], [36]. However, the defect was not detectable by microscopic examination. For this reason, it is suggested to comprehensively analyze each boule of Yb:Lu$_2$O$_3$ crystal material prior to the manufacturing of thin disks in order to be able to clearly identify the origin of such defects. In conclusion, the quality of the Yb:Lu$_2$O$_3$ material still varies strongly even at different areas of the same boule. However, certain Yb:Lu$_2$O$_3$ disks possess an adequate quality for high-power laser operation so that excellent laser performances can be obtained as reported in section 6.3.2.

6.3.2   CW multi-mode performance of ZPL-pumped Yb:Lu$_2$O$_3$ thin-disk lasers

To study the high-power laser performance of Yb:Lu$_2$O$_3$ thin-disk crystals, laser-active material of boules with an Yb^{3+} concentration of $8.55 \cdot 10^{-20}$cm^2 (corresponding to 3at.%) and $14.3 \cdot 10^{-20}$cm^2 (corresponding to 5at.%) was investigated. The laser disks had diameters of 11.3 mm (3at.%) and 7 mm (5at.%), respectively, and were mounted with their HR-coated backside on CVD-diamond heat sinks. The radii of curvature of the different Yb:Lu$_2$O$_3$ disks ranged between 1.8 and 4 m. All disks had a thickness of 250 μm. In a first set of experiments the optimum operation point of the Yb:Lu$_2$O$_3$ thin-disk lasers using 3at.% doped material was evaluated. For this purpose, different 3at.% doped Yb:Lu$_2$O$_3$ disks were mounted in a test-resonator with a simple V-shape design given in section 6.3.1. The performance of the resonator for three different output couplers having transmissions of 2%, 3% and 4.5% was determined. The results obtained with two selected disks are shown in figure 6.16. It can clearly be seen that up to a pump power of 863 W the output coupling of 3% led to the highest output power and efficiency of the laser. In this configuration an output power of 541 W could be extracted from disk 1 together with an optical efficiency of 63%. The corresponding slope efficiency was 77%. The same chart shows that the slope of the optical efficiency is slightly higher with 4.5% of output coupling when only the last three data points are considered. This indicates that an output coupler transmission of 4.5% will lead to the best performance at higher powers. An additional benefit of the higher transmission is the reduction of the heat load of the resonator elements due to the lower intra-cavity circulating power.
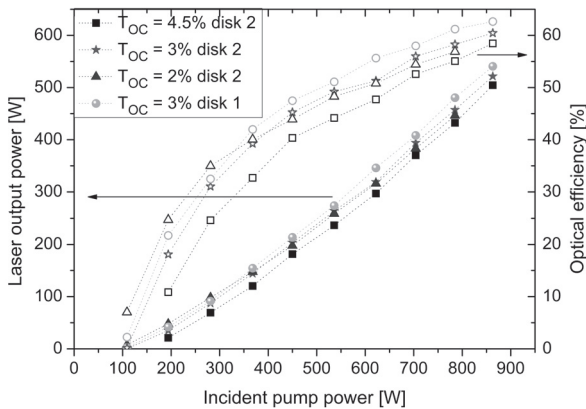
Figure 6.16: Laser output power and optical efficiency for two different Yb(3at.%):Lu_2O_3 thin-disk crystals with a thickness of 250 μm. For disk 2 the change of the performance for different output couplers is shown.

The knowledge gained during the study with the 3at.% doped Yb:Lu_2O_3 set the basis of the analysis regarding the high-power capability of this laser-active material in thin-disk configuration. From the previously reported temperature measurements (see figure 6.15), a maximum surface temperature of the Yb:Lu_2O_3 disks of about 140°C was extrapolated for an incident pump power of 2 kW. Although this temperature might be close to the practical limit it is sufficiently low to reach an output power of more than 1.3 kW without damaging the disk using the laser configuration described in section 6.3.1. The potential for an additional increase of the output power in future work is also indicated by the fact that 71% of the pump power were absorbed after 12 passes (measured by removing the rear mirror of the pump optics) through the 250 μm thick Yb:Lu_2O_3 crystal. Taking into account the losses in the pump optics, one can conclude that a crystal with a thickness of 170 μm would already be sufficient for an efficient operation when using 3at.% doped Yb:Lu_2O_3. Consequently, by combining thinner crystals (leading to better heat removal) and higher doping concentrations an increase of the pump power density is feasible which allows to scale the output power further. Further power scaling is also possible by an increase of the diameter of the pump spot.

In order to demonstrate that Yb:Lu_2O_3 shows good performances at higher doping concentrations, further experiments with 5at.% doped Yb:Lu_2O_3 were carried out. Figure 6.17 shows the results obtained in cw multi-mode operation with two different transmissions of the output coupler of 3 and 4.5%, respectively.
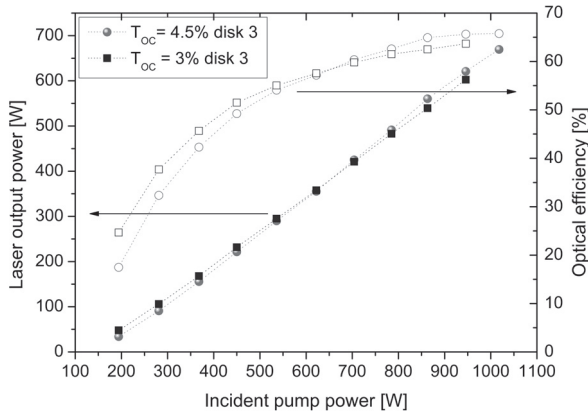
Figure 6.17: Output power and optical efficiency of an Yb(5at.%):Lu$_2$O$_3$ thin-disk laser in a V-shaped resonator configuration. The disk had a thickness of 250 μm and a diameter of 7 mm. Comparison of the laser performance with output couplers of 3% and 4.5%.

It is noticeable that at a certain point, the curves of the output power and the efficiency obtained with the two output coupler transmissions are crossing each other. This might be caused by a change of the sharpness of the pump spot image which was readjusted during the experiments. However, with 4.5% of output coupling, up to 670 W of laser output power was obtained with an optical efficiency of about 66% and a slope efficiency of 80% using a 250 μm thin disk with a diameter of 7 mm. This is the highest optical output power reached with the laser-active material Yb:Lu$_2$O$_3$ reported to date. Unfortunately, a further increase of the pump power density to approximately 4.6 kW/cm^2 caused a fracture of the Yb(5at.%):Lu$_2$O$_3$ disk so that the performance analysis of this disk could not be continued. The damage of the disk at this comparatively [94] low pump power density was most likely due to the unfavorable diameter ratio between pump spot (5.6 mm) and disk (7 mm) so that effects in the edge region of the disk implemented by the manufacturing and contacting process became critical. The lower efficiency in comparison to what was reported in [94] can be explained by the non-optimized pump spectrum due to the incomplete locking of the emitters of the diode laser stack (see section 6.1.2). This was verified by measuring the spectrum of the residual pump light after 12 passes through the crystal. It could clearly be seen that the unlocked part of the pump radiation was almost completely transmitted after the 12 passes.

6.3.3　CW high-brightness performance of ZPL-pumped Yb:Lu₂O₃ thin-disk lasers

Unlike the good performances of the Yb:Lu$_2$O$_3$ thin-disk lasers in multimode operation, the realization of high output power in fundamental-mode operation was rather challenging. A limiting factor thereby was the comparatively large diameter of the pump spot of 5.6 mm. This was already the minimum possible size that was defined by the brightness of the used pump diode in combination with the optical specifications of the thin-disk pump module. As a result of this large pump spot, the material quality, the polishing and the contacting of the Yb:Lu$_2$O$_3$ thin-disk crystals had to be excellent at least up to this diameter. Unfortunately this was not the case for the available thin-disk laser crystals. Even though the laser resonator was designed to obtain fundamental-mode operation and showed a near diffraction limited beam quality until approximately 120 W of output power, a degradation of the laser mode together with an efficiency drop at a pump power of about 580 W was observed, see figure 6.18 and 6.19. It is suspected that this effect was caused by a high internal stress of the Yb:Lu$_2$O$_3$ disk. The mounting of the disks on CVD diamond was not helpful in this context, but could not be changed anymore at this stage since the risk to damage the disk was high.
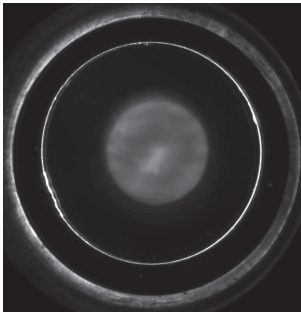
Figure 6.18: CCD-camera picture of the Yb:Lu$_2$O$_3$ disk showing the pump spot and the degraded laser mode at approximately 580 W of pump power.
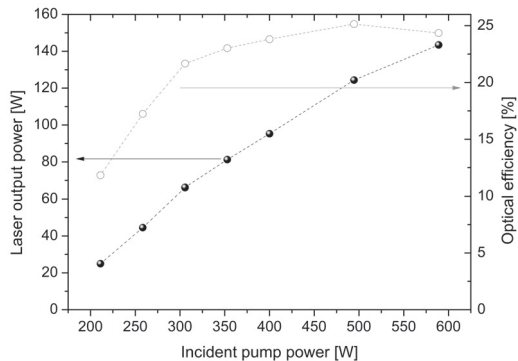
Figure 6.19: Laser output power and optical efficiency of the Yb:Lu$_2$O$_3$ laser. A drop of the optical efficiency at an incident pump power of ≈ 580 W can be observed.

However, the research to improve the crystal quality of Yb:Lu$_2$O$_3$ is still ongoing. Especially the reduction of stress implemented in the crystal during the growth is an important issue, but demanding due to the high melting temperature of this material. Alternative

methods to grow the crystals at lower temperatures are also existent but still at its beginning. Therefore, other possibilities like the usage of a heat sink with lower stiffness than CVD-diamond seems to currently be the best option to reduce the most likely stress-induced non-spherical deformation of the thin-disk crystal in laser operation. This seems to be the crucial factor for fundamental-mode operation. Finally, pump diodes that allow to obtain smaller pump spot sizes would also lower the constraints on the desired crystal quality and is suggested as investment in future work regarding this topic.

In conclusion, the power scaling capability of single-crystal Yb:Lu$_2$O$_3$ towards the kW output power range by ZPL-pumping was demonstrated. The temperature measurement of the crystal during laser operation allowed extrapolating the potential of this material for the multi-kW regime in thin-disk configuration. If Yb:Lu$_2$O$_3$ with good quality was available, the performance in multimode operation was only limited by the incomplete spectral narrowing of the pumping radiation and the unfavorable geometries of the thin-disk samples. A further improvement of the laser performance is expected by using thinner disks, but the polishing and contacting of Yb:Lu$_2$O$_3$ disks with thicknesses of less than 200 μm seems to be challenging. Taking into account this room for obvious improvements, the experiments nevertheless showed the promising potential of Yb:Lu$_2$O$_3$ for further power scaling.

7 Correction of the aspherical optical phase distortions in thin-disk lasers

Previous studies show that there is a limit in terms of beam quality of Yb:YAG and Yb:LuAG disk lasers at the multi-kilowatt output power level due to the thermally induced aspherical phase front distortion caused by the disk when using the conventional pumping wavelength of about 940 nm. To be able to use conventional pump diodes (spectral width about 3-6 nm) with a wavelength of 940 nm for technology and cost reasons and still reach good beam quality at this power level thus requires a compensating element inside the laser cavity like for example a static, actively-controlled, or adaptive aspherical mirror. In this context the rule of thumb applies that the higher the output power of the laser, the more evident becomes a compensation of the aspherical deformation of the disk to obtain a high optical efficiency together with a high brightness of the beam. This is particularly true for thin-disk lasers with beam parameter products of less than approximately 3 mm·mrad.

Indeed, the compensation of the aspherical part of the thermally induced deformations caused by the thin-disk crystal can be accomplished in different ways, but simplicity is always beneficial especially with regard to high-power laser operation. Therefore, a simple aspherical mirror concept was used as a starting point of the investigations. It was easily applicable and allowed to determine possible challenges for further research. The experimental results obtained with this promising mirror solution are presented in this chapter.

7.1 Aspherical mirrors for the use in thin-disk lasers at multi-kW output power level

In general, only fully dielectric mirrors on transparent dielectric substrates (e.g. fused silica) have shown to be suitable to reach the required high reflectivities (> 99.98%) and high surface quality for the implementation in high-power thin-disk laser cavities. This, and the high power densities exceeding 200 kW/ cm^2 inside the laser cavity restrict the choice of suitable optical elements. For this reason, high-power laser mirrors were

selected and geometrical and/or structural changes implemented to have a convenient basis for the investigations.

A static compensating mirror was developed in the first step. By using this concept complex control techniques are avoided. Furthermore, it is applicable to industrial thin-disk laser systems working at a fixed output power or with external power modulations. As previously explained in the sections 4.1 and 5.1.2, the required shape of the static aspherical mirror can be derived from the profile of the pump intensity in the thin-disk crystal and approximated by a Super-Gaussian function [16]. To obtain the appropriate height of the aspherical profile, the optical path difference ΔL_{opt} induced by an Yb:YAG disk with a thickness of 120 μm was estimated by [16]

$$\Delta L_{opt} = K_{th-opt} \cdot \frac{2}{3} \Delta T_{max} \cdot d_{crystal} \qquad (7.1)$$

For a large ratio between pump beam diameter and crystal thickness ($d_{crystal}$), the effective temperature in the laser disk converges to the value of 2/3 ΔT_{max}. This is a quite accurate assumption for the temperature averaged over the pumped volume and can be applied for disks with a thickness of up to a few hundreds of micrometers when the size of the pump spot is in the order of millimeters [16]. The temperature difference ΔT_{max} considers the heat power density which is defined by the part of the absorbed pump power which is transformed into heat. To correlate the change of the temperature with the change of the refractive index and the thermal expansion of the Yb:YAG disk the parameter K_{th-opt} ($\approx$13.4 $\cdot 10^{-6}$) is used. An optical path difference of about 130 nm was estimated when pumping the disk with a pump power of 7 kW on a spot diameter of 9.4 mm at the wavelength of 940 nm.

The value of $\approx$130 nm is valid for a single pass through the thin-disk crystal. However, the compensating mirror and the disk can be used either as end or folding mirror, whereby the step height can be the same, the double or the half of the calculated value. Performing the compensation of the aspherical distortions in the image plane of the disk avoids the appearance of any additional distortions, but a telescope has to be added in the resonator configuration which increases the number of mirrors and the complexity of the resonator. Another possibility is to use a sufficiently short distance between the mirror and the thin-disk crystal so that additionally induced wavefront distortions are negligible. This solution allows to use a simple resonator setup consisting of only two mirrors (see figure 7.1) and was therefore chosen for the experiments presented in the following.
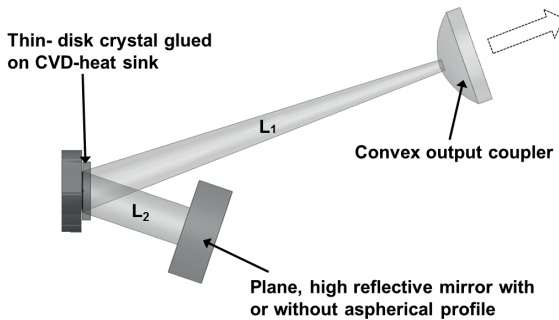
Figure 7.1: Drawing of the V-shaped resonator. A convex output coupler with a reflectivity of 97% and a radius of curvature of 2.3 m was placed in a distance L_1 of 1.8 m to the disk; a plane HR-mirror or aspherical HR-mirror was placed in a distance L_2 of 0.5m to the disk.

The proof of principle was performed with a compensating mirror having an aspherical step profile with a height of 100 nm and an edge contour with a 10th order Super-Gaussian profile. The development of a compensation mirror suitable for high-power laser operation appeared to be demanding since losses due to stray light and heating are significant factors. Particular attention had to be given to the achievable surface roughness and the substrate material itself. Furthermore, the achievable accuracy of the fabrication method in order to realize a step with a height of 100 nm. Several fabrication methods like etching or fluid jet polishing have been taken into consideration but exhibited an achievable surface roughness which was not sufficient for a good coating adhesion afterwards. Hence, an efficient operation of these mirrors in high-power thin-disk lasers could not be guaranteed. However, a simple method was found to fulfill the demands. It consisted of a coating of SiO_2 which was applied through an aperture as shown in figure 7.2. The aperture was positioned at a defined distance from a laser mirror substrate made of fused silica. Two samples, possessing the aforementioned aspherical profile and a high reflection coating on top were fabricated in a deposition process by a coating supplier. In the following section the characterization of these aspherical mirrors and the experimental results obtained in a high-power thin-disk laser system are presented.
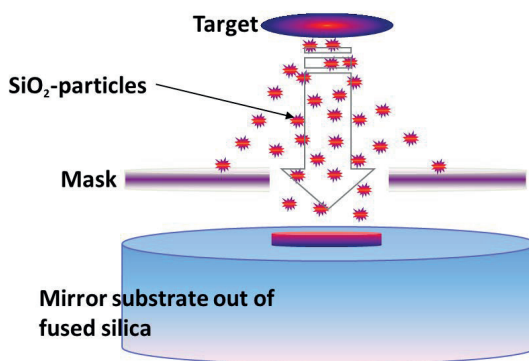
Figure 7.2: Drawing of the fabrication process of the aspherical surface by deposition of particles on a mirror substrate through a pinhole shaped mask.

First of all, interferometric measurements of the profile of the aspherical mirrors were conducted. The measured step heights of the two mirrors were approximately 85 nm and 90 nm, respectively. Both mirrors showed a good agreement of the edge profile to a 10th order Super-Gaussian function. The sharp step-profile was already clearly visible in the interferometric picture as shown in figure 7.3 and it was approved by the measured data as can be seen in figure 7.4.
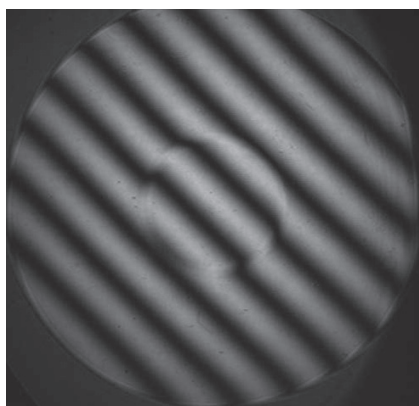
Figure 7.3: Interferometric picture (static fringe pattern) of an aspherical mirror after fabrication. The measurement wavelength of the interferometer was 980 nm.
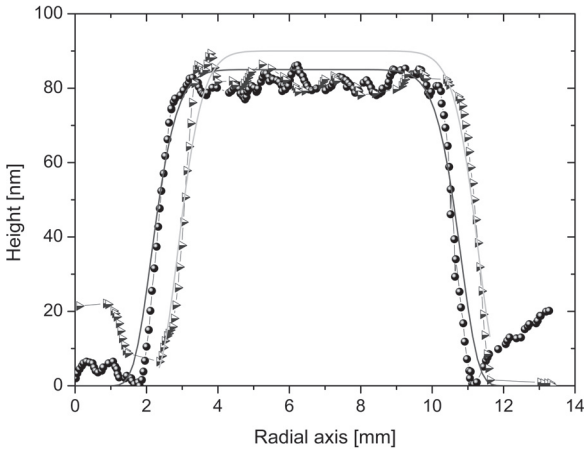
Figure 7.4: Measured step-profile of the aspherical mirrors. The solid lines indicate the equivalent Super-Gaussian fit-function with an exponent g=10 and heights of about 85nm and 90 nm, respectively.

The good quality of the aspheric profile realized with the coating method described above makes this fabrication technique also suitable for the generation of other axially symmetrical aspherical profiles. In total, it provides low surface roughness and high accuracy together with simplicity in comparison to other manufacturing processes.

A 120 μm thick Yb:YAG disk with a doping concentration of 11% mounted on a CVD diamond heat sink was used for the experimental investigations presented in the following. The deformation of this thin-disk crystal was previously analyzed for different pump power levels. The results of the conducted measurements (see figure 5.7) can be found in chapter 5 of this thesis, since they were used to exemplify the performance of the developed high-precision interferometer.

In this thin-disk laser setup, the pump radiation at a wavelength of 940 nm (configuration of diode stack with homogenizer) passed 20 times through the thin-disk crystal and was therefore efficiently absorbed. A pump cavity from TRUMPF Laser GmbH & Co KG was used for this purpose. The system was adapted in order to allow the laser to operate in helium atmosphere. To achieve a sufficient overlap of the emission spectrum of the pump diodes to the absorption peak of Yb:YAG, the complete system had to be operated at a cooling temperature of 30 °C. Thus, a further enhancement of the laser performance would be achieved when using a separate cooling unit with lower cooling

temperature for the disk. The resonator design was a simple V-shaped configuration (see figure 7.1) in order to easily implement it later in an industrial laser system. It consisted of the aspherical or plane rear mirror, the thin-disk crystal as folding mirror and a convex output coupler (ROC = 2.3 m, T = 3 %). The arm lengths of the resonator between the aspherical mirror and the disk was kept as short as possible to minimize distortions of the phase front of the laser mode due to an non-ideal compensation. For this reason, the adaption of the size of the resonator mode to the diameter of the pump spot was done with the radius of curvature of the convex output coupler. To experimentally verify the compensating effect of the aspherical mirror, a direct comparison to the results obtained with a flat rear mirror was performed. The performance of the laser with both mirror versions are given in figure 7.5 and figure 7.6. Without compensating aspherical mirror, the laser operation became so unstable that the laser was switched off automatically by a fluorescence light detection to avoid a damage of the thin-disk crystal. This safety shutdown was undertaken in case the detected fluorescence level from the disk exceeds a certain threshold.
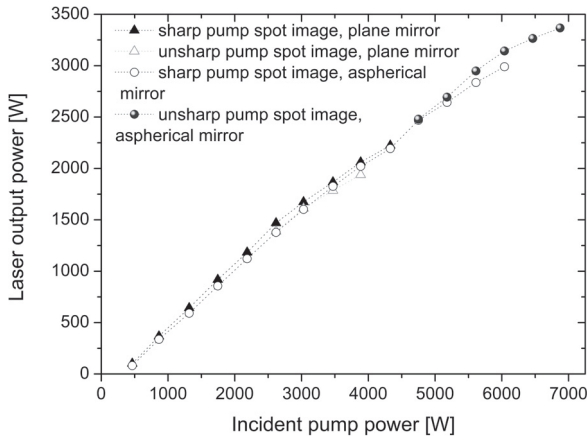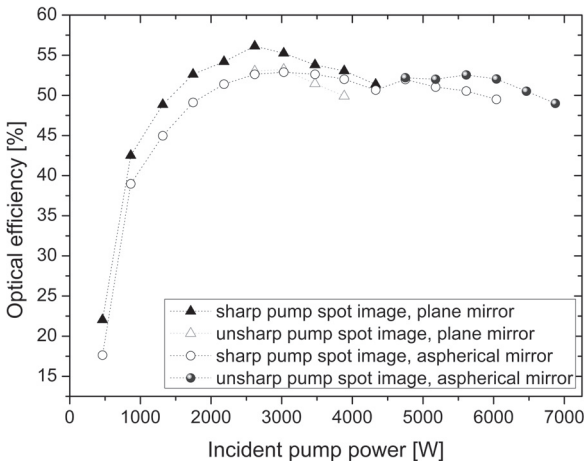

Figure 7.5: Laser output power versus incident pump power for sharp and unsharp pump spot images on the disk by using a plane or aspherical HR-mirror in the V-shaped resonator. The laser operation became unstable at about 4 kW of incident pump power when using the plane mirror so that the laser was switched off automatically by a fluorescence light detection to avoid a damage of the thin-disk crystal.

To realize a perfect match between the pump power distribution and the surface profile of the aspherical mirror, further experiments with a slight defocusing of the pump spot on the disk have been carried out. The obtained laser performance are also depicted

in figure 7.5 and figure 7.6. The defocusing of the pump image allowed an additional increase of the output power of the laser system. This was due to a resulting lower diffraction of the laser mode since the softer edges of the defocused pump spot are smoothing the aperture of the gain as well. A detailed description of this behavior based on interferometric measurements is given in section 5.2.2 of this thesis. As a result of the defocusing, a laser output power of 3.4 kW with an optical efficiency of 49 % and a beam parameter product of 2.4 mm ·mrad ($M^2 \approx 8$) was demonstrated by using the same resonator configuration described above.

Figure 7.6: Optical efficiency versus incident pump power for sharp and unsharp pump spot images onto the disk by using a plane or aspherical HR-mirror in the V-shaped resonator.

By analyzing the two figures it can clearly be seen that the implementation of the aspherical mirror makes it possible to achieve higher output powers due to the compensation it provides for the thermally induced phase front distortions caused by the laser disk. It can also be recognized that the aspherical profile creates more losses at lower incident pump powers which is why the output power and the optical efficiency are smaller than the ones obtained with the standard plane HR mirror. Despite this, the compensating effect takes place above a certain pump power causing a stabilization of the laser modes along with a rise of the efficiency.

A second method to produce a top-hat shaped profile in a fused silica substrate suitable to be used in high-power thin-disk lasers was presented in [95] and is based on a modified

laser lithography and ICP etching process. By using this method, the aspherical profile was directly written into a substrate with convex surface (ROC = 1 m) which served as the output coupling mirror of the resonator. These aspherical mirrors had a larger step height of about 190 nm, again with an approximately 10th order Super-Gaussian edge profile. The larger step height was a consequence of the consideration that the nominal working point should be shifted to output powers around 5 kW and the observations that the 1st generation of aspherical mirrors had their optimum working point at approximately 3 kW of output power. Using this kind of aspherical mirror a V-shaped resonator with an overall length of only 1.84 m allowed to generate 4.78 kW of output power with an optical efficiency of 48% featuring a beam quality factor M^2 of 7.8. A more detailed description of the setup and the conducted experiments can be found in [96].

The knowledge gained during the first successful demonstration and usage of an aspherical mirror in a thin-disk laser with output powers at the kilowatt level supported the further development of actively-controlled mirrors for the same purpose.

7.2 Actively-controlled mirrors for the use in thin-disk lasers at multi-kW output power level

As mentioned, the limitation of the static aspherical compensating mirrors is that they work only perfectly for a pre-defined point of operation. This may be enough for some industrial thin-disk laser systems but not sufficient for all. The next step of this research subject was therefore to increase the flexibility of these mirrors and thus the development of an actively-controlled aspherical mirror. The demands on the coating and substrates are equivalent to those of the static aspherical mirrors reported on previously, but with the additional requirement that the surface of the element has to be deformable up to a few hundred nanometers using defined steps.

In the presented approach, a specific deformation of the upper side of a laser mirror was produced by applying pneumatic pressure to the rear side of the thin or backside structured mirror substrate, see figures 7.7 and 7.8. Based on this method, a simple pneumatic mirror device was fabricated as follows. A circular recess was manufactured by ultrasonic drilling which was applied from the rear side of a conventional mirror. The ultrasonic drilling of the defined ring-shaped area was performed until only a few hundred micrometer of substrate material remained. The layout and the principle of operation of this mirror are shown schematically in figure 7.7. The diameter of the ring is directly related to the pump spot diameter on the thin-disk crystal, whereas the remaining substrate

thickness in combination with the applied air pressure defines the shape of the aspherical deformation. After the ultrasonic-drilling, the mirror was glued with its outer area onto a water-coolable mount by using a two-component, high-temperature epoxy. As a result, the central area at the backside of the mirror can be sealed and thus be subjected to a controllable air pressure. The diameter of this central area corresponds approximately to the pump spot diameter on the disk. By changing the pressure (typically up to 6 bar) applied to the small air volume, different aspherical step-shaped deformations in the order of one and up to a few hundred nanometers are obtained.
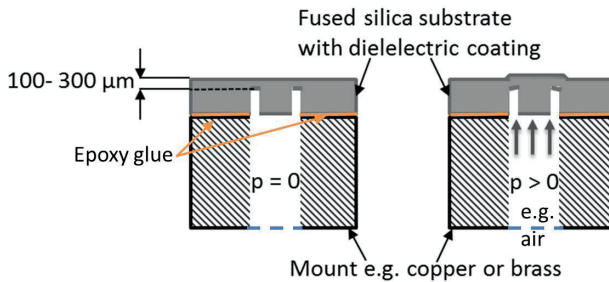
Figure 7.7: Principle of the actively-controlled mirror with structured mirror substrate which is deformed by an backside applied air pressure p.
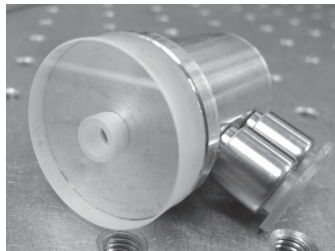
Figure 7.8: Picture of the 1st prototype of the actively-controlled mirror.

The proof of principle of this concept was demonstrated in the project ThermAO [97] which was funded by the Baden-Württemberg Stiftung. However, the pressure-based actively-controlled mirrors of these early developments were not suitable to operate at high output-powers of the thin-disk laser. Limitations with regard to the quality of these mirrors were due to the use of water in order to apply the backside pressure and a non-

optimized gluing process. We overcame these limitations with the design of the actively-controlled mirror prototype using compressed air as described above. By implementing such a mirror in the resonator, an Yb doped thin-disk laser with up to 815 W of output power and a beam quality factor M^2 better than 1.4 was demonstrated [98]. This topic was subject of further studies and afterwards addressed in the DFG-project "Methoden zur Regelung von adaptiven optischen Systemen in Hochleistungslaserresonatoren". A comprehensive overview of the results obtained during this project can be found in the thesis of Piehler [99].

8 Study of the novel laser-active material Yb:YAB for the use in high-power thin-disk lasers

Thin-disk lasers have a high potential to be used as laser source to generate femtosecond-pulses with an average output power at the kilowatt-level. For this aim the combination of a thin-disk laser crystal with a saturable absorber mirror (SAM) [100], [101], [102] is a promising approach. In view of a laser operation at high output powers, a thin-disk crystal and a SAM have one interesting feature in common. In theory and to a large extent also in practice, they can easily be scaled in power by increasing the pump spot diameter on the thin-disk crystal and likewise by increasing the mode size on the SAM. The presupposition in both cases is that laser-active material and absorber material exhibit a high optical quality with constant material parameters over large areas. Furthermore, the material has to be contacted over this area without distortion of the shape. If these conditions are fulfilled, a highly efficient heat extraction has additionally to be guaranteed for both components (disk and SAM). For these reasons, the realization of laser disks or SAMs, which are able to withstand power densities in the order of MW/cm^2 is still not state of the art technology.

Although the realization of a high-power laser oscillator generating femtosecond pulses is the final goal, a laser with high average output power and near-diffraction limited beam quality has to be demonstrated first. Of course, the choice of the laser-active material to obtain the desired high output power has to be made among those materials which facilitate the generation of ultrashort pulses. The list of laser-active materials discussed in the following is by no means exhaustive but refers to a few promising candidates in order to achieve the above mentioned goal.

As explained in chapter 3, laser-active materials have to fulfill certain requirements in order to be suitable for thin-disk lasers. At present, one can divide the laser-active materials which are appropriate to be integrated in thin-disk lasers into materials suitable to obtain output powers at the multi-kW level such as Yb:YAG and Yb:LuAG and into gain media featuring large spectral emission bandwidths sufficient to generate ultra-short pulses such as e.g. Yb:Lu$_2$O$_3$ [103], Yb:CALGO [104], Yb:SSO [105] or Yb:YAB [41]. To be able to scale mode-locked thin-disk lasers to the kW-level by using one of the latter

materials, a key technology has to be considered: the crystal growth process. Regarding this aspect, Yb:CALGO, Yb:SSO and Yb:YAB offer the advantage of a growth process at a comparatively low temperature which is close to or lower than the one of Yb:YAG (around 1940 °C). Moreover, the crystal structure of Yb:CALGO and Yb:SSO allows the growth by using the well-known Czochralski method. On the contrary, all sesquioxides including Yb:Lu$_2$O$_3$ have a comparatively high melting temperature (around 2430 °C). For this reason their growth process is quite demanding and still under intensive development until now. Nevertheless, not only Yb:Lu$_2$O$_3$, but also Yb:CALGO, Yb:SSO and Yb:YAB show a remarkable variation of the crystal quality from boule to boule. Issues are e.g. absorption and scattering defects and high internal stress inside the thin disks. Some of these aspects are discussed in chapter 3.3 and 6.3. Undeniably, the decision to use one of these material for an industrial thin-disk laser will depend to a large extent on the availability of crystals with high optical quality and only partly on the theoretical parameters the laser-active material is offering. In addition it should also be considered that for numerous industrial applications a difference of a few hundred femtoseconds of the pulse duration is only a minor aspect. Having said that, the laser-active material Yb:YAB has the prospect to enter into the field of high-power mode-locked thin-disk oscillators and was analyzed for the first time in thin-disk configuration (see chapter 3.2.4 for the thermal and spectral properties) as presented in the following.

8.1   Characterization of Yb:YAB for the use in thin-disk lasers

Yb:YAB-material was extensively studied for its use in microchip lasers. However, there was no demonstration in any other laser configuration so far. This was most likely due to the fact that by using other laser approaches than the microchip design certain requirements regarding the crystal quality and size have to be fulfilled. For the growth of the Yb:YAB material employed in the experiments presented here, the top seeded solution growth (TSSG) [106] was applied. The TSSG-process offers the advantage of low crystallization temperatures (of about 970 °C; solvent Li$_2$WO$_4$) which results in inherently small temperature gradients and therefore comparatively small dislocation densities [107]. For this reason, the internal stress of the crystals is likely to be also small. A sufficient crystal size was obtained by this growth method, allowing to manufacture thin-disk crystals with a diameter of 6.3 mm. The Yb-ion concentration of the grown crystal was 12 at.%, corresponding to an Yb^{3+} volume concentration of $6.6 \cdot 10^{-20}$ cm^3. To be able to analyse both, IR and self-frequency-doubled laser operation, the crystals were cut for

type I phase matching of 1030 nm under normal incidence with an angle of 31.3° to the c-axis. The growth and polishing of all Yb:YAB thin-disk crystals was carried out by the company FEE The polishing quality of the Yb:YAB thin-disk surfaces were similar to the one commonly obtained for Yb:YAG thin-disk crystals as can be seen in figure 8.1.
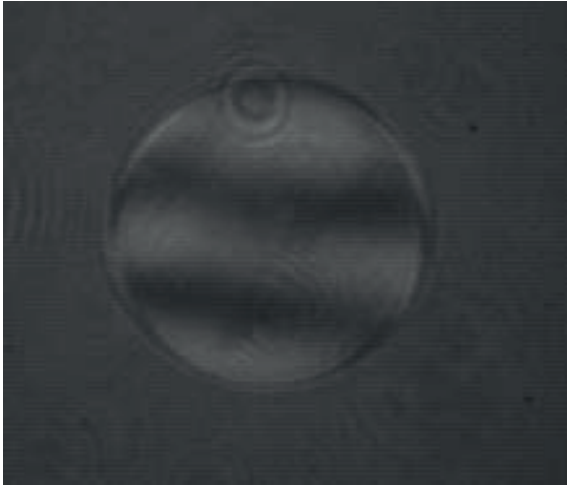

Figure 8.1: Interferogram of an Yb:(12at.%)YAB disk with a diameter of 6.3 mm and a thickness of 250 μm after polishing. The planarity of the disk is similar to the one commonly obtained for Yb:YAG thin-disk crystals.

Furthermore, no scattering defects or crack formation inside the thin disk could be observed by microscopic examination. However, using a Nomarski interference contrast microscope revealed changes of the optical path length in the disk as shown in figure 8.2. These areas can be recognized as the previously reported stacking faults from Dekker and Dawes [108] inside the Yb:YAB crystal structure. These defects are supposed to mainly influence the efficiency of the frequency conversion but not the achievable infrared output power. Nonetheless, a detailed analysis of these stacking faults, especially with regard to the influence on the polarization state of the laser emission has to be subject of future work. Despite this, an investigation of depolarization losses in the resonator, especially in the (polarized) fundamental-mode and mode-locked operation should be carried out as well. In addition, there is an on-going development in the crystal growth process at FEE with the aim to impede these defects.
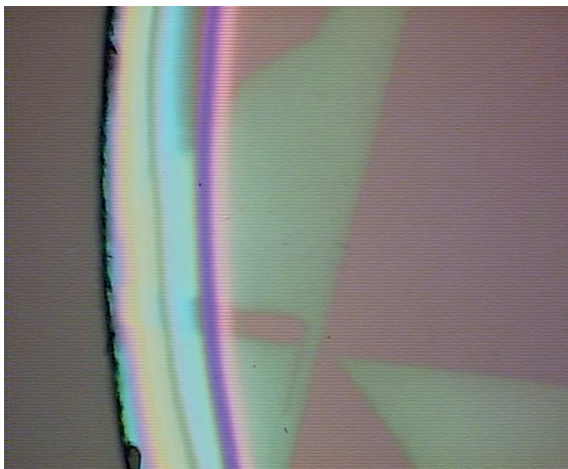
Figure 8.2: Microscope image of stacking defaults in an Yb:(12at.%)YAB disk.
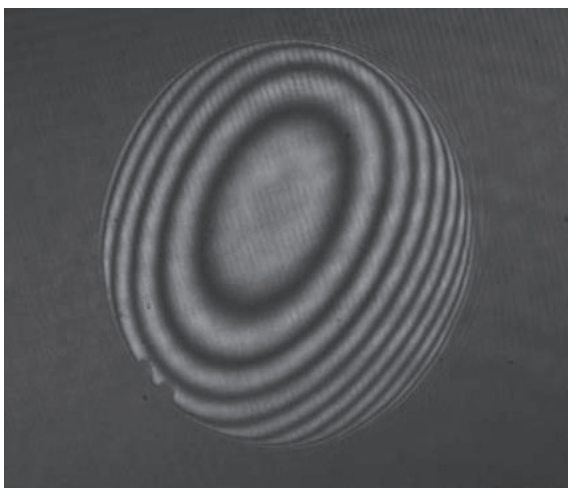
Figure 8.3: Interferogram of an Yb:(12at.%)YAB disk with a dimeter of 6.3 mm and a thickness of 250 μm after coating. As can be seen, the curvature of the disk was strongly asymmetric.

After the coating process, an asymmetric deformation of the Yb:YAB disk was observed, see figure 8.3, which was most probably due to the different heat expansion values along the a- and c-axis of Yb:YAB. During the bonding process the thin-disk crystal was damaged which reduced the usable optical aperture of the disk to less than 3 mm. The fracture might have been a result of the high internal stress inside the disk which was introduced by the coating process and can be seen in figure 8.3 by the strong difference of the radius of curvatures (ROCs) in vertical and horizontal axis of the disk.

8.2   Yb:YAB thin-disk lasers in high power CW-operation

The experimental investigations have been conducted by using a thin-disk laser pump cavity that allowed 24 passes of the pump radiation through the disk. To determine the suitable operation parameters for the Yb:YAB thin-disk laser, a thermal characterization as well as measurements providing the optimum output coupling were performed. It has to be mentioned in this context that the reflectivity of the AR-coating of the Yb:YAB disks was slightly higher than in the desired specifications given in section 3.3.3. This was due to the difference in the refractive index between Yb:YAG (n= 1.82) and Yb:YAB (n= 1.76) since the Yb:YAB disks were added to a coating batch optimized for Yb:YAG.

Our aim was to investigate the output performance of both, IR and self-frequency-doubled emission. Therefore, a trade-off with regard to the crystal thickness was made and a thickness of 250 μm was chosen. This is approximately 100 μm thicker than needed for efficient pump light absorption at this doping level when using 24 pump beam passes, but offers a longer conversion length for the frequency doubling with still reasonable heat removal. However, the results obtained in frequency-doubled operation shall not be presented here. The Yb:YAB thin-disk crystal was glued onto a copper heat sink and efficiently cooled by the typical impingement cooling.

To evaluate the power handling capability of the Yb:YAB laser disk, the temperature of the surface of the disk was measured as a function of the incident pump power density during fluorescence and laser operation. The temperature was recorded using a thermal imaging camera (InfraTec VarioCam). For a pump power density of 2.7 kW/cm^2, a maximum temperature of 71 °C without resonator feedback (fluorescence) and 56 °C during laser operation was measured. These values could be reduced even further by a lower thickness of the disk or by improving the heat extraction out of it e.g. with CVD-diamond heat sinks. Numerical calculations show (see section 4.1.3) that by using CVD-diamond a reduction of the temperature difference in the disk of $\approx$ 20 % can be achieved. Consequently, Yb:YAB has the potential to be scaled to the high-power level.

A performance analysis (by using a unpolarized, fiber coupled pump diode: $P_{max}=$ 60 W, $\lambda_p \approx 974$ nm) allowed to determine the optimum operation point of the Yb:YAB thin-disk lasers with I-shaped and V-shaped resonators. Thereto, different output couplers having transmissions between 0.5% and 3% were tested. For the I-shaped resonator the optimum output coupling was 1.5% and for the V-shape resonator 2%, respectively. Figure 8.4 and figure 8.5 show the experimental results. The slightly better performances with the V-shaped resonator were most likely due to the higher optical quality of the available output couplers. To give an example regarding the impact of the mirror quality on the output performance, the obtained results for two output couplers with nominally the same reflectivity of 97 % are depicted in figure 8.5 (squared- and sphere-symbols). A pump spot diameter of 1 mm was used for all experiments. The ROC_{disk} of the thin-disk crystal was about 4 m (concave, without incident pump radiation). For the sake of clarity, the resonator parameters of all configurations reported in this chapter are summarized in table 8.1.

Table 8.1: Resonator parameters

Fig.	d_p[mm]	ROC_1[mm]	ROC_2[mm]	L_1[m]	L_2[m]	M^2
8.4	1.0	0.5 cav	-	0.15	-	≈ 4
8.5	1.0	0.5 cav	0.5 cav	0.35	0.35	≈ 4
8.6	1.0	0.5 cav	0.5 cav	0.35	0.33	≈ 3
8.6	1.0	0.35 cav	0.5 cav	0.35	0.425	≈ 6
8.6	1.0	0.35 cav	0.5 cav	0.35	0.475	≈ 10
8.7	2.3	0.35 cav	0.5 cav	0.355	0.47	≈ 51
8.7	2.6	0.35 cav	0.5 cav	0.355	0.47	≈ 60
8.8	0.87	0.35 cav	0.5 cav	0.355	0.23	≈ 1
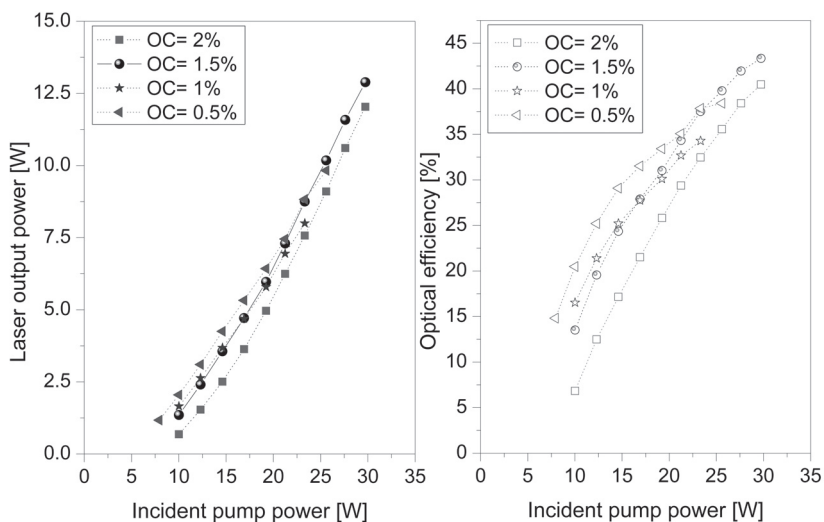
Figure 8.4: Output performance of the Yb:YAB thin-disk laser with I-shaped resonator configuration for different output coupling (OC).
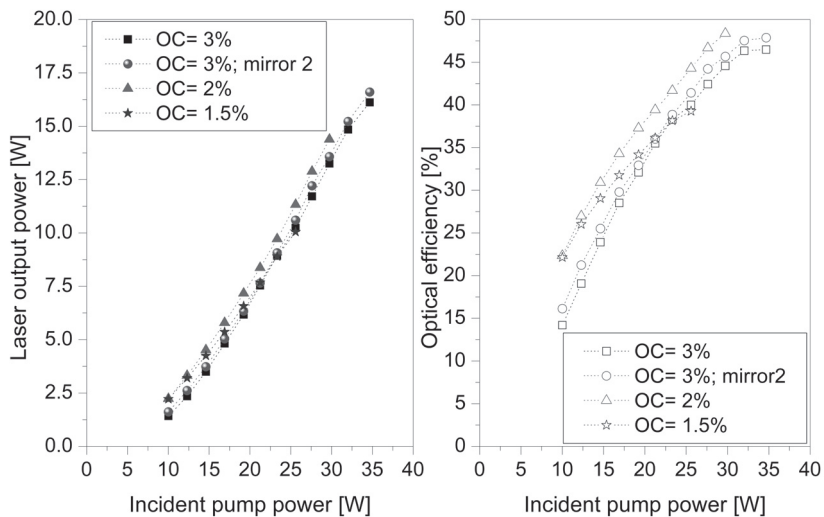
Figure 8.5: Output performance of the Yb:YAB thin-disk laser with V-shaped resonator configuration for different output coupling (OC).

By varying the ROC of the end mirror between 0.35 m and 0.5 m and adapting the reso-
nator length from 0.33 up to 0.475 m, multimode operation with different beam quality
factors was obtained. The best efficiency performance, with a maximum optical efficien-
cy of 60.4% corresponding to a slope efficiency of 76.4%, was achieved for a M^2 of 10
as shown in figure 8.6. The maximum output power was 19.3 W in this configuration.
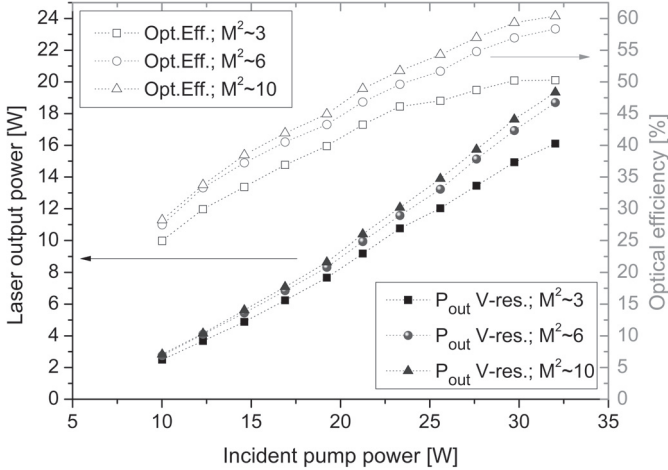
Figure 8.6: Output power and optical efficiency of Yb:YAB thin-disk lasers with different beam
quality factors. The highest optical efficiency was 60.4%.

To continue the analysis of the power handling capability, high-power tests (with an
unpolarized, fiber coupled pump diode: P_{max}= 1 kW, $\lambda_p \approx$ 975 nm) of the Yb:YAB
thin-disk crystal with larger pump spot diameters of 2.3 and 2.6 mm were performed.
For these experiments an HR end-mirror with a ROC of 0.35 m was used in the V-
shaped resonator described previously. The length of the arm with the output coupler was
0.47 m. With this resonator, a maximum output power of 93.1 W and an optical efficien-
cy of 50.7% was reached with a pump spot diameter of 2.3 mm. By increasing the pump
spot size to 2.6 mm, the output power was scaled further to 109 W with an optical effi-
ciency of 50.2%, see figure 8.7. The beam quality factor M^2 was $\approx$ 50...60.
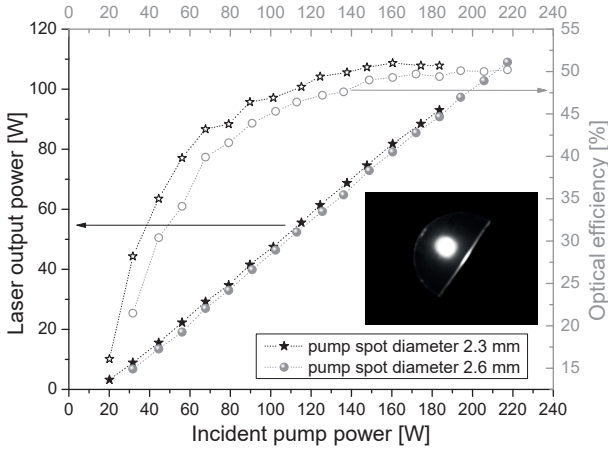
Figure 8.7: Output power and optical efficiency of the Yb:YAB thin-disk laser in high-power multimode operation for pump spot diameters of 2.3 and 2.6 mm.

As already mentioned, the Yb:YAB crystal was damaged during the mounting process so that the usable optical aperture of the disk was strongly reduced. The decrease of the optical efficiencies in these experiments can therefore be mainly attributed to the fact that the damage already interacted with the pump spot.

8.3   Fundamental-mode Yb:YAB thin-disk lasers and wavelength tuning capability

In order to continue the experimental investigations of Yb:YAB with regard to mode-locked operation, an analysis on the fundamental-mode operation was performed. For this purpose the pump spot diameter was reduced to 0.87 mm (pump diode: $P_{max} = 60$ W, $\lambda_p \approx 974$ nm). To efficiently suppress the oscillation of higher-order transverse modes, the diameter of the fundamental mode on the thin-disk was chosen to be 77% of the pump spot size. The V-shaped resonator with an overall length of 0.59 m (see table 8.1) consisted of a concave end mirror (ROC= 0.35 m) and a concave output coupler (ROC= 0.5 m) with a transmission of 2%. The beam quality was determined by a dual-knife-edge beam measurement using a Coherent ModeMaster. The output performance of the Yb:YAB laser together with the beam quality factor is shown in figure 8.8. At the

maximum output power of 10.4 W and an optical efficiency of 44.5%, the laser oscillated with a beam quality factor $M^2_R = 1.39$.
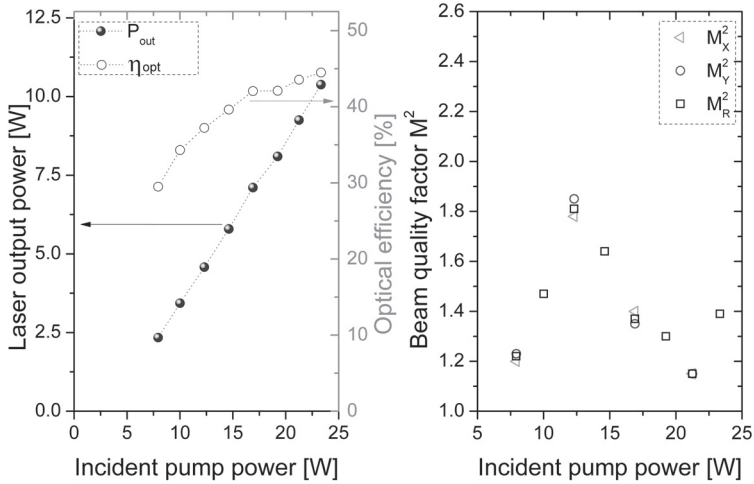
Figure 8.8: Left: Output performance of the Yb:YAB laser with near-diffraction limited beam quality. Right: Corresponding beam quality factors.

By demonstrating the fundamental-mode operation of the Yb:YAB thin-disk laser, the prerequisite for ultra-short pulse operation was fulfilled. Based on the broad fluorescence bandwidth one can expect that Yb:YAB should provide pulse durations down to about 200 fs or less in a passively mode-locked thin-disk oscillator. Thereby, the suppression of the self-frequency doubling of the laser crystal plays an important role for an efficient operation in mode-locked configuration since the radiation generated at the frequency-doubled wavelength acts as loss mechanism in the resonator. However, the frequency-conversion might be sufficiently suppressed by a proper selection of the cut-angle of future Yb:YAB laser disks.

To experimentally analyze the predicted large bandwidth of the laser emission of Yb:YAB, a wavelength tuning of the emission was performed. The tuning range of the IR laser emission was measured by inserting a mirror based on a grating waveguide structure (GWS) under Littrow configuration (for the principle see [109]) in a multimode ($M^2 \approx 5$) V-shaped resonator. A GWS-mirror with a diffraction efficiency of about 99.8% in the -1st order served as the output coupler (0.2% of output coupling). The 0.6 m long reso-

nator was completed with a concave HR mirror with a ROC of 1.5 m, see figure 8.9. A HR4000 spectrometer from Ocean Optics was used to record the emission spectra. The incident pump power during this experiment was 98 W.
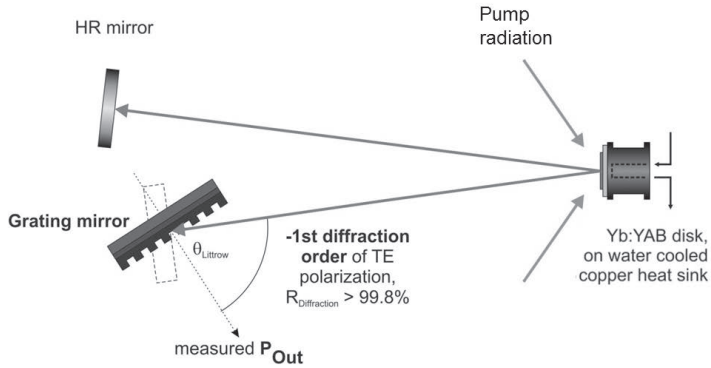

Figure 8.9: Yb:YAB thin-disk resonator setup with GWS-mirror as output coupler.

As can be seen in figure 8.10, a wavelength tuning range of 52 nm from 1001 nm to 1053 nm was obtained. For wavelengths above 1053 nm, the gain of Yb:YAB decreases strongly so that the resonator round-trip losses were too high to maintain laser operation at longer wavelengths. In a free-running Yb:YAB thin-disk laser resonator, the emitted laser wavelength is centered at a wavelength of ≈ 1040 nm with a FWHM spectral bandwidth of 4 nm (see dashed line in figure 8.10). This spectral bandwidth is reduced to a FWHM of ≈ 1 nm when a GWS-mirror in the resonator is used. Nevertheless, output powers higher than 10 W were achieved for the spectral range between 1009 nm and 1048 nm with a maximum of 36 W at a wavelength of 1040 nm.
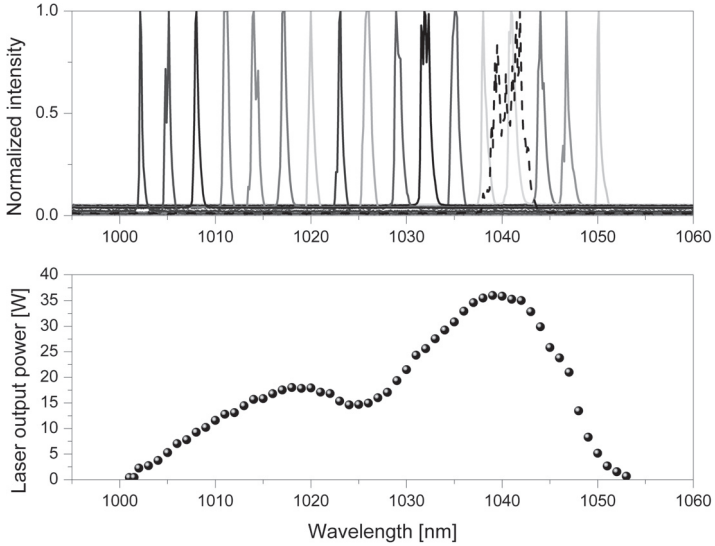
Figure 8.10: Top: Spectral tuning range of the Yb:YAB thin-disk crystal. Bottom: Corresponding output power for the wavelength range between 1001 and 1053 nm. To compare the spectral emission with and without GWS-mirror the spectrum of a free running Yb:YAB thin-disk resonator is shown by the dashed curve.

In conclusion, the good suitability of the laser-active material Yb:YAB for the thin-disk configuration was proven. Future work will push the laser performance further by taking into account the obvious room for improvements e.g. by applying an optimized AR-coating or using CVD-diamond heat sinks. Further investigations will concentrate in addition on the test of Yb:YAB thin-disk crystals configured (with regard to the cutting angle) for their use in mode-locked operation. Key point of this analysis will thereby be the successful suppression of unwanted frequency-conversion which is a source of loss of output power for this type of operation.

9   Summary

In the present thesis different methods to scale the output power of thin-disk lasers containing only one disk to the kilowatt level and beyond, whilst keeping the beam quality as close as possible to the diffraction limit, were presented and discussed. Two main approaches have been used to obtain this goal: 1st a reduction of the thermal load of the disk and 2nd a compensation of the thermally induced phasefront distortion caused by the thin-disk crystal. Part of this work provides the basis for the development of high-power mode-locked thin-disk oscillators. Therefore, the laser-active materials Yb:LuAG, Yb:Lu$_2$O$_3$ and Yb:YAB have been theoretically and experimentally analyzed in addition to the well known laser-active material Yb:YAG since they have favorable properties with regard to the generation of ultrashort pulses.

The innovative concept of Zero-Phonon-Line (ZPL) pumping was experimentally implemented to allow for pump powers of up to $\approx$ 2 kW at a narrow wavelength peak with a width of less than one Nanometer. The pumping of the laser-active materials Yb:YAG, Yb:LuAG and Yb:Lu$_2$O$_3$ at the ZPL-line allows to reduce the heat generation in the disk by approximately 30% which is due to the longer pump wavelength of 969 nm (Yb:YAG, Yb:LuAG) and 976 nm (Yb:Lu$_2$O$_3$) compared to the conventional pumping in the wavelength range of 940-950 nm. For this reason, the thermally induced deformations of the thin-disk crystal are strongly reduced and the Stokes efficiency is increased. Especially the reduction of the aspherical phase distortions which result in significantly lower diffraction losses of the fundamental mode is essential for the scaling of fundamental-mode thin-disk lasers to the kilowatt output power level. Using the ZPL-pump concept, an Yb:LuAG thin-disk laser with an optical output power of 742 W and nearly diffraction limited beam quality (M$^2 \approx$ 1.5) together with an unprecedented high optical efficiency of 58.5% was demonstrated. For an Yb:YAG laser in multimode operation (M$^2 \approx$ 15), this pumping principle allowed to achieve a maximum optical efficiency of 72%. Kilowatt level ZPL-pumping of an Yb:Lu$_2$O$_3$ thin-disk laser resulted in 670 W of output power which is the highest optical output power reported to date for this laser-active material. Despite the discussion of the high potential of the implementation of Yb:Lu$_2$O$_3$ for the use in thin-disk lasers, also (current) limitations especially regarding the crystal quality are addressed. It was determined that localized defects and high internal stress of the Yb:Lu$_2$O$_3$ thin-disk crystals limit currently the generation of fundamental-mode

radiation at high output powers. The method of ZPL-pumping reported in this thesis was used by the company TRUMPF later on to scale the output power of thin-disk lasers with high-brightness beams to output powers of several kilowatts. Gottwald et al. [110] used a ZPL pumping configuration with 44 passes of the pump beam through the thin-disk crystal and supposingly a quite thin Yb:YAG or Yb:LuAG disk of about 80 μm to demonstrate 4 kW of fundamental-mode output power. The optical efficiency of this laser was about 56%. This shows the high potential of ZPL-pumping and the applicability of this pump method to industrial systems. The combination of ZPL-pumping with aspherical mirror concepts will allow obtaining thin-disk oscillators with high brightness and output powers of 10 kW and beyond. A successful implementation of an aspherical mirror to compensate the aspherical contribution of the thermally induced deformations of the disk was described in chapter 7. This allowed demonstrating a thin-disk laser with an output power of about 4 kW with beam quality factors in the range of 8. Based on the knowledge gained during the first successful demonstration and usage of an aspherical mirror in a thin-disk laser with output powers at the kilowatt level an actively-controlled mirror for the same purpose was developed. As a result, an Yb:YAG thin-disk laser with an actively-controlled mirror at an output power close to the kilowatt level was realized later on by Piehler et al [98]. The described benefit of a vacuum environment for fundamental mode lasers was proven in [111], where 1.1 kW of output power was realized by using a simple I-resonator together with a comparatively long resonator length of several meters.

Aiming at a future use of this laser-active material to generate ultrashort pulses, the suitability of Yb:YAB in the thin-disk laser configuration was demonstrated for the first time. At an emission wavelength of 1040.7 nm, a maximum optical efficiency of 60.3% at an output power of 19.3 W was obtained by using a pump spot diameter of 1 mm. In high-power experiments, output powers exceeding 100 W together with 50.2% of optical efficiency were shown. To the best of our knowledge, this is the highest output power reported to date for a cw Yb:YAB laser. In a near-diffraction-limited operation the output power was 10.4 W with an optical efficiency of 44.5%. Moreover, the large emission bandwidth of Yb:YAB was verified by continuously tuning the emission wavelength from 1001 to 1053 nm using a GWS-mirror. Taking into account the obvious room for further improvements e.g. by applying an optimum AR-coating or using a CVD-diamond heat sink, power scaling of the Yb:YAB thin-disk laser to the multi-hundred watt level with high optical efficiencies seems to be within reach in the very near future. As FEM-simulations show, the temperature difference of the Yb:YAB disk can be reduced by $\approx 23\%$ when using a CVD-diamond heat sink instead of a copper one. Further investigations at the IFSW will also concentrate on the test of Yb:YAB thin-disk

crystals for their use in mode-locked resonators.

In order to realize a mode-locked thin-disk laser oscillator with an output power level of about 1 kW, the limiting factor is not only the aspherical optical phase distortion induced by the disk itself. Additional limits exist due to the high-energy densities in the cavity. Hence, future investigation should address the high-power/energy-suitability of the SESAM and the arising nonlinearities in the optical components, the air etcetera. The simplest approach to avoid nonlinearities in air is a set-up inside a vacuum chamber or at least in helium atmosphere. Both possibilities have already been demonstrated in scientific systems but are quite complex for industrial ones so that other solutions should be investigated for this purpose.

References

[1] J. Petit, B. Viana, P. Goldner, J. P. Roger, D. Fournier. *Thermomechanical pro-perties of Yb3+ doped laser crystals:Experiments and modeling*. J.Appl.Phys 108, 123108 (2010).

[2] B. Viana, J. Petit, R. Gaumé, P. Goldner, F. Druon, F. Balembois, and P. Geor-ges. *Crystal chemistry approach in Yb doped laser materials.* Materials Science Forum 494, 259-264, doi:10.4028/www.scientific.net/MSF.494.259 (2005).

[3] G.Boulon. *Fifty years of advances in solid-state laser materials.* Opt. Materials 34 (3), 499-512, http://dx.doi.org/10.1016/j.optmat.2011.04.018 (2012).

[4] T. Südmeyer, C. Kränkel, C.R.E. Baer, O.H. Heckl, C.J. Saraceno, M. Golling, R. Peters, K. Petermann, G. Huber, and U. Keller. *High-power ultrafast thin disk laser oscillators and their potential for sub-100-femtosecond pulse generation.* Appl. Phys. B 97, 281-295, doi 10.1007/s00340-009-3700-z (2009).

[5] M. Frede, R. Wilhelm, D. Kracht, C. Fallnich. *Nd:YAG ring laser with 213 W linearly polarized fundamental mode output power*. Opt. Express 13 (19), 7516-7519 (2005).

[6] E. Stiles. *New developments in IPG fiber laser technology*. Proceedings of the 5th International Workshop on Fiber Lasers (2009).

[7] A. Popp, A. Voss, Th. Graf, S. Kirchhof, and H. Bartelt. *Thin-disk laser-pumping of ytterbium-doped fiber laser.* Laser Phys. Lett. 8 (12), 887 doi:10.1002/lapl.201110083 (2011).

[8] D.J. Richardson, J. Nilsson, and W.A. Clarkson. *High power fiber lasers: current status and future perspectives.* J.Opt.Soc.Am.B 27 (11), B63-B92 (2010).

[9] P. Russbueldt, T. Mans, G. Rotarius, J. Weitenberg, H.D. Hoffmann, and R. Po-prawe. *400 W Yb:YAG Innoslab fs-amplifier.* Opt. Express 17 (15), 12230-12245 (2009).

[10] P. Russbueldt, T. Mans, J. Weitenberg, H.D. Hoffmann, and R. Poprawe. *Com-pact diode-pumped 1.1 kW Yb:YAG Innoslab femtosecond amplifier* Opt. Letters 35 (24), 4169-4171 (2010).

[11] C. Stewen, K. Contag, M. Larionov, A. Giesen, and H. Hügel. *A 1-kW CW Thin Disc Laser.* IEEE J.Sel.Top. Quantum Electron. 6 (4), 650-657 (2000).

[12] T. Gottwald, Ch. Stolzenburg, D. Bauer, J. Kleinbauer, V. Kuhn, Th. Metzger, S. Schad, D. Sutter, and A. Killi. *Recent disk laser development at Trumpf.*

Proc. SPIE 8547, High-Power Lasers 2012: Technology and Systems, 85470 C doi:10.1117/12.978990 (2012).

[13]   A. Killi, C. Stolzenburg, I. Zawischa, J. Kleinbauer, S. Schad, R. Brockmann, S. Weiler, J. Neuhaus, S. Kalfhues, E. Mehner, D. Bauer, H. Schlueter, C. Schmitz. *The broad applicability of the thin-disk laser principle-from cw to ps*. Proc. of SPIE 7193, 71931 T (2009).

[14]   J. Mende, G. Spindler, E. Schmid, J. Speiser, A. Giesen. *Thin- disk lasers with dynamically stable resonators*. OSA/ASSP (2009).

[15]   A. Giesen, H. Hügel, A. Voss, K. Wittig, U. Brauch, H. Opower. *Scalable concepts for diode-pumped high-power solid-state lasers.* Appl. Phys. B 58 (5), 365-372 (1994).

[16]   A. Voss. *Der Scheibenlaser: Theoretische Grundlagen des Dauerstrichbetriebs und erste experimentelle Ergebnisse anhand von Yb:YAG*. Dissertation, Stuttgart, Univ. (2002).

[17]   M. Larionov. *Kontaktierung und Charakterisierung von Kristallen für Scheibenlaser*. Dissertation, Stuttgart, Univ. (2009).

[18]   S. Erhard, M. Karszewski, C. Stewen, K. Contag, A. Voss, and A. Giesen *Pumping schemes for multi-kW thin disk lasers.* OSA Trends in Optics and Photonics/ Advanced Solid-State Laser, 34, 78-84 (2000).

[19]   W.Koechner. *Solid-State Laser Engineering.* 6th revised and updated edition, Springer Series in Optical Sciences (2006).

[20]   K. Petermann, D. Fagundes-Peters, J. Johannsen, M. Mond, V. Peters, J. J.Romero, S. Kutovoi, J. Speiser and A. Giesen. *Highly Yb-doped oxides for thin-disc lasers.* Journal of Crystal Growth, 275, 135-140 (2005).

[21]   A. Ahmad *Handbook of optomechanical engineering.* Edited by A. Ahmad, TA1750.h36 (1997).

[22]   K. Contag. *Modellierung und numerische Auslegung des Yb:YAG-Scheibenlasers*. Dissertation Universität Stuttgart, Herbert Utz Verlag GmbH (2002).

[23]   C. E. Webb, J. D. C. Jones. *Handbook of Laser Technology and Applications: Laser design and laser systems.* Band 2, CRC Press (2004).

[24]   A. Sennaroglu (editor), B. Viana, J. Petit, R. Gaumé, P. Goldner, M. Jacquernet, F. Druon, S. Chénais, F. Balembois and P. Georges. *Solid-State Lasers and Applications, Chapter 2: Yb-Doped Solid-State Lasers and Materials*. Taylor and Francis Group, LLC, pp 86-87 (2007).

[25]   K. Beil, S. T. Fredrich-Thornton, F. Tellkamp, R. Peters, C. Kränkel, K. Petermann and G. Huber. *Thermal and laser properties of Yb:LuAG for kW thin disk lasers*. Opt. Express 18 (20), 20712-20722 (2010).

[26] L. Parthier, G. Wehrhan, F. Seifert, M. Ansorg, T. Aichele, Ch. Seitz. *High-Index Lens Material LuAG: Development Status and Progress.* SCHOTT AG, Division Schott Lithotec, Litho Forum 2008, Bolton Landing, NY (2008).

[27] T. Kasamatsu, H. Sekita, and Y. Kuwano. *Temperature dependence and optimization of 970-nm diode-pumped Yb:YAG and Yb:LuAG lasers.* Appl. Opt. 38(24), 5149-5153 (1999).

[28] http://www.crytur.cz/pages/10/laser-rods

[29] R. Peters, Ch. Kränkel, K. Petermann, G. Huber. *Crystal growth by the heat exchanger method, spectroscopic characterization and laser operation of high-purity Yb:Lu$_2$O$_3$.* Journal of Crystal Growth 310, 1934-1938 (2008).

[30] A.A. Kaminskii, S.N. Bagayev, K. Ueda, K. Takaichi, A.Shirakawa, S.N. Ivanov, E.N. Khazanov, A.V. Taranov, H.Yagi, and T. Yanagitani. *New results on characterization of highly transparent nanocrystalline C-modification Lu$_2$O$_3$ nanocrystalline ceramics: room-temperature tunable CW laser action of Yb^{3+} ions under LD-pumping and the propagation kinetics of non-equilibrium acoustic phonons.* Laser Phys. Lett. 3 (8), 375-379 (2006).

[31] M. Tokurakawa, K. Takaichi, A. Shirakawa, K. Ueda, H.Yagi, S. Hosokawa, T. Yanagitani, and A.A. Kaminskii. *Diode-pumped mode-locked Yb^{3+}:Lu$_2$O$_3$ ceramic laser.* Opt. Express 14 (26), 12832-12838 (2006).

[32] M. Tokurakawa, A. Shirakawa, K. Ueda, H. Yagi, S.Hosokawa, T. Yanagitani, and A.A. Kaminskii. *Diode-pumped 65 fs Kerr-lens mode-locked Yb^{3+}:Lu$_2$O$_3$ and nondoped Y$_2$O$_3$ combined ceramic laser.* Opt. Letters 33 (12), 1380-1382 (2008).

[33] J. Sanghera, J. Frantz, W. Kim, G. Villalobos, C. Baker, B. Shaw, B. Sadowski, M. Hunt, F. Miklos, A. Lutz, and I. Aggarwal. *10% Yb^{3+}-Lu$_2$O$_3$ ceramic laser with 74% efficiency.* Opt. Letters 36 (4), 576-578 (2011).

[34] C. McMillen, D. Thompson, T. Tritt, and J. Kolis. *Hydrothermal Single-Crystal Growth of Lu$_2$O$_3$ and Lanthanide-Doped Lu$_2$O$_3$.* Cryst. Growth Des. 11 (10), 4386-4391 (2011).

[35] R. Peters. *Ytterbium-dotierte Sesquioxide als hocheffiziente Lasermaterialien.* Dissertation, Institut für Laser-Physik, Universität Hamburg (2009).

[36] V. Peters. *Growth and Spectroscopy of Ytterbium-Doped Sesquioxides.* Dissertation, Institut für Laser-Physik, Universität Hamburg (2001).

[37] P. Wang, J.M. Dawes, P. Dekker, D. M. Knowles, and J. Piper, Baosheng Lu. *Growth and evaluation of ytterbium-doped yttrium aluminum borate as a potential self-doubling laser crystal.* J. Opt. Soc.Am.B 16, 63-69 (1999).

[38] P. Dekker, P. A. Burns, J. M. Dawes and J. Piper, J.Li, X. Hu, and J. Wang. *Widely tunable yellow-green lasers based on the self-frequency-doubling material*

Yb:YAB. J. Opt. Soc. Am. B 20, 706-712 (2003).

[39]   D. Rytz, A. Gross, S. Vernay, V. Wesemann. *YAl$_3$(BO$_3$)$_4$: a novel NLO crystal for frequency conversion to UV wavelengths.* Proc. SPIE 6998, Solid State Lasers and Amplifiers III, 699814, doi:10.1117/12.780027 (2008).

[40]   M. J. Lederer, M. Hildebrandt, V. Z. Kolev, B. Luther-Davies, B. Taylor, J. Dawes, P. Dekker, J. Piper, H. H. Tan, and C. Jagadish. *Passive mode locking of a self-frequency-doubling Yb:YAl$_3$(BO$_3$)$_4$ laser*. Opt. Letters 27 (6), 436-438 (2002).

[41]   S. Rivier, U. Griebner, V. Petrov, H. Zhang, J. Li, J. Wang, and J. Liu. *Sub-90 fs pulses from a passively mode-locked Yb:YAl$_3$(BO$_3$)$_4$ laser*. Appl. Phys. B 93, 753-757 (2008).

[42]   J. Liu, X. Mateos, H. Zhang, J. Li, J. Wang, and V. Petrov. *High-power laser performance of Yb:YAl$_3$(BO$_3$)$_4$ crystals cut along the crystallographic axes*. IEEE Journ. of Quant. Electronics 43, 385-390 (2007).

[43]   J. Liu, X. Mateos, H. Zhang, J. Li, J. Wang, and V. Petrov. *Compact diode-pumped Yb:YAl$_3$(BO$_3$)$_4$ laser generating 14.0 W of continuous-wave and 8.5 W of pulsed output power.* Appl. Phys. B 111, 233-237, doi 10.1007/s00340-012-5323-z (2013).

[44]   D.E. McCumber. *Einstein relations connecting broadband emission and absorption spectra*. Phys. Rev. 136, A954-A957 (1964).

[45]   P. Le Boulanger, J.L. Doulan, S. Girard, J. Marjerie, and R. Moncorgé. *Excited-state absorption spectroscopy of Er^{3+}-doped Y$_3$Al$_5$O$_{12}$, YVO$_4$, and phosphate glass*. Phys. Rev. B60, 11380-11390 (1999).

[46]   P.H. Haumesser, R. Gaumé, B. Viana, and D. Vivien. *Determination of laser parameters of ytterbium-doped oxide crystalline materials.* J. Opt. Soc. Am. B, 19 (10), 2365-2375 (2002).

[47]   G. Boulon, Y. Guyot, H. Canibano, S. Hraich, and A. Yoshikawa. *Characterization and comparison of Yb3+ -doped YAlO$_3$ perovskite crystals (Yb:YAP) with Yb3+-doped Y$_3$Al$_5$O$_{12}$ garnet crystals (Yb:YAG) for laser application*. J. Opt. Soc. Am. B 25, 884-896 (2008).

[48]   R. L. Aggarwal, D. J. Ripin, J. R. Ochoa, and T. Y. Fan. *Measurement of thermo-optic properties of Y$_3$Al$_5$O$_{12}$, Lu$_3$Al$_5$O$_{12}$, YAlO$_3$, LiYF$_4$, LiLuF$_4$, BaY$_2$F$_8$, KGd(WO$_4$)$_2$, and KY(WO$_4$)$_2$ laser crystals in the 80-300 K temperature range*. J. Appl. Phys. 98, 103514-1-103514-14 (2005).

[49]   A. Brenier, Y. Guyot, H. Canibano, G. Boulon, A. Ródenas, D. Jaque, A. Eganyan, and A. G. Petrosyan. *Growth, spectroscopic, and laser properties of Yb^{3+}-doped Lu$_3$Al$_5$O$_{12}$ garnet crystal.* J. Opt. Soc. Am. B 23(4), 676-683 (2006).

[50]   F. Euler, and J. A. Bruce. *Oxygen coordinates of compounds with garnet struc-*

ture. Acta Crystallogr. 19(6), 971-978 (1965).

[51]   H. Jiang, J. Li, J. Wang, X.-B. Hu, H. Liu, B. Teng, C.-Q. Zhang, P. Dekker, P. Wang. *Growth of Yb:YAl$_3$(BO$_3$)$_4$ crystals and their optical and self-frequency-doubling properties.* J. Cryst. Growth 233(1-2), 248-252 (2001).

[52]   A.A. Filimonov, N.I. Leonyuk, L.B. Meissner, T.I. Timchenko, I.S. Rez. *Nonlinear optical properties of isomorphic family of crystals with yttrium-aluminium borate (YAB) structure.* Kristall und Technik 9(1), 63-66 (1974).

[53]   Y. Xu, X. Gong, Y. Chen, M. Huang, Z. Luo, Y. Huang. *Crystal growth and optical properties of YbYAl$_3$(BO$_3$)$_4$: a promising stoichiometric laser crystal.* J. Cryst. Growth 252(1-3), 241-245 (2003).

[54]   J. Li, J. Wang, X. Cheng, X. Hu, P.A. Burns, J.M. Dawes. *Thermal and laser properties of Yb:YAl$_3$(BO$_3$)$_4$ crystal.* J. Cryst. Growth 250(3-4), 458-462 (2003).

[55]   http://www.opticsbalzers.com/en/284/Coating-Technologies.htm

[56]   L. Kirschlager. *Aufbau und Automatisierung eines Messplatzes zur Bestimmung der Absorption optischer Komponenten für den Nah IR-Wellenlängenbereich.* Studienarbeit, Stuttgart, Univ. (2012).

[57]   K. Mori. *Transient Colour Centres Caused by UV Light Irradiation in Yttrium Aluminium Garnet Crystals.* Phys.Stat.Sol. (a) 42, 375- 384 (1977).

[58]   Norm DIN EN ISO 11551 2003. *Optik und optische Instrumente, Laser und Laseranlagen, Prüfverfahren für den Absorptionsgrad von optischen Laserkomponenten.*

[59]   DIN ISO 10110 *Optik und Photonik - Erstellung von Zeichnungen für optische Elemente und Systeme DIN ISO 10110 Teil 1-8* www.beuth.de

[60]   B. Weichelt, A. Voss. *Innovative Disklaser-Module: Charakterisierung von Laserkristallen, Beschichtungen und Disklaser-Modulen, Kurzbezeichnung: DiskModul: Abschlussbericht zum Innonet-Projekt.* Univ., Inst. für Strahlwerkzeuge., Stuttgart, Hannover (2011).

[61]   S. Günster, D. Ristau, B. Weichelt and A. Voss. *Coatings for thin-disk laser systems.* Proc. of SPIE, p.81680J. (2011).

[62]   D. Ristau. *Ion beam sputter coatings for laser technology.* Proc. of Advances in Optical Thin Films, SPIE [5963 pp13-1 to 13-12], (2005).

[63]   *In-situ stress measurement system SIG-2000SP, sigma-physik.* http://www.sigma-physik.de/insitu_en.html

[64]   P.J. Kelly and R.D. Arnell. *Magnetron sputtering: a review of recent developments and applications.* Vacuum 56, 159 - 172 (2000).

[65]   A.J. Waldorf, J.A. Dobrowolski, B.T. Sullivan and L.M. Plante. *Optical coatings deposited by reactive ion plating.* Applied Optics 32 (28), 5583-5593 (1993).

[66]   V. Magni. *Resonators for solid-state lasers with large-volume fundamental mode*

and high alignment stability. Applied Optics 25 (1), pp 107 (1986).

[67]   J. Schwarz, M. Geissel, P. Rambo, J. Porter, D. Headley, M. Ramsey. *Development of a variable focal length concave mirror for on-shot thermal lens correction in rod amplifiers*. Opt. Express 14 (23), pp 10957-10969 (2006).

[68]   E.Anashkina and O. Antipov. *Electronic (population) lensing versus thermal lensing in Yb:YAG and Nd:YAG laser rods and disks.* J. Opt. Soc. Am. B 27 (3), 363-369 (2010).

[69]   S. Chénais, F. Balembois, F. Druon, G. Lucas-Leclin, and P. Georges. *Thermal Lensing in Diode-Pumped Ytterbium Lasers-Part II: Evaluation of Quantum Efficiencies and Thermo-Optic Coefficients.* IEEE Journ. of Quant. Electronics 40 (9), 1235-1243 (2004).

[70]   Personal communication with B. Vrolijk, Element Six Ltd.

[71]   Physical properties of AuSn, Indium Cooperation.
       http://www.indium.com/solders/gold/

[72]   Thermal properties of copper.
       http://www.engin.brown.edu/organizations/EWB/GISP/Callster%20-
       %20chapter_17.pdf

[73]   Thermal properties of CuW.
       https://www.plansee.com/de/produkte/komponenten/elektronik-
       thermal-management-komponenten/waermeshysspreizer-und-
       gehaeusekomponenten.html

[74]   Silicon Carbide Product Specification.
       SiC-6H Substrates. www.sicrystal.de/index.php/de/produkt-spezifikationen-de
       (2014).

[75]   CVD-diamond Product Specification.
       The CVD diamond booklet.
       www.diamond-materials.com/downloads/cvd_diamond_booklet.pdf (2008).

[76]   Technical Data Sheet curamik® Ceramic Substrates.
       https://www.rogerscorp.com/pes/curamik/product/13/curamik-Thermal.aspx

[77]   R. Paschotta. *Beam quality deterioration of lasers caused by intracavity beam distortions* Opt. Express 14 (13), 6069-6074 (2006).

[78]   R. Pereira, B. Weichelt, D. Liang, P. Morais, H. Gouveia, M. Abdou-Ahmed, A. Voss and T. Graf. *Efficient pump beam shaping for high-power thin-disk laser systems* Appl. Optics 49 (279), 5157-5162 (2010).

[79]   K. Contag, M. Karszewski, C. Stewen, A. Giesen and H. Hügel. *Theoretical modeling and experimental investigations of the diode- pumped thin-disk Yb:YAG laser.* Quantum Electron. 29 (8), 697 (1999).

[80]   J. Speiser, A. Giesen. *Numerical Modeling of High Power Continuous-Wave*

Yb:YAG Thin Disk Lasers, Scaling to 14 kW. Opt. Soc. Am. ASSP (2007).

[81]   S. Chenais, F. Druon, S. Forget, F. Balembois, P. Georges. *On thermal effects in solid-state lasers: The case of ytterbium- doped materials.* Progress in Quantum Electron. 30, 89-153 (2006).

[82]   A. Antognini, K. Schuhmann, F. D. Amaro, F. Biraben, A. Dax, A. Giesen, Th. Graf, Th. W. Hänsch, P. Indelicato, L. Julien, Ch.-Y. Kao, Paul E. Knowles, F. Kottmann, E. Le Bigot, Y.-W. Liu, L. Ludhova, N. Moschüring, F. Mulhauser, T. Nebel, F. Nez, P. Rabinowitz, C. Schwob, D. Taqqu, and R. Pohl. *Thin-Disk Yb:YAG Oscillator-Amplifier Laser, ASE, and Effective Yb:YAG Lifetime.* IEEE Journ. of Quant. Electronics 45 (8), 993-1005 (2009).

[83]   J. Mende, E. Schmid, J. Speiser, G.Spindler, A.Giesen. *Thin- disk laser - Power scaling to the kW regime in fundamental mode operation.* Proc. of SPIE 7193, (2009).

[84]   T.Y. Fan and J.L. Daneu. *Thermal coefficients of the optical path length and refractive index in YAG.* Appl. Optics, 37 (9), 1635-1637 (1998).

[85]   P.Hariharan. *Optical interferometry.* 2nd ed. Elsevier Science (2003).

[86]   H.J. Tiziani. *Rechnerunterstützte Laser-Meßtechnik. Computer aided laser measurement techniques.* Technisches Messen tm, 54. Jahrgang, Heft 6/1987, V436-24 (1987).

[87]   S. Timoshenko. *Theory of Plates and Shells* McGraw-Hill (1987).

[88]   *Gaussian beam shapers. Advanced microoptic systems GmbH.* http://www.amus.de/gaussian-beam-shapers—lbh.html

[89]   J.J. Romero, J. Johannsen, M. Mond, K. Petermann, G. Huber and E. Heumann. *Continuous-wave laser action of Yb^{3+}-doped lanthanum scandium borate.* Appl. Physics B 80, 159-163 (2005).

[90]   D. Sangla, M. Castaing, F. Balembois and P. Georges. *Highly efficient Nd:YVO$_4$ laser by direct in-band diode pumping at 914 nm.* Opt. Letters 34 (14), 2159-2161 (2009).

[91]   G. B. Venus, A.Sevian, V.I. Smirnov and L.B.Glebov. *High- brightness narrow-line laser diode source with volume Bragg-grating feedback.* Proc. of SPIE, (5711), pp 166-176 (2005).

[92]   L.B. Glebov, L.N. Glebova, V.I. Smirnov, M. Dubinskii, L.D. Merkle, S. Papernov, A.W. Schmid. *Laser damage resistance of photo-thermo-refractive glass Bragg gratings*. Proc. of Solid State and Diode Lasers Technical Review, Albuquerque (2004).

[93]   B. Weichelt, K. Wentsch, A. Voss, M. Abdou Ahmed and T. Graf. *A 670 W Yb:Lu$_2$O$_3$ thin-disk laser.* Laser Phys. Lett., 9 (2), 110-115 (2011).

[94]   R. Peters, C. Kränkel, S.T. Fredrich-Thornton, K. Beil, K. Petermann, G. Huber,

O.H. Heckl, C.R.E. Baer, C.J. Saraceno, T. Südmeyer, and U. Keller. *Thermal analysis and efficient high power continuous-wave and mode-locked thin disk laser operation of Yb-doped sesquioxides* Applied Phys. B 102, 509-514 (2011).

[95]   D. Radtke, U.D. Zeitner. *Laser-lithography on non-planar surfaces*. Opt. Express 15, 1167-1174 (2007).

[96]   D. Blázquez-Sánchez, B. Weichelt, A. Austerschulte, A. Voss, Th. Graf, A. Killi, H. Ch. Eckstein, M. Stumpf, A. L. Matthes, and U. D. Zeitner. *Improving the brightness of a 5-kW single thin-disk laser by an aspherical phase-front correction*. Opt. Letters 36, 799-801 (2011).

[97]   Final report, project Baden Württemberg Stiftung. *Thermisch aktivierte Bauelemente für die adaptive Optik (ThermAO).* (2008).

[98]   S. Piehler, B. Weichelt, A. Voss, M. Abdou Ahmed and T. Graf. *Power scaling of fundamental-mode thin-disk lasers using intra-cavity deformable mirror*. Opt. Letters 37 (24), 5033-5035 (2012).

[99]   S. Piehler. *Resonatorinterne Kompensation thermisch induzierter Wellenfront-störungen in hochbrillanten Scheibenlasern*. Dissertation Universität Stuttgart, Herbert Utz Verlag GmbH (2017).

[100] M. N. Islam, E. R. Sunderman, C. E. Soccolich, I. Bar-Joseph, N. Sauer, T. Y. Chang, and B. I. Miller. *Color Center Lasers Passively Mode Locked by Quantum Wells.* IEEE J. Quantum Electron. 25, 2454-2463 (1989).

[101] S. Tsuda, W. H. Knox, E. A. de Souza, W. Y. Jan, and J. E. Cunningham. *Mode-Locking Ultrafast Solid-State Lasers with Saturable-Bragg Reflectors.* IEEE J. Sel. Top. Quantum Electron. 2, 454-464 (1996).

[102] U. Keller. *Semiconductor nonlinearities for solid-state laser modelocking and Q-switching.* in Semiconductors and Semimetals, Vol. 59A, edited by A. Kost and E. Garmire, Academic Press, Boston (1999).

[103] C.R.E. Baer, Ch. Kränkel, C. J. Saraceno, O. H. Heckl, M. Golling, R. Peters, K. Petermann, Th. Südmeyer, G. Huber, and U. Keller. *Femtosecond thin-disk laser with 141 W of average power*. Opt. Letters 35, 2302-2304 (2010).

[104] S. Ricaud, A. Jaffres, K. Wentsch, A. Suganuma, B. Viana, P. Loiseau, B. Weichelt, M. Abdou-Ahmed, A. Voss, T. Graf, D. Rytz, C. Hönninger, E. Mottay, P. Georges, and F. Druon. *Femtosecond Yb:CaGdAlO$_4$ thin-disk oscillator*. Opt. Letters 37, 3984-3986 (2012).

[105] K. S. Wentsch, L. Zheng, J. Xu, M. Abdou Ahmed, and Th. Graf. *Passively mode-locked Yb$^{(3+)}$:Sc$_2$SiO$_5$ thin-disk laser*. Opt. Letters 37, 4750-4752 (2012).

[106] V. Belruss, J. Kalnajs, A. Linz, R.C. Folweiler. *Top-seeded solution growth of oxide crystals from non-stoichiometric melts*. Materials Research Bulletin, 6,

10, 899-905 (1971).

[107] Personal communication with D. Rytz., Forschungsinstitut für mineralische und metallische Werkstoffe -Edelsteine/Edelmetalle- GmbH (FEE).

[108] P. Dekker and J.M. Dawes. *Characterisation of nonlinear conversion and crystal quality in Nd- and Yb-doped YAB.* Opt. Express 12 (24), 5922-5930 (2004).

[109] M. Rumpel, A. Voss, M. Moeller, F. Habel, Ch. Moormann, M. Schacht, Th. Graf, and M. Abdou Ahmed. *Linearly polarized, narrow-linewidth, and tunable Yb:YAG thin-disk laser.* Opt. Letters 37, 4188-4190 (2012).

[110] T. Gottwald, V. Kuhn, S.S. Schad, Ch. Stolzenburg, A. Killi. *Recent developments in high power thin disk lasers at TRUMPF Laser.* Proc. SPIE 8898, Technologies for Optical Countermeasures X; and High-Power Lasers 2013: Technology and Systems, 88980P, doi:10.1117/12.2028656 (2013).

[111] Y.H. Peng, Y.X. Lim, J. Cheng, Y. Guo, Y.Y. Cheah, and K.S. Lai. *Near fundamental mode 1.1 kW Yb:YAG thin-disk laser.* Opt. Letters 38, 1709-1711 (2013).

Acknowledgment

Laser in der Materialbearbeitung
Forschungsberichte des IFSW (Institut für Strahlwerkzeuge)

Herausgegeben von
Prof. Dr.-Ing. habil. Helmut Hügel, Universität Stuttgart
Forschungsberichte des IFSW von 1992 bis 1999 erschienen im Teubner Verlag, Stuttgart

Zoske, Uwe
Modell zur rechnerischen Simulation von Laser-resonatoren und Strahlführungssystemen
1992, 186 Seiten, ISBN 3-519-06205-4

Gorriz, Michael
Adaptive Optik und Sensorik im Strahlführungs-system von Laserbearbeitungsanlagen
1992, vergriffen, ISBN 3-519-06206-2

Mohr, Ursula
Geschwindigkeitsbestimmende Strahleigenschaf-ten und Einkoppelmechanismen beim CO_2-Laserschneiden von Metallen
1993, 130 Seiten, ISBN 3-519-06207-0

Rudlaff, Thomas
Arbeiten zur Optimierung des Umwandlungshär-tens mit Laserstrahlen
1993, 152 Seiten, ISBN 3-519-06208-9

Borik, Stefan
Einfluß optischer Komponenten auf die Strahl-qualität von Hochleistungslasern
1993, 200 Seiten, ISBN 3-519-06209-7

Paul, Rüdiger
Optimierung von HF-Gasentladungen für schnell längsgeströmte CO_2-Laser
1994, 149 Seiten, ISBN 3-519-06210-0

Wahl, Roland
Robotergeführtes Laserstrahlschweißen mit Steuerung der Polarisationsrichtung
1994, 150 Seiten, ISBN 3-519-06211-9

Frederking, Klaus-Dieter
Laserlöten kleiner Kupferbauteile mit geregelter Lotdrahtzufuhr
1994, 139 Seiten, ISBN 3-519-06212-7

Grünewald, Karin M.
Modellierung der Energietransferprozesse in längsgeströmten CO_2-Lasern
1994, 158 Seiten, ISBN 3-519-06213-5

Shen, Jialin
Optimierung von Verfahren der Laseroberflä-chenbehandlung mit gleichzeitiger Pulverzufuhr
1994, 160 Seiten, ISBN 3-519-06214-3

Arnold, Johannes M.
Abtragen metallischer und keramischer Werkstof-fe mit Excimerlasern
1994, 192 Seiten, ISBN 3-519-06215-1

Holzwarth, Achim
Ausbreitung und Dämpfung von Stoßwellen in Excimerlasern
1994, 153 Seiten, ISBN 3-519-06216-X

Dausinger, Friedrich
Strahlwerkzeug Laser: Energieeinkopplung und Prozeßeffektivität
1995, 143 Seiten, ISBN 3-519-06217-8

Meiners, Eckhard
Abtragende Bearbeitung von Keramiken und Metallen mit gepulstem Nd:YAG-Laser als zwei-stufiger Prozeß
1995, 120 Seiten, ISBN 3-519-06222-4

Beck, Markus
Modellierung des Lasertiefschweißens
1996, 160 Seiten, ISBN 3-519-06218-6

Breining, Klaus
Auslegung und Vermessung von Gasentladungs-strecken für CO_2-Hochleistungslaser
1996, 131 Seiten, ISBN 3-519-06219-4

Griebsch, Jürgen
Grundlagenuntersuchungen zur Qualitätssiche-rung beim gepulsten Lasertiefschweißen
1996, 133 Seiten, ISBN 3-519-06220-8

Krepulat, Walter
Aerodynamische Fenster für industrielle Hoch-leistungslaser
1996, 144 Seiten, ISBN 3-519-06221-6

Xiao, Min
Vergleichende Untersuchungen zum Schneiden dünner Bleche mit CO_2- und Nd:YAG-Lasern
1996, 118 Seiten, ISBN 3-519-06223-2

Glumann, Christiane
Verbesserte Prozeßsicherheit und Qualität durch Strahlkombination beim Laserschweißen
1996, 143 Seiten, ISBN 3-519-06224-0

Gross, Herbert
Propagation höhermodiger Laserstrahlung und deren Wechselwirkung mit optischen Systemen
1996, 191 Seiten, ISBN 3-519-06225-9

Rapp, Jürgen
Laserschweißeignung von Aluminiumwerkstoffen für Anwendungen im Leichtbau
1996, 202 Seiten, ISBN 3-519-06226-7

Wittig, Klaus
Theoretische Methoden und experimentelle Verfahren zur Charakterisierung von Hochleistungslaserstrahlung
1996, 198 Seiten, ISBN 3-519-06227-5

Grünenwald, Bernd
Verfahrensoptimierung und Schichtcharakterisierung beim einstufigen Cermet-Beschichten mittels CO_2-Hochleistungslaser
1996, 160 Seiten, ISBN 3-519-06229-1

Lee, Jae-Hoon
Laserverfahren zur strukturierten Metallisierung
1996, 154 Seiten, ISBN 3-519-06232-1

Albinus, Uwe N. W.
Metallisches Beschichten mittels PLD-Verfahren
1996, 144 Seiten, ISBN 3-519-06233-X

Wiedmaier, Matthias
Konstruktive und verfahrenstechnische Entwicklungen zur Komplettbearbeitung in Drehzentren mit integrierten Laserverfahren
1997, 129 Seiten, ISBN 3-519-06228-3

Bloehs, Wolfgang
Laserstrahlhärten mit angepaßten Strahlformungssystemen
1997, 143 Seiten, ISBN 3-519-06230-5

Bea, Martin
Adaptive Optik für die Materialbearbeitung mit CO_2-Laserstrahlung
1997, 143 Seiten, ISBN 3-519-06231-3

Stöhr, Michael
Beeinflussung der Lichtemission bei mikrokanalgekühlten Laserdioden
1997, 147 Seiten, ISBN 3-519-06234-8

Plaß, Wilfried
Zerstörschwellen und Degradation von CO_2-Laseroptiken
1998, 158 Seiten, ISBN 3-519-06235-6

Schaller, Markus K. R.
Lasergestützte Abscheidung dünner Edelmetallschichten zum Heißgaskorrosionsschutz für Molybdän
1998, 163 Seiten, ISBN 3-519-06236-4

Hack, Rüdiger
System- und verfahrenstechnischer Vergleich von Nd:YAG- und CO_2-Lasern im Leistungsbereich bis 5 kW
1998, 165 Seiten, ISBN 3-519-06237-2

Krupka, René
Photothermische Charakterisierung optischer Komponenten für Hochleistungslaser
1998, 139 Seiten, ISBN 3-519-06238-0

Pfeiffer, Wolfgang
Fluiddynamische und elektrophysikalisch optimierte Entladungsstrecken für CO_2-Hochleistungslaser
1998, 152 Seiten, ISBN 3-519-06239-9

Volz, Robert
Optimiertes Beschichten von Gußeisen-, Aluminium- und Kupfergrundwerkstoffen mit Lasern
1998, 133 Seiten, ISBN 3-519-06240-2

Bartelt-Berger, Lars
Lasersystem aus kohärent gekoppelten Grundmode-Diodenlasern
1999, 135 Seiten, ISBN 3-519-06241-0

Müller-Hummel, Peter
Entwicklung einer Inprozeßtemperaturmeßvorrichtung zur Optimierung der laserunterstützten Zerspanung
1999, 139 Seiten, ISBN 3-519-06242-9

Rohde, Hansjörg
Qualitätsbestimmende Prozeßparameter beim Einzelpulsbohren mit einem Nd:YAG-Slablaser
1999, 171 Seiten, ISBN 3-519-06243-7

Huonker, Martin
Strahlführung in CO_2-Hochleistungslasersystemen zur Materialbearbeitung
1999, 121 Seiten, ISBN 3-519-06244-5

Callies, Gert
Modellierung von qualitäts- und effektivitätsbestimmenden Mechanismen beim Laserabtragen
1999, 119 Seiten, ISBN 3-519-06245-3

Schubert, Michael E.
Leistungsskalierbares Lasersystem aus fasergekoppelten Singlemode-Diodenlasern
1999, 105 Seiten, ISBN 3-519-06246-1

Kern, Markus
Gas- und magnetofluiddynamische Maßnahmen zur Beeinflussung der Nahtqualität beim Laserstrahlschweißen
1999, 132 Seiten, ISBN 3-519-06247-X

Raiber, Armin
Grundlagen und Prozeßtechnik für das Lasermikrobohren technischer Keramiken
1999, 135 Seiten, ISBN 3-519-06248-8

Laser in der Materialbearbeitung
Forschungsberichte des IFSW (Institut für Strahlwerkzeuge)

Herausgegeben von
Prof. Dr.-Ing. habil. Helmut Hügel, Universität Stuttgart
Forschungsberichte des IFSW ab 2000 erschienen im Herbert Utz Verlag, München

Lücke, Bernd
Kohärente Kopplung von Vertikalemitter-Arrays
2003, 120 Seiten, ISBN 3-8316-0224-7

Hohenberger, Bernd
Laserstrahlschweißen mit Nd:YAG-Doppelfokustechnik – Steigerung von Prozeßsicherheit, Flexibilität und verfügbarer Strahlleistung
2003, 128 Seiten, ISBN 3-8316-0223-9

Jasper, Knut
Neue Konzepte der Laserstrahlformung und -führung für die Mikrotechnik
2003, 152 Seiten, ISBN 3-8316-0205-0

Heimerdinger, Christoph
Laserstrahlschweißen von Aluminiumlegierungen für die Luftfahrt
2003, 112 Seiten, ISBN 3-8316-0256-5

Christoph Fleig
Evaluierung eines Messverfahrens zur genauen Bestimmung des Reflexionsgrades optischer Komponenten
2003, 150 Seiten, ISBN 3-8316-0274-3

Joachim Radtke
Herstellung von Präzisionsdurchbrüchen in keramischen Werkstoffen mittels repetierender Laserbearbeitung
2003, 150 Seiten, ISBN 3-8316-0285-9

Michael Brandner
Steigerung der Prozesseffizienz beim Löten und Kleben mit Hochleistungsdiodenlasern
2003, 195 Seiten, ISBN 3-8316-0288-3

Reinhard Winkler
Porenbildung beim Laserstrahlschweissen von Aluminium-Druckguss
2004, 153 Seiten, ISBN 3-8316-0313-8

Helmut Kindler
Optische und gerätetechnische Entwicklungen zum Laserstrahlspritzen
2004, 117 Seiten, ISBN 3-8316-0315-4

Andreas Ruf
Modellierung des Perkussionsbohrens von Metallen mit kurz- und ultrakurzgepulsten Lasern
2004, 140 Seiten, ISBN 3-8316-0372-3

Guido Hergenhan
Kohärente Kopplung von Vertikalemittern – Systemkonzept und experimentelle Verifizierung
2004, 115 Seiten, ISBN 3-8316-0376-6

Klaus Goth
Schweißen von Mischverbindungen aus Aluminiumguß- und Knetlegierungen mit CO_2-Laser unter besonderer Berücksichtigung der Nahtart
2004, 143 Seiten, ISBN 3-8316-0427-4

Armin Strauch
Effiziente Lösung des inversen Problems beim Laserstrahlschweißen durch Simulation und Experiment
2004, 169 Seiten, ISBN 3-8316-0425-8

Thomas Wawra
Verfahrensstrategien für Bohrungen hoher Präzision mittels Laserstrahlung
2004, 162 Seiten, ISBN 3-8316-0453-3

Michael Honer
Prozesssicherungsmaßnahmen beim Bohren metallischer Werkstoffe mittels Laserstrahlung
2004, 113 Seiten, ISBN 3-8316-0441-x

Thomas Herzinger
Prozessüberwachung beim Laserbohren von Turbinenschaufeln
2004, 143 Seiten, ISBN 3-8316-0443-6

Reiner Heigl
Herstellung von Randschichten auf Aluminiumgusslegierungen mittels Laserstrahlung
2004, 173 Seiten, ISBN 3-8316-0460-6

Laser in der Materialbearbeitung
Forschungsberichte des IFSW (Institut für Strahlwerkzeuge)

Herausgegeben von
Prof. Dr. phil. nat. Thomas Graf, Universität Stuttgart
Forschungsberichte des IFSW ab 2005 erschienen im Herbert Utz Verlag, München

Thomas Fuhrich
Marangoni-effekt beim Laserstrahltiefschweißen von Stahl
2005, 163 Seiten, ISBN 3-8316-0493-2

Daniel Müller
Pulsenergiestabilität bei regenerativen Kurzpulsverstärkern im Scheibenlaserdesign
2005, 172 Seiten, ISBN 3-8316-0508-4

Jiancun Gao
Neodym-dotierte Quasi-Drei-Niveau-Scheibenlaser: Hohe Ausgangsleistung und Frequenzverdopplung
2005, 148 Seiten, ISBN 3-8316-0521-1

Wolfgang Gref
Laserstrahlschweißen von Aluminiumwerkstoffen mit der Fokusmatrixtechnik
2005, 136 Seiten, ISBN 3-8316-0537-8

Michael Weikert
Oberflächenstrukturieren mit ultrakurzen Laserpulsen
2005, 116 Seiten, ISBN 3-8316-0573-4

Julian Sigel
Lasergenerieren metallischer Bauteile mit variablem Laserstrahldurchmesser in modularen Fertigungssystemen
2006, 132 Seiten, ISBN 3-8316-0572-6

Andreas Ruß
Schweißen mit dem Scheibenlaser-Potentiale der guten Fokussierbarkeit
2006, 142 Seiten, ISBN 3-8316-0580-7

Gabriele Seibold
Absorption technischer Oberflächen in der Lasermaterialbearbeitung
2006, 156 Seiten, ISBN 3-8316-0618-8

Dirk Lindenau
Magnetisch beeinflusstes Laserstrahlschweißen
2007, 180 Seiten, ISBN 978-3-8316-0687-0

Jens Walter
Gesetzmäßigkeiten beim Lasergenerieren als Basis für die Prozesssteuerung und –regelung
2008, 140 Seiten, ISBN 978-3-8316-0770-9

Heiko Ridderbusch
Longitudinal angeregte passiv gütegeschaltete Laserzündkerze
2008, 175 Seiten, ISBN 978-3-8316-0840-9

Markus Leimser
Strömungsinduzierte Einflüsse auf die Nahteigenschaften beim Laserstrahlschweißen von Aluminiumwerkstoffen
2009, 150 Seiten, ISBN 978-3-8316-0854-6

Mikhail Larionov
Kontaktierung und Charakterisierung von Kristallen für Scheibenlaser
2009, 186 Seiten, ISBN 978-3-8316-0855-3

Jürgen Müller-Borhanian
Kamerabasierte In-Prozessüberwachung beim Laserstrahlschweißen
2009, 162 Seiten, ISBN 978-3-8316-0890-4

Andreas Letsch
Charakterisierung allgemein astigmatischer Laserstrahlung mit der Methode der zweiten Momente
2009, 176 Seiten, ISBN 978-3-8316-0896-6

Thomas Kübler
Modellierung und Simulation des Halbleiterscheibenlasers
2009, 152 Seiten, ISBN 978-3-8316-0918-5

Günter Ambrosy
Nutzung elektromagnetischer Volumenkräfte beim Laserstrahlschweißen
2009, 170 Seiten, ISBN 978-3-8316-0925-3

Agnes Ott
Oberflächenmodifikation von Aluminiumlegierungen mit Laserstrahlung: Prozessverständnis und Schichtcharakterisierung
2010, 226 Seiten, ISBN 978-3-8316-0959-8

Detlef Breitling
Gasphaseneinflüsse beim Abtragen und Bohren mit ultrakurz gepulster Laserstrahlung
2010, 200 Seiten, ISBN 978-3-8316-0960-4

Dmitrij Walter
Online-Qualitätssicherung beim Bohren mittels ultrakurz gepulster Laserstrahlung
2010, 156 Seiten, ISBN 978-3-8316-0968-0

Jan-Philipp Weberpals
Nutzen und Grenzen guter Fokussierbarkeit beim Laserstrahlschweißen
2010, 154 Seiten, ISBN 978-3-8316-0995-6

Angelika Beyertt
Yb:KYW regenerativer Verstärker für ultrakurze Pulse
2010, 166 Seiten, ISBN 978-3-8316-4002-7

Christian Stolzenburg
Hochrepetierende Kurzpuls-Scheibenlaser im infraroten und grünen Spektralbereich
2011, 184 Seiten, ISBN 978-3-8316-4041-6

Svent-Simon Beyertt
Quantenfilm-Pumpen zur Leistungsskalierung von Halbleiter-Scheibenlasern
2011, 130 Seiten, ISBN 978-3-8316-4051-5

Sonja Kittel
Verzugsarmes Laserstrahlschweißen an axial-symmetrischen Bauteilen
2011, 162 Seiten, ISBN 978-3-8316-4088-1

Andrey Andreev
Schweißen mit dem Scheibenlaser im Getriebe-bau – Prozessmerkmale und Anlagenkonzepte
2011, 140 Seiten, ISBN 978-3-8316-4103-1

Christian Föhl
Einsatz ultrakurz gepulster Laserstrahlung zum Präzisionsbohren von Metallen
2011, 156 Seiten, ISBN 978-3-8316-4120-8

Andreas Josef Birnesser
Prozessregelung beim Laserstrahlschweißen
2011, 150 Seiten, ISBN 978-3-8316-4133-8

Christoph Neugebauer
Thermisch aktive optische Bauelemente für den resonatorinternen Einsatz beim Scheibenlaser
2012, 220 Seiten, ISBN 978-3-8316-4178-9

Andreas Dauner
Fluidmechanische Maßnahmen zur Reduzierung von Schmelzablagerungen beim Hochgeschwindigkeitslaserbohren
2012, 150 Seiten, ISBN 978-3-8316-4194-9

Axel Heß
Vorteile und Herausforderungen beim Laserstrahlschweißen mit Strahlquellen höchster Fokussierbarkeit
2012, 164 Seiten, ISBN 978-3-8316-4198-7

Christian Gehrke
Überwachung der Struktureigenschaften beim Oberflächenstrukturieren mit ultrakurzen Laserpulsen
2013, 164 Seiten, ISBN 978-3-8316-4271-7

David Schindhelm
In-Prozess Qualitätssicherung für das Laserstrahlschneiden von Metallen
2013, 150 Seiten, ISBN 978-3-8316-4345-5

Tilman Froschmeier-Hanss
Festigkeitsverhalten laserstrahlgeschweißter belastungsangepasster Stahlwerkstoffverbindun-gen
2014, 200 Seiten, ISBN 978-3-8316-4347-9

Moritz Vogel
Speciality Fibers for High Brightness Laser Beam Delivery
2014, 187 Seiten, ISBN 978-3-8316-4382-0

Andreas Michalowski
Untersuchungen zur Mikrobearbeitung von Stahl mit ultrakurzen Laserpulsen
2014, 176 Seiten, ISBN 978-3-8316-4424-7

Georg Stöppler
Untersuchung eines OPOs im mittleren Infrarot im Hinblick auf Anwendungen für minimalinvasive Chirurgie
2015, 144 Seiten, ISBN 978-3-8316-4437-7

Patrick Mucha
Qualitäts- und produktivitätsbeeinflussende Mechanismen beim Laserschneiden von CF und CFK
2015, 120 Seiten, ISBN 978-3-8316-4516-9

Claus-Dieter Reiniger
Fluiddynamische Effekte beim Remote-Laserstrahlschweißen von Blechen mit Fügespalt
2015, 188 Seiten, ISBN 978-3-8316-4528-2

Andreas Leitz
Laserstrahlschweißen von Kupfer- und Aluminiumwerkstoffen in Mischverbindung
2016, 172 Seiten, ISBN 978-3-8316-4549-7

Peter Stritt
Prozessstrategien zur Vermeidung von Heißrissen beim Remote-Laserstrahlschweißen von AlMgSi 6016
2016, 194 Seiten, ISBN 978-3-8316-4555-8

Katrin Sarah Wentsch
Analyse Ytterbium-dotierter Materialien für den Einsatz in ultrakurz-gepulsten Scheibenlasersystemen
2016, 162 Seiten, ISBN 978-3-8316-4578-7

Jan-Philipp Negel
Scheibenlaser-Multipassverstärker für ultrakurze Laserpulse mit Ausgangsleistungen im kW-Bereich
2017, 142 Seiten, ISBN 978-3-8316-4632-6

Christian Freitag
Energietransportmechanismen bei der gepulsten Laserbearbeitung Carbonfaser verstärkter Kunst-stoffe
2017, 152 Seiten, ISBN 978-3-8316-4638-8

Andreas Popp
Faserlaser und Faserlaserverstärker als Brillanz-konverter für Scheibenlaserstrahlen
2017, 242 Seiten, ISBN 978-3-8316-4643-2

Karin Heller
Analytische Temperaturfeldbeschreibung beim
Laserstrahlschweißen für thermographische
Prozessbeobachtung
2017, 130 Seiten, ISBN 978-3-8316-4654-8

Stefan Piehler
Resonatorinterne Kompensation thermisch indu-
zierter Wellenfrontstörungen in hochbrillanten
Scheibenlasern
2017, 148 Seiten, ISBN 978-3-8316-4690-6

Felix Abt
Bildbasierte Charakterisierung und Regelung von
Laserschweißprozessen
2017, 232 Seiten, ISBN 978-3-8316-4691-3

Volker Rominger
Untersuchungen der Prozessvorgänge bei Ein-
schweißungen in Baustahl mit Lasern hoher Bril-
lanz
2017, 186 Seiten, ISBN 978-3-8316-4692-0

Thomas Rataj
Hochleistungstaugliche faserintegrierte Strahl-
weichen
2018, 142 Seiten, ISBN 978-3-8316-4733-0

Michael Diez
Pulsformung zur schädigungsarmen Laserbear-
beitung von Silizium
2018, 194 Seiten, ISBN 978-3-8316-4737-8

Andreas Heider
Erweitern der Prozessgrenzen beim Laserstrahl-
schweißen von Kupfer mit Einschweißtiefen zwi-
schen 1 mm und 10 mm
2018, 156 Seiten, ISBN 978-3-8316-4738-5

Marcel Schäfer
Energetische Beeinflussung von Schmelzefluss
und Heißrissbildung beim Laserstrahlschweißen
von Vergütungsstahl
2018, 146 Seiten, ISBN 978-3-8316-4742-2

Laser in der Materialbearbeitung
Forschungsberichte des IFSW (Institut für Strahlwerkzeuge)
Herausgegeben von
Prof. Dr. phil. nat. Thomas Graf, Universität Stuttgart
Forschungsberichte des IFSW ab 2019 erschienen im utzverlag, München

Tom Dietrich
Gitterwellenleiterstrukturen zur Strahlformung in
Hochleistungsscheibenlasern
2019, 154 Seiten, ISBN 978-3-8316-4785-9

Martin Rumpel
Applications of Grating Waveguide Structures in
Solid-State Lasers
2019, 112 Seiten, ISBN 978-3-8316-4801-6

Michael Eckerle
Generation and amplification of ultrashort pulsed
high-power cylindrical vector beams
2019, 112 Seiten, ISBN 978-3-8316-4804-7

Martin Stubenvoll
Messung und Kompensation thermisch induzier-
ter Wellenfrontdeformationen in optischen Ele-
menten
2019, 118 Seiten, ISBN 978-3-8316-4819-1

Christian Hagenlocher
Die Kornstruktur und der Heißrisswiderstand
von Laserstrahlschweißnähten in Aluminium-
legierungen
2020, 150 Seiten, ISBN 978-3-8316-4864-1

Florian Fetzer
Analyse der Geometrie und Stabilität der Kapilla-
re beim Laserstrahltiefschweißen mittels redu-
zierter Modelle.
2020, 180 Seiten, ISBN 978-3-8316-4874-0

Michael Jarwitz
Laserstrahlschweißen von Metallen mit unter-
schiedlichen thermophysikalischen Eigenschaf-
ten.
2020, 154 Seiten, ISBN 978-3-8316-4882-5

Christian Röhrer
Flexible Führung hochbrillanter Laserstrahlen mit
optischen Fasern
2020, 130 Seiten, ISBN 978-3-8316-4888-7

Martin Sommer
Laserstrahlschweißen der Aluminiumlegierung
AlMgSi mittels Strahloszillation
2021, 110 Seiten, ISBN 978-3-8316-4898-6

Birgit Weichelt
Experimental Investigations on Power Scaling of
High-Brightness cw Ytterbium-Doped Thin-Disk
Lasers.
2021, 166 Seiten, ISBN 978-3-8316-4914-3